UILU-ENG-83-2002

CIVIL ENGINEERING STUDIES

STRUCTURAL RESEARCH SERIES NO. 503

ISSN: 0069-4274

SPATIAL CORRELATION STUDY OF STRONG MOTION ARRAY DATA WITH APPLICATION TO LIFELINE EARTHQUAKE ENGINEERING

By
C. H. LOH
A. H-S. ANG
and
Y. K. WEN

Technical Report of Research
Supported by the
NATIONAL SCIENCE FOUNDATION
Division of Civil & Environmental Engineering
(Under Grants CEE 80-02584 and CEE 82-13729)

UNIVERSITY OF ILLINOIS
at URBANA-CHAMPAIGN
URBANA, ILLINOIS
MARCH 1983

50272-101

REPORT DOCUMENTATION PAGE	1. REPORT NO. UILU-ENG-83-2002	2.	3. Recipient's Accession No.

4. Title and Subtitle
SPATIAL CORRELATION STUDY OF STRONG MOTION ARRAY DATA WITH APPLICATION TO LIFELINE EARTHQUAKE ENGINEERING

5. Report Date March 1983

6.

7. Author(s)
C. H. Loh, A. H-S. Ang, Y. K. Wen

8. Performing Organization Rept. No. SRS No. 503

9. Performing Organization Name and Address
Department of Civil Engineering
University of Illinois
208 N. Romine Street
Urbana, IL 61801

10. Project/Task/Work Unit No.

11. Contract(C) or Grant(G) No.
(C) NSF CEE 80-02584
(G) NSF CEE 82-13729

12. Sponsoring Organization Name and Address
National Science Foundation
Washington, D.C.

13. Type of Report & Period Covered

14.

15. Supplementary Notes

16. Abstract (Limit: 200 words)

Seismic design of structures with long dimensions located at the ground surface such as bridges, pipelines, are usually controlled by strains and differential movements caused by body and surface waves generated by earthquakes. Based on the observed strong motion array data, in particular the SMART-1 array, a theoretical model is developed to estimate the ground strains and differential movements. With the use of conversion factors by which structural strains are derived from ground strains, methods for assessing the potential damage and safety of a lifeline system under strong ground shaking during an earthquake are studied.

A cross-spectrum model for surface waves is developed based on the SMART-1 data. Numerical evaluation of parameters shows the attenuation is less important than the loss of coherence as waves propagate from the source to the site. The dynamic response (deterministic as well as stochastic) of structures subject to spatial seismic waves is also studied. The contribution of both in-phase and out-of-phase input motions to the response of an extended structure (such as a lifeline) is calculated. The sensitivity of lifeline longitudinal response to change in epicenter direction was also examined. The root-mean-square response is evaluated for the purpose of reliability assessment.

17. Document Analysis a. Descriptors
Earthquake
Seismograph Array
Lifeline
Correlation
Ground Motions

b. Identifiers/Open-Ended Terms

c. COSATI Field/Group

18. Availability Statement	19. Security Class (This Report) UNCLASSIFIED	21. No. of Pages 108
	20. Security Class (This Page) UNCLASSIFIED	22. Price

ACKNOWLEDGMENTS

This report is based on a study by Dr. C. H. Loh of the National Central University, Taiwan during his tenure as Visiting Scholar in 1982 at the University of Illinois at Urbana-Champaign. The study is part of the research program on seismic hazard and structural damage prediction supported by the Division of Civil and Environmental Engineering of the National Science Foundation under Grants CEE 80-02584 and CEE 82-13729.

TABLE OF CONTENTS

CHAPTER 1

INTRODUCTION

Structures with long dimensions (pipes, bridges, dams, tunnels) located at or near the ground surface may be damaged by large strains and differential movements caused by body and surface waves during earthquakes (Kubo, et al., 1979). Theoretical modeling is needed to estimate the amplitude of strains and differential movements which can be expected for given ground conditions and earthquake source parameters. This model may be obtained realistically by using data from dense instrument arrays (e.g., the SMART-1). The ground strain and differential movement are the most important factors in the analysis of lifeline earthquake engineering. Most risk analysis of lifeline systems (e.g., Der-Kiureghian and Ang, 1977) are based on the criterion that the ground strain exceeds a specified limiting value. Although this type of failure is important in causing possible local damage, the failure at the joint of a lifeline due to relative ground motions has been seldom investigated; such failure may be equally important. The incoherent (out-of-phase) motion sometimes may cause the failure of the system prior to the local strain failure. This report will discuss these two failure modes in the analysis of lifelines. To study the incoherent motion, the SMART-1 array data is used.

1.1 General Description of SMART-1 Array

The SMART-1 (Strong Motion Array in Taiwan) is located at Lotung in the northeast corner of Taiwan. It consists of a center element C00 and other instruments arranged on three concentric circles (inner I, middle M, and outer O), each with 12 strong-motion seismographs having a common time base and with radii of 200 meters, 1 km, and 2 km, respectively, see Fig. 1.1. This specially designed array provides information about the spatial variation of surface ground motions that

is useful for the study of the seismic response of large structures (Loh, et al., 1982).

1.2 Objectives and Scope of Present Study

The purpose of this study is to investigate the effect of time and spatial variation of surface ground motion on the response of lifeline systems, such as buried pipeline, bridges and large structural systems. Deterministic model is first developed to study the variation of ground strain and differential movement between two points. A cross-spectrum model for surface waves is then developed based on the SMART-1 data, and the influence of spatial variations on the response of lifelines is investigated. The seismic safety of a lifeline system based on the potential damage from a strong ground shaking during an earthquake is also examined.

Chapter 2 presents an analytical method to identify the wave directions, wave types, and wave velocities. The phase difference between two stations can be calculated based on the identified wave velocity, which is important for the mathematical modeling of the cross-spectral density function between two points. Chapter 3 uses the SMART-1 data to calculate the ground strain and differential movement, and also to develop a methematical model to calculate ground strain and relative displacement. A quasi-static solution of the soil-pipeline interaction, when subject to longitudinal and transverse seismic waves propagating along the lifeline axis, is formulated in Chapter 4, whereas, Chapter 5 presents a dynamic analysis of the interaction problem. Both deterministic and non-deterministic cases are studied. Chapter 6 discusses the sensitivity of lifeline longitudinal response to earthquakes with changing epicenter direction. Chapter 7 outlines a procedure for the reliability of lifelines.

Much of the uncertainty in the reliability analysis of lifeline systems is associated with the wave attenuation (Der-Kiureghian and Ang, 1977; Moghtaderizadeh, et al., 1982; and Taleb-Agha, 1977). This

is especially true when the lifeline system covers a large area and the wave attenuation is important. For a small area, the coherence of waves may be more important than the attenuation of waves. The study includes the response of lifeline systems subjected to waves that may not be completely coherent.

CHAPTER 2

IDENTIFICATION OF WAVES

2.1 Identification of Wave Types and Directions

Different kinds of waves exist in a strong-motion acceleration record. Each kind of wave has different wave velocity and propagate in different directions. An effective analytical method is available (Loh and Penzien, 1984) for identifying the dominant wave types, directions and velocity using data of strong earthquake ground accelerations.

For a stationary random process, the power spectral density function of a ground acceleration in any direction can be represented as a combination of the motions in the two original orthogonal directions,

$$\tilde{x}_i(t) = x_i(t)\cos\phi + y_i(t)\sin\phi$$

as shown in Fig. 2.1. The power spectral density function of $\tilde{x}_i(t)$ is represented as

$$S_{\tilde{x}_i\tilde{x}_i}(\omega) = S_{x_ix_i}(\omega)\cos^2\phi + S_{y_iy_i}(\omega)\sin^2\phi + 2\mathrm{Re}[S_{x_iy_i}(\omega)]\cos\phi\sin\phi \qquad (2.1)$$

where $S_{\tilde{x}_i\tilde{x}_i}(\omega)$ is the auto-spectral density of $\tilde{x}_i(t)$ and $\mathrm{Re}[S_{x_iy_i}(\omega)]$ is the real part of the cross-spectral density of $S_{x_iy_i}(\omega)$. The direction of maximum power spectral density at each frequency can be obtained by maximizing Eq. 2.1, and the dominant direction ϕ_o is

defined as the value of ϕ that maximizes $S_{\tilde{x}_i \tilde{x}_i}(\omega)$; i.e., $\partial S_{\tilde{x}_i \tilde{x}_i}(\omega)/\partial\phi = 0$. Then,

$$\phi_o(\omega) = 1/2 \arctan \frac{2\mathrm{Re}[S_{x_i y_i}(\omega)]}{S_{x_i x_i}(\omega) - S_{y_i y_i}(\omega)} \tag{2.2}$$

where $\phi_o(\omega)$ is the principal direction and the spectrum associated with this direction is called the major power spectrum; $\phi_o(\omega) + \pi/2$ is the minor direction which is orthogonal to the principal direction. The corresponding spectrum is called the minor power spectrum. $R(\omega)$ is defined as the ratio of the major power spectral density to the minor power spectral density; namely,

$$R(\omega) = \frac{S_{\tilde{y}_i \tilde{y}_i}(\omega)}{S_{\tilde{x}_i \tilde{x}_i}(\omega)} \tag{2.3}$$

where $0 < R(\omega) < 1$ in all frequency bands. When $R(\omega) = 1$, there is no principal direction, whereas when $R(\omega) \ll 1$, a principal direction exists and the particle motion almost follows a simple harmonic motion in that direction.

From the SMART-1 array data, especially that of the January 29, 1981 earthquake, the principal direction is close to the epicenter direction. Figure 2.2 is a plot of the ratio of $R(\omega)$ with different moving time windows. For a detailed analysis of the array data, see Appendix. From $R(\omega)$ and $\phi(\omega)$, the wave type may be identified. For example, from Fig. 2.2, at frequencies 1.17 Hz and 2.85 Hz, there is a low value of R. One is caused by surface waves and the other is caused by shear waves. Once the wave type and wave direction have been identified, the delay time for the maximum cross correlation between

each station pair can be calculated, from which the wave velocity at this specific frequency can be estimated.

2.2 Identification of Wave Velocity

In the previous section, the wave velocity is identified at a frequency band for small values of $R(\omega)$. This is because at that specific frequency band, the wave can be regarded as a simple harmonic wave propagating along a certain direction. For other frequencies (large values of $R(\omega)$), the method cannot be applied.

In this section, a simple method is discussed to identify the wave number and wave velocity at frequency bands where no definite wave direction exists (Iyer and Hlaby, 1972).

First, consider the omni-directional wave train of frequency f,

$$x(t) = A(f)\exp[2\pi i(ft + \alpha(f))] \tag{2.4}$$

where $x(t)$ is the horizontal ground motion and $\alpha(f)$ is the phase at frequency f. Take the Fourier transform

$$R(f) = A(f)[\cos 2\pi\alpha(f) - i \sin 2\pi\alpha(f)] \tag{2.5}$$

where $A(f)$ is the amplitude of the wave train at frequency f. Assume $x(t)$ and $y(t)$ to be the waves recorded at two points in the array. The cross-spectral density C_r^{xy} between x and y is represented as

$$C_r^{xy} = A_r^2 [\cos 2\pi(\alpha_r - \beta_r) - i \sin 2\pi(\alpha_r - \beta_r)] = P_r^{xy} - iQ_r^{xy} \tag{2.6}$$

where P_r^{xy} and Q_r^{xy} are the real (co-spectrum) and imaginary parts (quadra-spectrum), respectively, of the cross-spectral density at frequency r. $\alpha_r - \beta_r$ is the phase difference between two stations.

Consider the propagation of waves across an array as shown in Fig. 2.3. The phase difference at some specific frequency between two instruments along the wave direction is

$$\phi_{ij} = KD\cos\theta \tag{2.7}$$

where K is the wave number, and D is the separation between stations i and j. Then the co-spectrum P_r^{xy} can be represented in the form

$$P_r^{xy} = A_r^2\cos[2\pi\phi_{ij}] = A_r^2\cos[2\pi KD\cos\theta] \tag{2.8}$$

This equation can be expanded in Bessel function (Iyer and Hlaby, 1972)

$$P_r^{xy} = A_r^2[J_0(K) - 2J_2(K)\cos2\theta_i + 2J_4(K)\cos4\theta_i - \ldots] \tag{2.9}$$

where $K = 2\pi KD$, and D is the separation.

Now assume the waves arriving at the two stations from several directions but with the same wave number K at every frequency. The wave direction θ_i may vary from 0 to 2π. Since there is no definite propagation direction, θ_i can be assumed to take discrete values, e.g., $\theta_i = 0^o, 30^o, 60^o, 90^o, \text{-------} 330^o$. Substitute all these different values of θ_i in Eq. 2.9 and take the summation (because waves are coming from all directions). After cancelling the J_2 and J_4 terms,

$$\sum_{i=1}^{12} P_i^{xy} = \sum_{i=1}^{12} A_i^2 [J_o(2\pi KD) - J_6(2\pi KD)\cos 6\theta_i + \ldots] \tag{2.10}$$

If the higher order Bessel functions can be neglected, Eq. 2.10 becomes

$$\sum_{i=1}^{12} P_i^{xy} = \sum_{i=1}^{12} A_i^2 J_o(2\pi KD) \tag{2.11}$$

then,

$$J_o(2\pi KD) = \frac{\sum_{i=1}^{12} P_i^{xy}}{\sum_{i=1}^{12} A_i^2} \tag{2.12}$$

where P_r^{xy} is the co-spectrum of two adjacent signals along $\theta = \theta_i$ and A_i^2 is the average power spectral density function of two signals. The summation is with respect to different values of θ_i.

Based on Eq. 2.12, the wave number K can be evaluated at different frequencies, from which the wave velocity can be determined from $V_c = f/K$.

Using the SMART-1 array data, the wave velocity is calculated up to 7 Hz except for the frequency range of small values of $R(\omega)$. From station pairs M06-006 and I06-I12, the wave velocity is plotted in Fig. 2.4. The results are quite similar. It is interesting to note that the wave velocity increases linearly up to 5.5 km/sec at 3.0 Hz and remains constant up to 7.0 Hz. This method is valid only when there is no dominant wave direction and for waves having the same wave number.

CHAPTER 3

ANALYSIS OF GROUND STRAIN AND DIFFERENTIAL MOVEMENT

The design of a lifeline facility to withstand an earthquake must permit the joints between its parts to accommodate relative motions as well as permit the links between two joints to sustain the local strains induced by the ground motions. Both the local ground strain and differential movement between two stations induced by earthquakes are important factors in the consideration of safety of lifelines.

3.1 Formulation of Ground Strain

The maximum strain in a pipeline may not necessarily occur during the maximum acceleration of the ground. Following Goto, et al. (1981), the estimation of ground strain from the passage of surface waves may be estimated from the relative ground displacement between two points. Suppose a wave propagates along the x-direction from station i to station i+1. The phase difference caused by the wave propagation between two consecutive stations can be represented as

$$\exp[iK(x + D/2)] - \exp[iK(x - D/2)]$$

where K is the wave number (frequency dependent), and D is the separation between stations i and i+1. The relative ground displacement can be written as the inverse Fourier transform of the relative ground displacement, namely

$$\Delta u(x,D,t) = \int_{-\infty}^{\infty} F(i\omega)\exp(i\omega t)[\exp(iK(x + D/2) - \exp(iK(x - D/2))]d\omega$$

$$= 2i\int_{-\infty}^{\infty} F(i\omega)\sin(\tfrac{KD}{2})\exp(iKx - i\omega t)d\omega \qquad (3.1)$$

where $F(i\omega)$ is the Fourier transform of the ground displacement. The strain can be estimated as the limit,

$$\lim_{D\to 0} \frac{\Delta u(x,D,t)}{D}\Big|_{x=0} = \varepsilon(t) \tag{3.2}$$

Then

$$\varepsilon(t) = \int_{-\infty}^{\infty} F(i\omega) \cdot iK \cdot \exp(i\omega t)d\omega \tag{3.3}$$

In Eq. 3.3, it is important to note that the wave number $K = \omega/V$ is a function of the frequency identified in the previous chapter. If there is only a single dominant wave that exists in a certain frequency band, Eq. 3.3, applies in that frequency band and the wave number K can be taken as a constant. From the analysis of the SMART-1 data, Tables 3.1 and 3.2 show the maximum strain, maximum velocity, and maximum displacement along stations 006 to 012. The maximum ground strain is proportional to the maximum amplitude of the ground velocity and the time to maximum value is almost the same. The suggested estimation of the free-field ground strain can be expressed in the following form (Shinozuka, et al., 1981),

$$\varepsilon_{max} = V_{max}/C(\omega_o) \tag{3.4}$$

where V_{max} is the maximum ground velocity and C is the ground wave velocity at frequency ω_o, which is the predominant frequency of the ground acceleration. From the SMART-1 data, it is found that Eq. 3.4 gives good estimation of the maximum ground strain. Under the assumption that the ground shaking is dominated by surface waves

propagating along the epicentral direction, the wave velocity $C(\omega_o)$ can be estimated as indicated in Chapter 2.

To study the ground strain along the axis of a pipeline, two types of waves are important. From Fig. 3.1a, assume the surface wave as a harmonic wave that propagates in a direction with an angle θ from the x-direction (pipeline axis). The axial particle wave velocity along the x-direction is $V = \dot{u}_g \cos\theta$, where $\dot{u}_g$ is the ground velocity, and the wave velocity is $C = V_{rc}/\cos\theta$. Then the ground strain is represented by,

$$\varepsilon_a = V/C = \dot{u}_g/V_{rc} \cdot \cos^2\theta \tag{3.5a}$$

From Fig. 3.1b, it is clear that the shear wave can also propagate along the same direction as the Rayleigh surface wave. The axial particle wave velocity due to the S-wave is $V = \dot{u}_g \cos\theta$. The ground strain due to the S-wave is, therefore,

$$\varepsilon_a = V/C = \dot{u}_g/V_{sc} \cdot \sin\theta\cos\theta \tag{3.5b}$$

Equations 3.5a and 3.5b show the contribution of surface waves and shear waves to the ground strain along the x-direction.

3.2 Formulation of Relative Ground Displacement

From the SMART-1 data of January 29, 1981 earthquake, Figs. 3.2 and 3.3 show the relative displacement between two stations as a function of separation. It is reasonable to assume that the relative displacement increases with the separation distance. It is also clear that the relative ground displacement is sensitive to the phase difference as the wave propagates through the soil along the lifeline

axis (Christian, 1976). The relative ground displacement may be expressed as

$$R = \begin{cases} V_{max}(\omega_o) \cdot \frac{D}{V_c} & , \quad D \leq \lambda/2 \\ |d_{max} - d_{min}| & , \quad D > \lambda/2 \end{cases} \tag{3.6}$$

where R is the relative displacement; $V_{max}(\omega_o)$ is the maximum ground velocity at the predominant ground frequency ω_o; V_c is the wave velocity, and D is the separation. d_{max} and d_{min} represent the maximum and minimum ground displacement. When the separation D between the stations is greater than half the wave length $\lambda = V_c/f$, R is almost equal to the absolute value of the difference between the maximum and minimum values of the site displacement (this value is about 1.5 times the maximum ground displacement).

Both ground strain and relative ground displacement are important for the analysis of pipeline response and performance during earthquakes.

CHAPTER 4

SOIL-BURIED PIPELINE INTERACTION (QUASI-STATIC SOLUTION)

The shaking of a pipeline caused by an earthquake has been studied by several investigators (Kameda and Shinozuka, 1982; Hindy and Novak, 1979, 1980). Using the SMART-1 data, the quasi-static solution of the interaction between a buried pipeline and the surrounding soil is examined, for buried pipelines in both the lateral and longitudinal directions.

4.1 Axial Response to Longitudinal Traveling Waves

The model of a pipeline is shown in Fig. 4.1. The axial response of the pipeline is investigated by assuming that the ground displacement, $u_g(z,t)$, is in the direction of the pipeline axis. The equation of motion of the pipeline is

$$\mu \frac{\partial^2 u_s(z,t)}{\partial t^2} + K_z u_s(z,t) - EA \frac{\partial^2 u_s(z,t)}{\partial z^2} = K_z u_g(z,t) \tag{4.1}$$

where μ is the mass of the pipe per unit length, G is the shear modulus, and K_z is the dynamic soil property. The quasi-static solution for the axial response can be obtained by assuming the ground acceleration as

$$\ddot{u}_g(z,t) = a \exp[i(\omega t - \frac{2\pi}{\lambda} z)] \tag{4.2}$$

The ground displacement can, therefore, be evaluated through double integration of Eq. 4.2; yielding

$$u_g(z,t) = -\frac{a}{\omega^2}\exp[i(\omega t - \frac{2\pi}{\lambda} z)] \tag{4.3}$$

Now assume that the pipeline displacement is

$$u_s(z,t) = \tilde{A}\exp[i(\omega t - \frac{2\pi}{\lambda} z)] \tag{4.4}$$

Using Eqs. 4.2 and 4.4 in Eq. 4.1, the quasi-static solution for the amplification $\tilde{A}$ (neglecting the dynamic term) is

$$\tilde{A} = \frac{-aD_L(\alpha,T)}{(\frac{2\pi}{\lambda})^2 V^2} \quad , \quad D_L = \frac{1}{1 + (\frac{\alpha}{T})^2} \tag{4.5}$$

in which $\alpha = 2\pi\sqrt{AE/K}/V$, is called the "rigidity ratio period" (Aoki and Hayashi, 1973).[z] α depends on the relative rigidity of the buried pipe and the soil. Then Eq. 4.4 becomes,

$$u_s(z,t) = \frac{-aD_L(\alpha,t)}{(\frac{2\pi}{\lambda})^2 V^2}\exp[i(\omega t - \frac{2\pi}{\lambda} z)] \tag{4.6}$$

The strain and axial load in the pipeline, therefore, are

$$\varepsilon_s(z,t) = \frac{\partial u_s}{\partial z} = i\,\frac{aD_L(\alpha,T)}{(\frac{2\pi}{T})^2}(\frac{2\pi}{\lambda})\exp[i(\omega t - \frac{2\pi}{\lambda} z)]$$

$$q(z,t) = EA\frac{\partial^2 u_s}{\partial z^2} = aD_L(\alpha,T)\exp[i(\omega t - \frac{2T}{\lambda} z)] \tag{4.7}$$

The ratio of the structural strain to the ground strain is

$$\beta = \frac{\varepsilon_s}{\varepsilon_g} = D_L(\alpha,T) = \frac{1}{1 + (\frac{\alpha}{T})^2} \tag{4.8}$$

For an arbitrary ground acceleration, Eq. 4.2 can be extended for all frequency band as,

$$\ddot{u}_g(z,t) = \sum_n a_n \exp[i(\omega_n t - \frac{2\pi}{\lambda} z)] \tag{4.9}$$

On this basis, the maximum axial pipeline strain and axial load due to longitudinal traveling waves are (Penzien),

$$S_\varepsilon(z,t) = |\sum_n i a_n \frac{T_n}{2\pi} D_L(\alpha,T_n) \exp[i(\omega_n t - \frac{2\pi}{\lambda} z)]|_{max}$$

$$S_q(z,t) = |\sum_n a_n D_L(\alpha,T_n) \exp[i(\omega_n t - \frac{2\pi}{\lambda} z)]|_{max} \tag{4.10}$$

4.2 Response to Transverse Waves

Consider a horizontal pipeline subject to ground acceleration $\ddot{w}_g(z,t)$. The differential equation of the pipe response is

$$\mu \frac{\partial^2 w_s(z,t)}{\partial t^2} + K_x w_s(z,t) + EI \frac{\partial^4 w_s(z,t)}{\partial z^4} = K_x w_g(z,t) \tag{4.11}$$

where $w_g(z,t)$ is the motion of the soil particles in the direction perpendicular to that of the pipe axis, and K_x is the dynamic soil

property in the x-direction. Assume the structural response and ground displacement to be in the form

$$w_s(z,t) = \tilde{B} \exp[i(\omega t - \frac{2\pi}{\lambda} z)]$$

$$w_g(z,t) = -\frac{a}{\omega^2} \exp[i(\omega t - \frac{2\pi}{\lambda} z)] \tag{4.12}$$

For quasi-static solution, the amplification factor $\tilde{B}$ is calculated as

$$\tilde{B} = \frac{-aD_T(\alpha,t)}{(\frac{2\pi}{\lambda})^2 V^2} \tag{4.13}$$

where

$$D_T(\alpha,T) = \frac{1}{1 + (\frac{\alpha}{T})^4} \quad , \qquad \alpha = \frac{2\pi}{V} \sqrt[4]{\frac{EI}{K_x}} \tag{4.14}$$

On the bases of Eqs. 4.12 and 4.13, the curvature $\rho(z,t)$, shear force $S(z,t)$ and lateral soil loading $P(z,t)$ can be expressed as follows:

$$\rho(z,t) = \frac{\partial^2 w_s(z,t)}{\partial z^2} = -(\frac{2\pi}{\lambda})^2 \tilde{B} \exp[i(\omega t - \frac{2\pi}{\lambda} z)]$$

$$S(z,t) = EI \frac{\partial^3 w_s(z,t)}{\partial z^3} = -i(\frac{2\pi}{\lambda})^3 EI\tilde{B} \exp[i(\omega t - \frac{2\pi}{\lambda} z)] \tag{4.15}$$

$$P(z,t) = EI \frac{\partial^4 w_s(z,t)}{\partial z^4} = EI(\frac{2\pi}{\lambda})^4 \tilde{B} \exp[i(\omega t - \frac{2\pi}{\lambda} z)]$$

For an arbitrary ground motion,

$$\ddot{w}_g(z,t) = \sum_n a_n \exp[i(\omega_n t - \frac{2\pi}{\lambda_n} z)]$$

the curvature spectrum, shear force spectrum, and lateral spectrum can be calculated as,

$$S_p(z,t) = |\sum_n a_n D_T(\alpha,T_n)\exp[i(\omega_n t - \frac{2\pi}{\lambda} z)]|_{max} = |V^2 \rho(z,t)|_{max}$$

$$S_s(z,t) = |\frac{V^3 S(z,t)}{EI}|_{max} \qquad (4.16)$$

$$S_p(z,t) = |\frac{V^4 P(z,t)}{EI}|_{max}$$

4.3 Case Study

Using the records of station C00 as the ground motion, Fig. 4.2 shows the change in the axial strain S_ε, axial load S_q, and curvature S_p for different values of α. Figure 4.3 shows the time of the maximum axial strain and axial load as the wave propagates from Station 006 to 012. The value of the axial strain and axial load produced by the January 29, 1981 earthquake are also presented. Because of the site condition, the values S_ε and S_q change irregularly.

CHAPTER 5

DYNAMIC ANALYSIS OF LIFELINES

Extended lifeline structures such as bridges, tunnels, and buried pipelines, interact with the ground at many points along the lifeline and are subject to spatially varying seismic motions at their supports. Spatially varying seismic waves have a profound impact on the response characteristics of these long extended structures. The difference in ground displacement caused by a phase delay between adjacent foundation points will be the only source of this non-coherent motion (Esteva, et al., 1980; Fong and Hu, 1982; Loh, et al., 1982; and Pazargadi, 1980). The spatial variation of seismic waves and their effects on the response of lifelines are examined.

5.1 Theoretical Modeling of Cross-Spectral Density Function

The cross-spectral density function between two stations may contain two important parts: the amplitude and the phase difference. Traveling waves may be idealized as having no change in wave forms or amplitude at a given frequency. In reality, even uniform plane waves involve scattering due to the inhomogeneity of the medium between the stations; consequently, the loss of correlation of the signals is to be expected. From Chapter 2, there is a certain kind of predominant wave at a given frequency band in each seismogram propagating in the direction of the epicenter direction. The study of correlation and cross-spectral density at this particular frequency band is important. Within this predominant frequency band, the cross-spectral density function can be assumed as

$$S_{ij}^{q}(f) = S_{o}^{q}(f)\exp\left[-\frac{|D_{ij}|}{\lambda_e}\right]\exp\left[i2\pi f\,\frac{D_{ij}}{V_c}\right] \quad , \quad f-\Delta f/2 \leq f \leq 1+\Delta f/2 \qquad (5.1)$$

where $S_o^q(f)$ is the power spectral density function common to all stations, λ_e is a constant value representing the spatial correlation of the signals, D_{ij} is the separation between Stations i and j, and V_c is the relevant wave velocity (surface wave or shear wave). Equation 5.1 is true for a given type of wave propagating in certain directions within a specific frequency band. The same equation may be extended to other frequency bands. λ_e, the wave velocity is frequency dependent.

From the SMART-1 data, Figs. 5.1 and 5.2 show the coherence $\gamma^2(f)$ versus separation. The loss of coherence for surface waves that propagate along the epicenter direction is faster than that of shear waves propagating along the same direction. This is because the surface waves propagate at or near the ground surface and the shear waves are coming directly from the soil layer beneath the array, so the site condition may have greater influence on the coherence of surface waves than that of the shear waves. More detailed analysis in the other frequency bands, is given in the Appendix. From the plot of $R(\omega)$, Fig. 2.2, we can easily separate the frequency axis into several frequency bands according to the value of $R(\omega)$. High values of $R(\omega)$ mean that no definite waves exist at that frequency that may be used as a separation point. In each frequency band, the coherence between each station pair and their phase difference can be evaluated. This makes it easy to estimate the parameter λ_e and the phase part of Eq. 5.1.

The effectiveness of using the cross-spectral density model is related to the correlation length of the ground acceleration, that is defined as

$$L_a(f_o) = \int_0^\infty \gamma_{ij}^2(f_o,r)dr \qquad (5.2)$$

where L_a is the acceleration correlation length, and $\gamma_{ij}^2(f,r)$ is the coherence between stations i and i+1, i.e., defined as

$$\gamma_{ij}^2(f) = \frac{|S_{ij}(f)|^2}{S_{ii}(f)S_{jj}(f)} \tag{5.3}$$

Substitute Eqs. 5.3 and 5.1 into Eq. 5.2; thus,

$$L_a(f_o) = \int_0^\infty \exp(-\frac{r}{\lambda_e})dr = \int_0^\infty \exp(-C\frac{f_o r}{V})dr = \frac{V}{Cf_o} \tag{5.4}$$

where V is the wave velocity, and f_o is the dominant frequency. The relation between C and the correlation length L_a of the seismic ground acceleration is shown in Fig. 5.3. From the SMART-1 data, at the predominant frequency of f = 1.17 Hz (surface wave), the correlation length is about 2.8 km (C = 0.83). This means that the seismic waves for this particular earthquake have a high correlation even though the separation between stations is 2.8 km apart. The cross-spectrum model established from stations located within this correlation length is more meaningful.

5.2 Equation of Motion and Response Spectrum Analysis

Following Nelson and Weidlinger (1979), consider a segment of a long pipeline as shown in Fig. 5.4, where L is the finite difference interval and K_p is the axial stiffness of the element. The equation of motion of this typical i-th link is given by

$$m\ddot{X}_i + C_g\dot{X}_i - C_p(\dot{X}_{i-1} - 2\dot{X}_i + \dot{X}_{i+1}) + K_g X_i - K_p(X_{i-1} - 2X_i + X_{i+1}) = C_g\dot{Z}_i + K_g Z_i \tag{5.5}$$

where X_i is the absolute motion of the i-th link, and Z_i is the free-field ground displacement at the center of i-th link. If the joint between segments is soft, i.e., $K_p/K_g \to 0$ and $C_p/C_g \to 0$, Eq. 5.5 is completely uncoupled and reduced to the form,

$$\ddot{X}_i + 2\omega_g \xi_g \dot{X}_i + \omega_g^2 X_i = \omega_g^2 Z_i + 2\omega_g \xi_g \dot{Z}_i \tag{5.6}$$

where i is for structural element i. Consider two consecutive elements and set

$$\Delta X = X_{i+1} - X_i \quad , \quad \Delta Z = Z_{i+1} - Z_i \quad , \quad \Delta y = \Delta X - \Delta Z$$

Equation 5.6 then transforms to

$$\Delta\ddot{y} + 2\xi_g \omega_g \Delta\dot{y} + \omega_g^2 \Delta y = -\Delta\ddot{Z} \tag{5.7}$$

This is the equation for a SDF system with out-of-phase component of the input $\Delta\ddot{Z}$. From this, the absolute relative displacement between element i and i+1, $\Delta X = \Delta y + \Delta Z$, can be calculated. Based on Eq. 5.7, the displacement response spectrum S_D (for maximum displacement) can be evaluated as a function of the structural period T and the delay time Δt due to the incoherent input motion, i.e.,

$$S_D(\omega, \xi, \Delta t) = \text{Max}|\Delta x(t)|$$

or (5.8)

$$S_D(\omega, \xi, \ell) = \text{Max}|\Delta x(t)|$$

where ℓ is the separation. From the SMART-1 data, the response spectra due to the in-phase and out-of-phase inputs are plotted for different separations in Figs. 5.5 and 5.6. It is clear that for different separation ℓ, the response spectrum curves have different amplification. At the dominant frequency, the out-of-phase motion

displacement response spectrum S_D increases as the phase difference increases, as shown in Fig. 5.9. This is due to the phase delay of wave propagation. In the case of multiple inputs, this phase difference between inputs is an important factor to consider in the study of the response spectrum. When the separation between two stations reach half the wave length, S_D will reach a minimum value for in-phase inputs and a maximum value for out-of-phase inputs.

A simplified method is suggested for calculating the S_D. Once the wave types and wave velocity have been identified at certain frequency, the out-of-phase motion inputs can be replaced by

$$\Delta\ddot{Z} = \ddot{X}_i(t) - \ddot{X}_i(t + \tau) \tag{5.9}$$

where τ is equal to ℓ/V (V is the wave velocity). The response spectrum under the input of Eq. 5.9 is shown in Figs. 5.7 and 5.8. Because the SMART-1 data of January 29, 1981 earthquake show a concentration of energy at frequency 1.17 Hz in the epicenter direction and the wave velocity and wave type at this particular frequency have been identified, one can simulate the response spectrum using a single station data with a phase delay, as defined in Eq. 5.9, without losing much accuracy.

5.3 Random Vibration Analysis of Multiple Inputs

From Eq. 5.7, the input-output relation can be represented in the frequency domain as

$$S_{\Delta X}(\omega) = |H(\omega)|^2 S_{\Delta Z}(\omega) \tag{5.10}$$

where $|H(\omega)|^2$ is the transfer function for the absolute acceleration output. For multiple inputs, the input spectral density is represented as

$$S_{\Delta Z}(\omega) = S_{z_i}(\omega) + S_{z_{i+1}}(\omega) \pm 2\mathrm{Re}[S_{z_i z_{i+1}}(\omega)] \tag{5.11}$$

where the positive sign is for in-phase inputs and the negative sign designates out-of-phase inputs. Define the ratio $\eta(\omega)$ as

$$\eta(\omega) = \frac{\mathrm{Re}[S_{z_i z_{i+1}}(\omega)]}{S_{z_i}(\omega) + S_{z_{i+1}}(\omega)} \tag{5.12}$$

Substitute the cross-spectral density model, Eq. 5.1, in Eq. 5.12, obtaining

$$\eta(\omega) = \frac{S_0(\omega)}{S_{z_i}(\omega) + S_{z_{i+1}}(\omega)} \exp\left[-\frac{|D_{ij}|}{\lambda_e}\right] \cos\left[\omega \frac{D_{ij}}{V_c}\right] \tag{5.13}$$

The mean square response value is

$$\sigma^2_{\Delta X} = \int_{-\infty}^{\infty} |H(\omega)|^2 S_{\Delta Z}(\omega) d\omega \tag{5.14}$$

Substituting Eqs. 5.10 through 5.12 into Eq. 5.13, giving

$$\sigma^2_{\Delta X} = \int_{-\infty}^{\infty} |H(\omega)|^2 (S_{z_i}(\omega) + S_{z_{i+1}}(\omega))\ (1-2\eta(\omega)) d\omega \tag{5.15}$$

Since $S_o(\omega)$ represents the power spectral density common to stations i and j, it is reasonable to assume $S_o(\omega) = (S_{z_i}(\omega) + S_{z_{i+1}}(\omega))/2$. Then Eq. 5.14 reduces to the form

$$\sigma^2_{\Delta X} = \int_{-\infty}^{\infty} |H(\omega)|^2 (S_{z_i}(\omega) + S_{z_{i+1}}(\omega))(1 - \exp[-\frac{D}{\lambda_e}]\cos(\omega \frac{D}{V_c}))d$$

If λ_e is independent of the frequency and the phase part is also frequency-independent and concentrated at frequency ω_o, then

$$\sigma^2_{\Delta X} = (1-\exp[-\frac{D}{\lambda_e}]\cos(\omega_o \frac{D}{V_o})) \int_{-\infty}^{\infty} |H(\omega)|^2 (S_{z_i}(\omega)+S_{z_{i+1}}(\omega))d\omega \quad (5.16)$$

where ω_o is the dominant frequency of the ground motion. This is true if the dominant wave contains most of the energy in the seismogram. For mutually uncorrelated inputs, Eq. 5.15 reduces to

$$\sigma^2_{\Delta X} = \int_{-\infty}^{\infty} |H(\omega)|^2 (S_{z_i}(\omega)+S_{z_{i+1}}(\omega))d\omega \quad (5.17)$$

The importance of input correlation can be evaluated from The following equation,

$$\frac{\sigma^2_{\Delta X}(\text{input correlated})}{\sigma^2_{\Delta X}(\text{input uncorrelated})} = 1 - \exp(-\frac{D_{ij}}{\lambda_e})\cos(\omega_o \frac{D_{ij}}{V_o}) \quad (5.18)$$

From the analysis of the January 29, 1981 earthquake data, the ratio of $\eta(\omega)$ is plotted for different station pairs (different separation). For small separation, the variation of $\eta(\omega)$ with respect to frequency

is quite smooth, as shown in Fig. 5.10. It is interesting to point out that the variation of $R(\omega)$ with respect to separation at frequency $f = 1.17$ Hz is a cosine function with an exponentially decaying amplitude, as shown in Fig. 5.11. Based on Eq. 5.18, the ratio of the mean square response of correlated input to the uncorrelated input for different values of ω_o/V_c is shown in Fig. 5.12. For the case of out-of-phase inputs with low values of ω_o/V_c, this ratio increases with increasing separation.

CHAPTER 6

SENSITIVITY OF MAXIMUM RESPONSE TO EPICENTER DIRECTION

The emphasis of this investigation was to determine the significance of coupling between the longitudinal motions and transverse motions of the ground to the response of a lifeline structure. The relative displacement between two adjacent points of a lifeline was studied through the random vibration approach. The design of a lifeline system may be dictated by future earthquakes producing the maximum response for a given geological condition. This section is aimed at examining the maximum relative displacement of a lifeline along the longitudinal direction based on linear elastic analysis; in particular, the effect of the epicenter direction of an earthquake on the maximum response is investigated.

6.1 Formulation

Any ground motion can be decomposed into two motions, i.e., the motion in the epicenter direction and that normal to the epicenter direction. Suppose a lifeline structure is constructed along the x-direction making an angle ϕ with respect to the epicenter direction (x-direction), as shown in Fig. 6.1.

The ground acceleration along the x-direction is represented as

$$x(t) = \tilde{x}(t)\cos\phi - \tilde{y}(t)\sin\phi \tag{6.1}$$

in which $x(t)$ is the ground acceleration along the lifeline direction, and ϕ is the structural orientation with respect to the epicenter direction. If the duration of the strong motion part of the earthquake is much longer than the fundamental period of the ground motion, the earthquake motions may be modeled as a stationary random process (Yang,

et al., 1982). The power spectral density of the ground acceleration along the x-direction can be represented as

$$S_{xx}(\omega) = S_{\tilde{x}\tilde{x}}(\omega)\cos^2\phi + S_{\tilde{y}\tilde{y}}(\omega)\sin^2\phi - 2\mathrm{Re}[S_{\tilde{x}\tilde{y}}(\omega)]\cos\phi\sin\phi \qquad (6.2)$$

where x is along the epicenter direction, and y is normal to the x-direction, and $\mathrm{Re}[S_{\tilde{x}\tilde{y}}(\omega)]$ is the real part of the cross-spectral density between the $\tilde{x}$ and $\tilde{y}$ motions. $S_{\tilde{x}\tilde{x}}(\omega)$ and $S_{\tilde{y}\tilde{y}}(\omega)$ are the respective power spectral density functions along and normal to the epicenter direction.

As mentioned in the previous chapter, different kinds of waves may exist in either of the two directions. This is especially true near the source and for shallow earthquakes. The frequency contents of the motions in both directions may be also independent (for example, the motions in the epicenter direction contain high energy of surface waves, whereas the motions in the normal direction may be largely shear waves).

Let the ground motions in the x- and y-directions be stationary processes that are characterized by the spectral densities $S_{\tilde{x}\tilde{x}}(\omega)$ and $S_{\tilde{y}\tilde{y}}(\omega)$, and cross-spectral density $S_{\tilde{x}\tilde{y}}(\omega)$. The spectral densities of the ground accelerations may be assumed to be of the following forms:

$$S_{\tilde{x}\tilde{x}}(\omega) = S_{ox}\,\frac{1 + 4\xi_1^2(\frac{\omega}{\omega_1})^2}{[1 - (\frac{\omega}{\omega_1})^2]^2 + 4\xi_1^2(\frac{\omega}{\omega_1})^2}\,\frac{(\frac{\omega}{\omega_2})^2}{[1 - (\frac{\omega}{\omega_2})^2] + 4\xi_2^2(\frac{\omega}{\omega_2})^2}$$

$$S_{\tilde{y}\tilde{y}}(\omega) = S_{oy}\,\frac{1 + 4\xi_3^2(\frac{\omega}{\omega_3})^2}{[1 - (\frac{\omega}{\omega_3})^2]^2 + 4\xi_3^2(\frac{\omega}{\omega_3})^2}\,\frac{(\frac{\omega}{\omega_4})^2}{[1 - (\frac{\omega}{\omega_4})^2]^2 + 4\xi_4^2(\frac{\omega}{\omega_4})^2}$$

$$\mathrm{Re}[S_{\tilde{x}\tilde{y}}(\omega)] = q(\omega) \cdot \sqrt{S_{\tilde{x}\tilde{x}}(\omega)S_{\tilde{y}\tilde{y}}(\omega)} \qquad (6.3)$$

where

$$q(\omega) = \frac{\mathrm{Re}[S_{\tilde{x}\tilde{y}}(\omega)]}{\sqrt{S_{\tilde{x}\tilde{x}}(\omega) \cdot S_{\tilde{y}\tilde{y}}(\omega)}} \tag{6.4}$$

in which S_{ox} and S_{oy} are two constants, ν_1, ω_3 are characteristic frequencies, and ξ_1 and ξ_3 are characteristic damping. These constants are dependent on the local geological conditions.

Based on the finite difference model of a long lifeline, as mentioned in the previous chapter, the equation of motion of a structural element is represented as (the same as Eq. 5.7))

$$\Delta\ddot{y} + 2\xi_n \omega_n \Delta\dot{y} + \omega_n^2 \Delta y = -\Delta\ddot{Z}$$

where Δy is the relative displacement of the lifeline element. In frequency domain representation,

$$S_{\Delta x}(\omega) = |H(\omega)|^2 S_{\Delta\ddot{Z}}(\omega) \tag{6.5}$$

where $\Delta\ddot{Z}$ is the relative motion of ground acceleration between two adjacent stations along the lifeline axis (x-direction), $|H(\omega)|$ is the absolute response transfer function, and ΔX is the relative displacement response of two consecutive structural elements. The spectral density function of the input, $\Delta\ddot{Z}$, can be expressed as the auto-spectral and cross-spectral density functions of the ground motions at two adjacent elements, i.e.,

$$S_{\Delta\ddot{Z}}(\omega) = S_{\ddot{x}_i}(\omega) + S_{\ddot{x}_{i+1}}(\omega) - S_{\ddot{x}_i \ddot{x}_{i+1}}(\omega) - S_{\ddot{x}_{i+1} \ddot{x}_i}(\omega) \tag{6.6}$$

Equation 6.6 can also be expressed in terms of the power spectral density of the motion along and normal to the epicenter direction, i.e.,

$$S_{\Delta\ddot{z}}(\omega) = (S_{\ddot{x}_i}(\omega) + S_{\ddot{x}_{i+1}}(\omega) - 2\mathrm{Re}[S_{\ddot{x}_i\ddot{x}_{i+1}}(\omega)]\cos^2\phi$$

$$+ (S_{\ddot{y}_i}(\omega) + S_{\ddot{y}_{i+1}}(\omega) - 2\mathrm{Re}[S_{\ddot{y}_i\ddot{y}_{i+1}}(\omega)]\sin^2\phi$$

$$+ 2(\mathrm{Re}[S_{\ddot{x}_i\ddot{y}_{i+1}}(\omega)] + \mathrm{Re}[S_{\ddot{y}_i\ddot{x}_{i+1}}(\omega)] - \mathrm{Re}[S_{\ddot{x}_i\ddot{y}_i}(\omega)]$$

$$- \mathrm{Re}[S_{\ddot{x}_{i+1}\ddot{y}_{i+1}}(\omega)])\cos\phi\sin\phi \qquad (6.7)$$

Combining Eqs. 6.5 and 6.7, the response spectral density function can be expressed as a function of the structural orientation with respect to the epicenter direction.

The mean square structural response follows from

$$E[\Delta X^2(t)] = \int_{-\infty}^{\infty} |H(\omega)|^2 S_{\Delta\ddot{Z}}(\omega)\,d\omega$$

$$= \int_{-\infty}^{\infty} \frac{1}{\omega^2} \frac{1 + (2\xi_n \frac{\omega}{\omega_n})^2}{[1 - (\frac{\omega}{\omega_n})^2]^2 + (2\xi_n \frac{\omega}{\omega_n})^2} \cdot S_{\Delta\ddot{x}}(\omega)\,d\omega \qquad (6.8)$$

The information required to perform a response analysis are the spectral density of the ground acceleration, the frequency response function, and the angle of structural orientation with respect to the epicenter direction ϕ. This root mean square response is useful for design purposes.

If the excitation and the response are approximated as a stationary process, the extreme value of $\Delta X(t)$ over the duration T, can be expressed as

$$\Delta Y_m = (\Delta y(t))_{max} \tag{6.9}$$

The mean maximum response can be approximated by using the relation

$$E[\Delta y_m] \simeq \sigma_{\Delta y}(\sqrt{2\ell n\nu T} + 0.5772/\sqrt{2\ell n\nu T}) \tag{6.10}$$

where

$$\nu \simeq \frac{1}{2\pi} \int_{-\infty}^{\infty} \omega^2 S_{\Delta z}(\omega) d\omega / \int_{-\infty}^{\infty} S_{\Delta z}(\omega) d\omega$$

$$\sigma_{\Delta y_m} \simeq \frac{\pi}{6} \frac{1}{\sqrt{2\ell n\nu T}} \sigma_{\Delta y} \tag{6.11}$$

6.2 Transverse Response

The sensitivity of the transverse response of a lifeline to earthquake with uncertain epicenter direction is also required. From Fig. 6.1, the ground acceleration along the transverse y direction is represented as,

$$y(t) = \tilde{x}(t)\sin\phi + \tilde{y}(t)\cos\phi \tag{6.12}$$

The power spectral density of the transverse response can be written as the combination of two original horizontal ground motions

$$S_{yy}(\omega) = S_{\tilde{x}\tilde{x}}(\omega)\sin^2\phi + S_{\tilde{y}\tilde{y}}(\omega)\cos^2\phi + 2\mathrm{Re}[S_{\tilde{x}\tilde{y}}(\omega)]\sin\phi\cos\phi \qquad (6.13)$$

The auto-spectral density and cross-spectral density in Eq. 6.13, may be represented as in Eqs. 6.3 and 6.4. Then the equation of motion of the structural response is

$$\Delta\ddot{y}(t) + 2\xi_n\omega_n\Delta\dot{y}(t) + \omega_n^2\Delta y(t) = -\Delta\ddot{Z}(t)$$

and (6.14)

$$\Delta x = y_{i+1} - y_i \quad , \quad \Delta Z = Z_{i+1} - Z_i \quad , \quad \Delta y = \Delta X - \Delta z$$

The input power spectral density can be expressed as Eq. 6.7

$$\begin{aligned} S_{\Delta\ddot{x}}(\omega) = {} & (S_{\ddot{x}_i}(\omega) + S_{\ddot{x}_{i+1}}(\omega) - 2\mathrm{Re}[S_{\ddot{x}_i\ddot{x}_{i+1}}(\omega)])\sin^2\phi \\ & + (S_{\ddot{y}_i}(\omega) + S_{\ddot{y}_{i+1}}(\omega) - 2\mathrm{Re}[S_{\ddot{y}_i\ddot{y}_{i+1}}(\omega)])\cos^2\phi \\ & + 2(\mathrm{Re}[S_{\ddot{x}_i\ddot{y}_i}(\omega)] + \mathrm{Re}[S_{\ddot{x}_{i+1}\ddot{y}_{i+1}}(\omega)] - \mathrm{Re}[S_{\ddot{x}_i\ddot{y}_{i+1}}(\omega)] \\ & - \mathrm{Re}[S_{\ddot{y}_i\ddot{x}_{i+1}}(\omega)])\cos\phi\sin\phi \end{aligned} \qquad (6.15)$$

Following the same model for the auto-spectral and cross-spectral densities, the mean square response of a structural system due to changing epicenter direction may be calculated.

6.3 Example

Before calculating the mean square response of a pipeline due to uncertain epicentral direction of an earthquake, two mathematical models have to be established. One is the cross-spectral density of the spatial ground acceleration between two stations along the same direction; the other model is the cross-spectral density between two orthogonal directions at one point (i.e., along and normal to epicentral direction). From the SMART-1 data, the parameters of the first model have been discussed and estimated. The second model, based on Eq. 6.4, is given in the Appendix. The shape of q(f) does not change much from station to station according to the calculations based on the inner ring data, as shown in Fig. 6.4. Table 6.1 and 6.2 give the parameters of the power spectral densities along two orthogonal directions. Their shapes are shown in Figs. 6.3 and 6.4. The difference between these two examples is that there is a strong coupling between the power spectral densities of the motions along and normal to the epicentral direction. Figures 6.5 and 6.6 show the change of $\sigma_{\Delta X}$ with respect to the epicenter direction θ. For out-of-phase motions, when the pipeline axis coincides with the earthquake epicentral direction, the root mean square response ($\sigma_{\Delta X}$) reaches a maximum value. This is true because most of the earthquake energy is concentrated along the epicentral direction and also the natural frequency of the structural system coincides with that of the peak power spectral density of the input along the epicentral direction. As the separation between two inputs increases (i.e., D increases), for out-of-phase motion, the RMS $\sigma_{\Delta X}$ will also increase. For Example 2, the change of $\sigma_{\Delta X}$ is smoother than that in Example 1. This is due to the strong coupling between the input power spectral densities along the two directions. If the cross-spectral density between two inputs is neglected, for out-of-motion, it is conservative

as shown in Fig. 6.7. The previous discussion is to consider the effect of the out-of-phase input on the response of a pipeline along its axis. Figure 6.8 suggests a model to calculate the transverse motion between two pipeline elements. From Fig. 6.9, the variation of the RMS $\sigma_{\Delta X}$ with θ is also shown. Compare these figures with Fig. 6.6, for D = 0.4 km; the longitudinal response is much more important than the transverse response. The results for the two examples may be summarized as follows:

(1) The shape of the input power spectral density and the system natural frequency may have significant influence on the RMS response $\sigma_{\Delta X}$.

(2) The coupling of the power spectral densities of the motions along and normal to the epicenter direction has a great influence on the calculation of $\sigma_{\Delta X}$, especially at $\theta = 90^{o}$.

(3) The separation between two pipeline elements or the phase difference as a wave propagates from element i to i+1 is important to the out-of-phase response of the pipeline.

CHAPTER 7

RELIABILITY ANALYSIS OF LIFELINES

7.1 Probability of Damage of Lifeline

Consider the axial strain of a pipeline caused by earthquakes. Assume that the pipe strain can be estimated by multiplying the free field ground strain by a factor β (conversion factor) (Shinozuka, et al., 1981), i.e.,

$$\varepsilon_S = \beta \varepsilon_G \tag{7.1}$$

where ε_G is the ground strain, and ε_S is the structural strain. For a straight buried pipe, the evaluation of β was discussed in the previous chapter. To evaluate the probability of failure of a buried pipeline, the mean value ε_o and standard deviation σ_ε of the ground strain have to be evaluated. These values may be different at different stations because of varying site conditions. The correlation length of the ground motion, as defined in Chapter 5, is used. Within this length the variation of the ground strain is not large. Of course, for different earthquakes, the predominant frequency of the ground motion and wave velocity may be different, thus leading to different correlation lengths. Within a given correlation length, the mean value of the ground strain ε_o and corresponding standard deviation σ_ε can be evaluated as

$$\varepsilon_o = \sum_{i=1}^{n} \varepsilon_i / n$$

$$\sigma_\varepsilon = \sum_{i=1}^{n} (\varepsilon_i - \varepsilon_o)^2 / (n - 1) \tag{7.2}$$

where n is the number of points selected to evaluate the ground strain.

The probability of damage of pipeline per unit length may be defined as

$$P_D = P_r(\beta\varepsilon_G \geq \varepsilon_f) \tag{7.3}$$

where ε_f is the failure strain and ε_G is the earthquake-induced ground strain. If both ε_G and ε_f are normal variates with $N(\mu_{\varepsilon_G}, \sigma_{\varepsilon_G})$ and $N(\mu_{\varepsilon_f}, \sigma_{\varepsilon_f})$, then

$$P_D = 1 - \Phi\left(\frac{\mu_{\varepsilon_f} - \beta\mu_{\varepsilon_G}}{\sqrt{\sigma^2_{\varepsilon_f} + \beta^2\sigma^2_{\varepsilon_f}}}\right) \tag{7.4}$$

where $\Phi(\cdot)$ is the standard normal distribution.

From the January 29, 1981 earthquake data, the mean value of the ground strain is calculated as 0.0000463. The probability of damage of a pipeline of length L may be given as,

$$P_F = 1 - (1 - P_D)^{L/1} \tag{7.5}$$

where L/1 means the number of unit element within the pipeline length L. Figure 7.1 shows the probability of damage for different values of the failure strain ε_f.

7.2 Extreme-Value Response Distribution

From Eq. 6.9, the mean and mean square values of the maximum relative displacement are estimated. Using the Gumbel Type I distribution (Wirsching and Yao, 1971) to express the extreme-value response distribution of $\Delta\tilde{X}_m$,

$$F_{\Delta X_m}(\Delta X,T) = \exp\{-\exp[-\alpha_x - (\Delta X - \beta_x)]\} \tag{7.6}$$

where ΔX_m is the maximum relative displacement and α_x, β_x are two constants. Finding an exact distribution function of the maximum value of a random process within an arbitrary time interval is equivalent to finding the distribution function of the first passage time. For a zero-mean, narrow-band process and a high level crossing, the barrier crossing may be approximated as a Poisson process. The probability of failure of one structural component i, during a time interval (0,T), may then be expressed as (Wirsching and Yao, 1971),

$$\begin{aligned} P_{F_i} &= 1 - P_r[|\Delta X_m| < \Delta\tilde{X}] \\ &= 1 - \exp\{-2\nu_o \exp[-1/2(\frac{\Delta\tilde{X}}{\sigma_{\Delta X_m}})^2 T]\} \end{aligned} \tag{7.7}$$

where ν_o is the mean zero crossing rate, equal to

$$\nu_o = \frac{1}{2\pi}\sqrt{\frac{\lambda_2}{\lambda_o}} \quad , \quad \lambda_j = \int_0^\infty \omega^j S(\omega)d\omega \tag{7.8}$$

where $\sigma_{\Delta X_m}$ is the root mean square value of ΔX_m, which is a function of epicenter direction and can be evaluated from previous chapters.

Table 3.1 Maximum Ground Strain, Velocity and Displacement Along Epicenter Direction. (Surface wave dominant.)

January 29, 1981 Earthquake	Strain ($x10^{-5}$)*		Velocity (cm/sec)		Displacement (cm)	
	Max. Strain	Time for Max.	Max. Vel.	Time for Max.	Max. Disp.	Time for Max.
012	5.03	6.48	14.82	6.49	2.09	6.30
M12	4.49	6.22	14.74	6.23	2.06	6.03
I12	4.02	6.13	12.61	6.14	2.04	5.92
C00	4.60	6.12	13.78	6.13	1.93	5.92
I06	4.13	6.09	11.36	6.08	1.86	5.85
M06	5.04	5.80	11.12	5.79	1.98	5.55
006	5.13	5.37	10.42	5.40	1.95	5.09

*Maximum strain was calculated along calculated epicenter direction (ϕ = 77.36°), with frequency band 0.49 ~ 2.93 Hz. Wave No. = 3.13.

Table 3.2 Maximum Ground Strain, Velocity and Displacement Normal to Epicenter Direction. (Shear wave dominant.)

January 29, 1981 Earthquake	Strain ($x10^{-5}$)*		Velocity (cm/sec)		Displacement (cm)	
	Max. Strain	Time for Max.	Max. Vel.	Time for Max.	Max. Disp.	Time for Max.
012	4.55	6.48	10.01	6.46	1.92	6.33
M12	3.44	6.52	7.86	6.21	1.72	6.10
I12	4.89	6.36	7.31	6.38	1.34	7.15
C00	4.56	6.34	6.52	6.35	1.29	5.97
I06	4.32	6.26	4.95	6.29	1.42	5.94
M06	1.36	18.37	2.45	6.32	0.64	17.83
006	3.29	5.62	5.86	6.49	1.09	6.36

*Maximum strain was calculated along the normal of epicenter direction (ϕ = -34.0°), with frequency band 0.24 ~ 6.05 Hz.

Table 6.1 Parameters of Simulated Power Spectral Density in Example 1

EXAMPLE 1		S_o	1st Mode		2nd Mode	
			f_1	ξ_1	f_2	ξ_2
Epicenter Direction	Station i	790.	1.10	0.14	2.13	0.13
	Station i+1	890.	1.10	0.15	2.23	0.15
Normal to Epicenter Direction	Station i	190.	2.80	0.11	4.40	0.14
	Station i+1	140.	2.72	0.09	4.34	0.11

Table 6.2 Parameters of Simulated Power Spectral Density in Example 2

EXAMPLE 2		S_o	1st Mode		2nd Mode	
			f_1	ξ_1	f_2	ξ_2
Epicenter Direction	Station i	740.	1.11	0.14	2.20	0.14
	Station i+1	940.	1.11	0.15	2.34	0.10
Normal to Epicenter Direction	Station i	440.	1.14	0.40	2.90	0.11
	Station i+1	870.	1.14	0.45	2.94	0.10

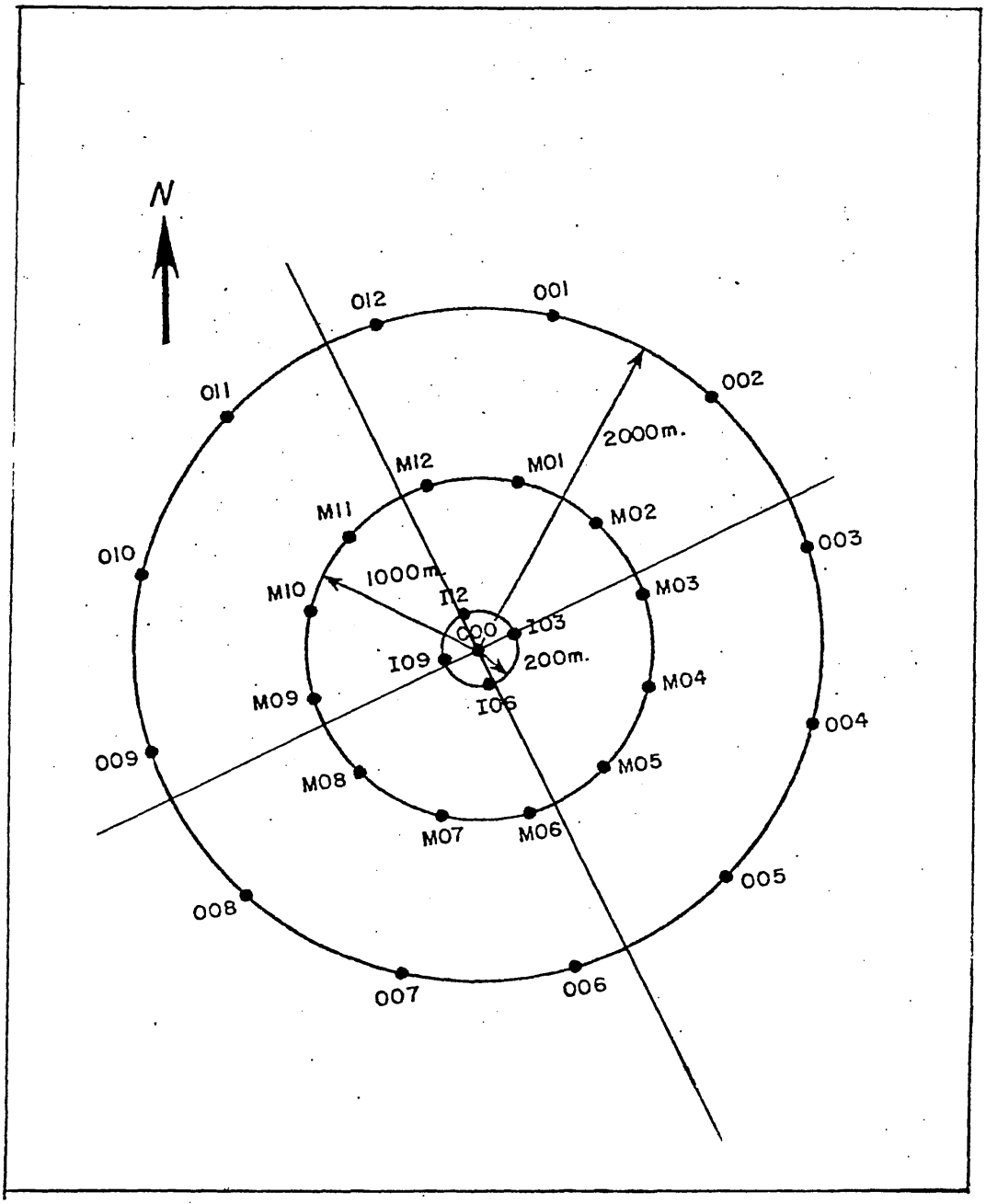

Figure 1.1 Configuration of the SMART-1 Array

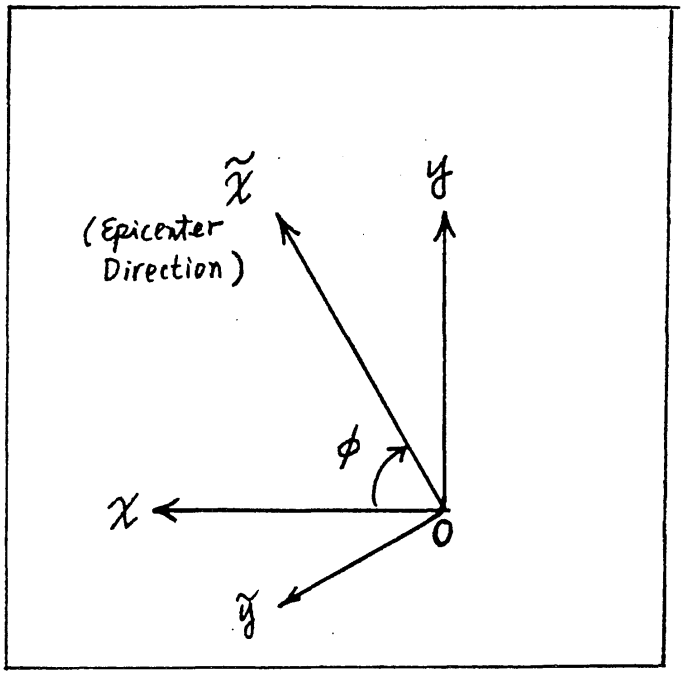

Figure 2.1 Coordinate Transformation of Two Horizontal Components

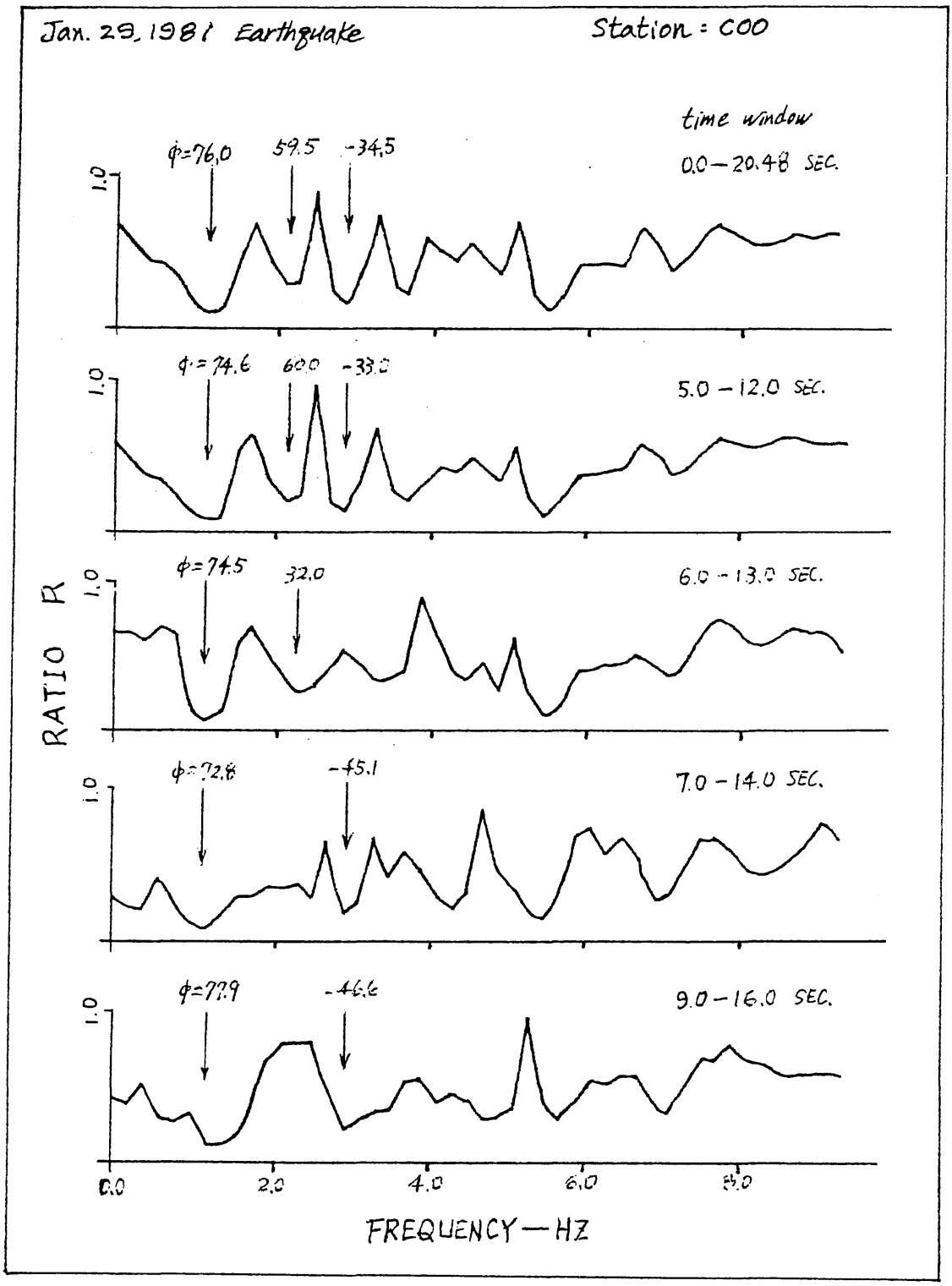

Figure 2.2 Variation of R(f) with Frequency at Different Time Window (Station = COO)

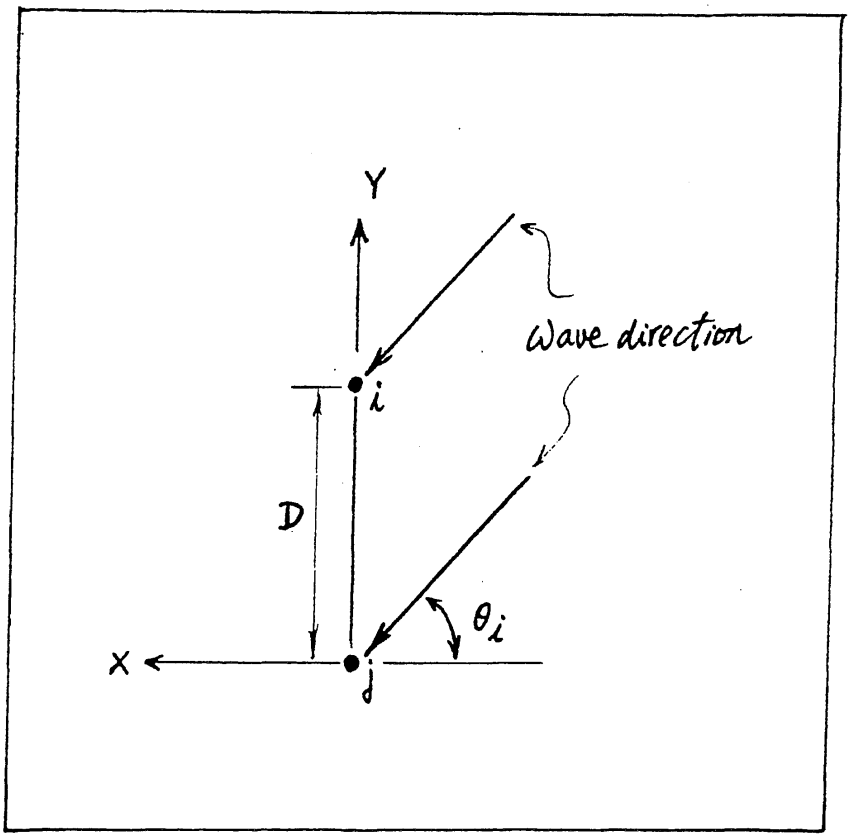

Figure 2.3 Wave Propagation in Direction θ_i

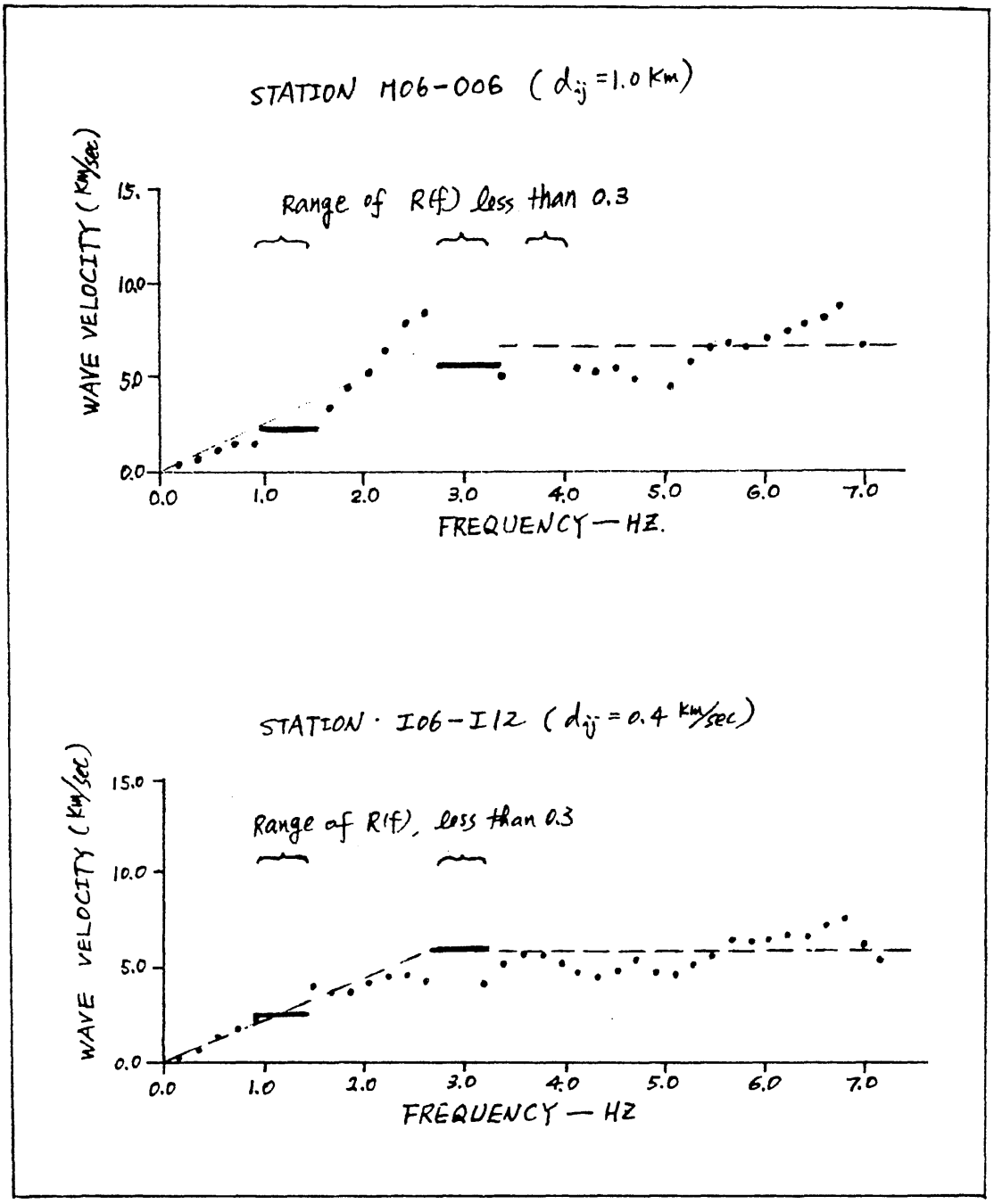

•••• Calculated value
---- Fitted one
——— By other method (which the type of waves can be identified)

Figure 2.4 Variation of Wave Velocity with Respect to Frequency (Data From M06-006 and I06-I12)

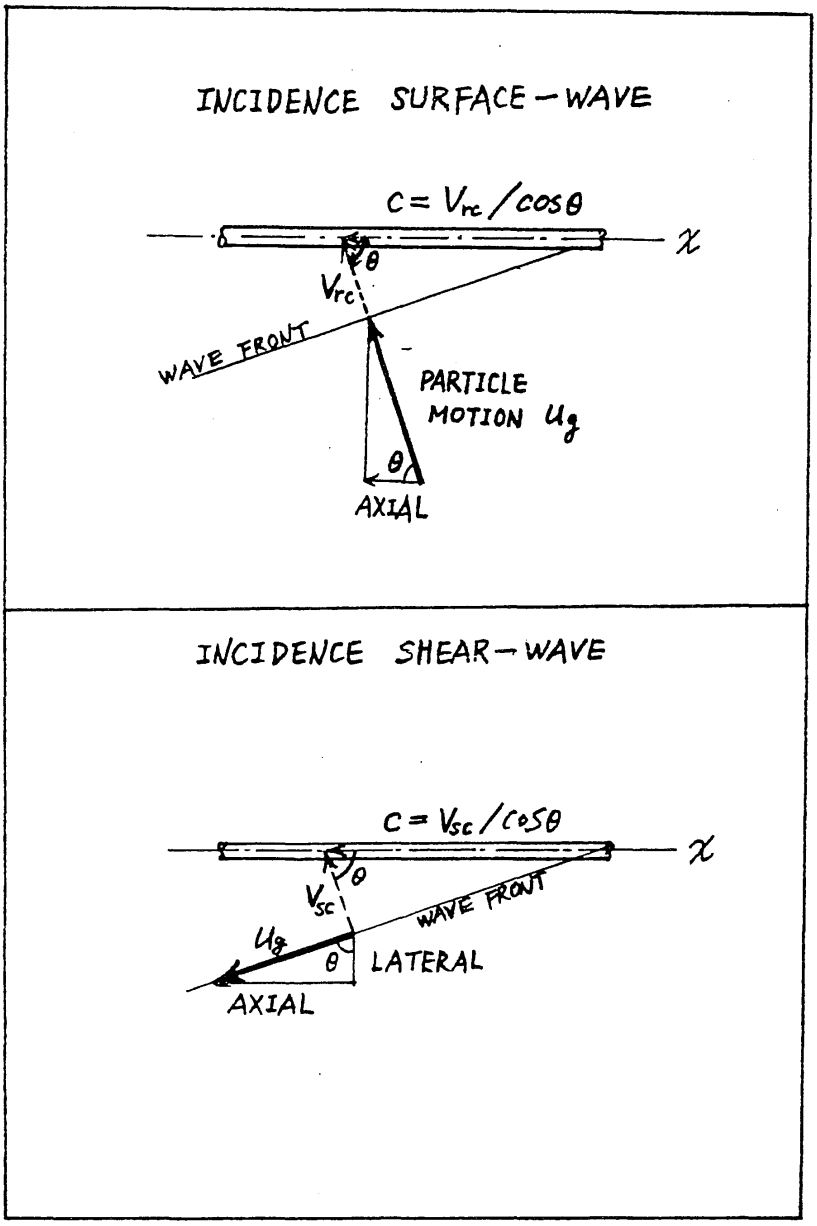

Figure 2.5 Relationship Between Particle Motion and Buried Pipeline for Incident Surface and Shear Waves

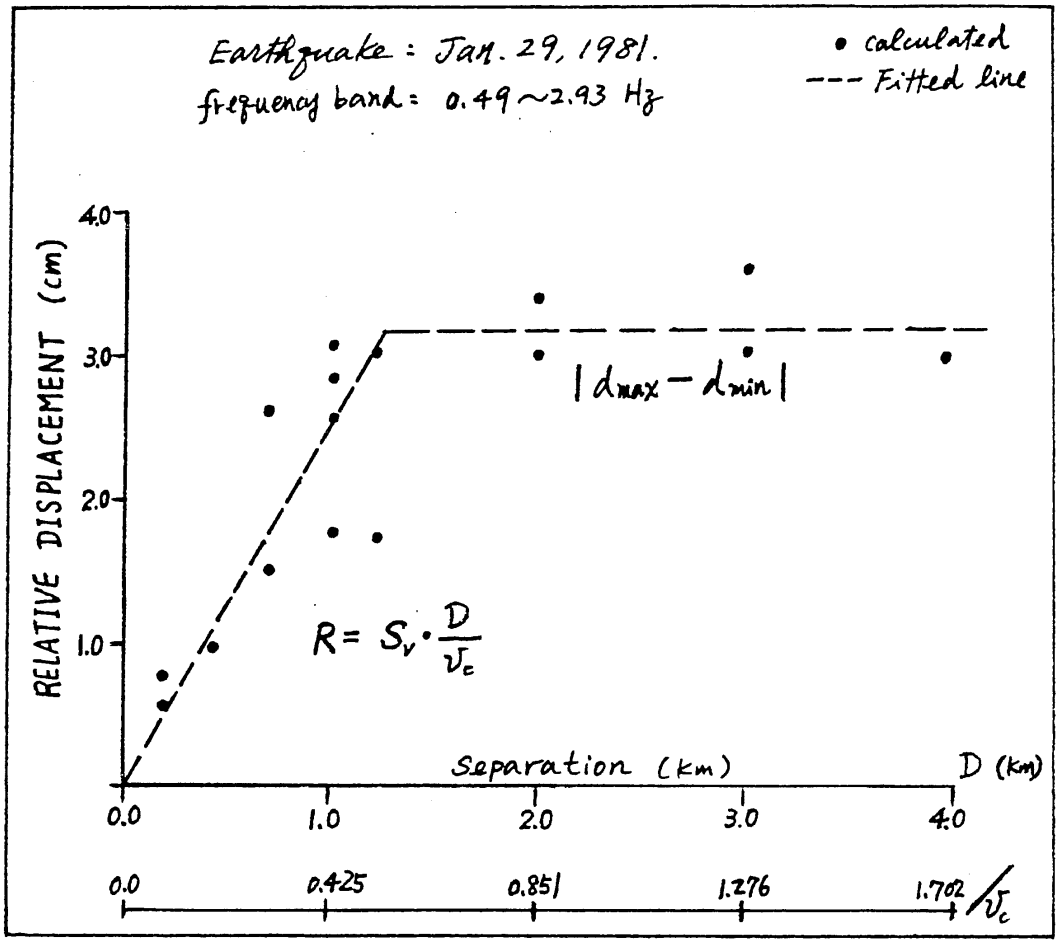

Figure 3.1 Relation Between Relative Displacement R and Separation D (Data Along Epicenter Direction)

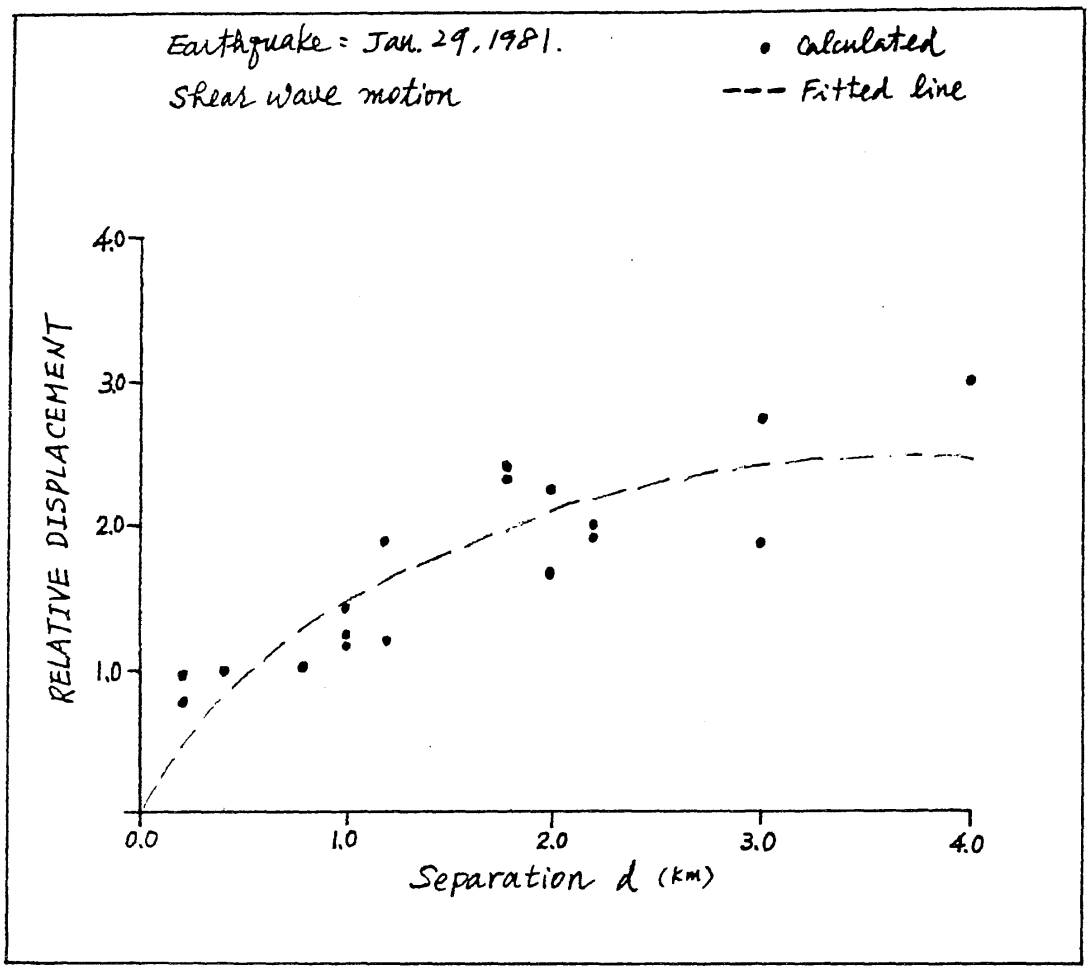

Figure 3.2 Relative Displacement Between Station Pairs Normal to Epicenter Direction

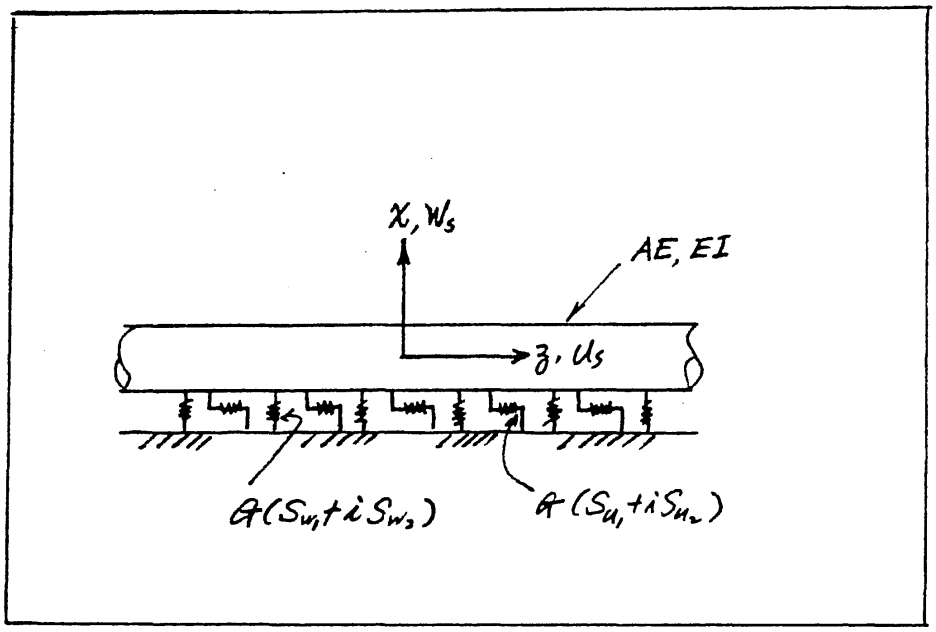

Figure 4.1 Model of Buried Pipeline

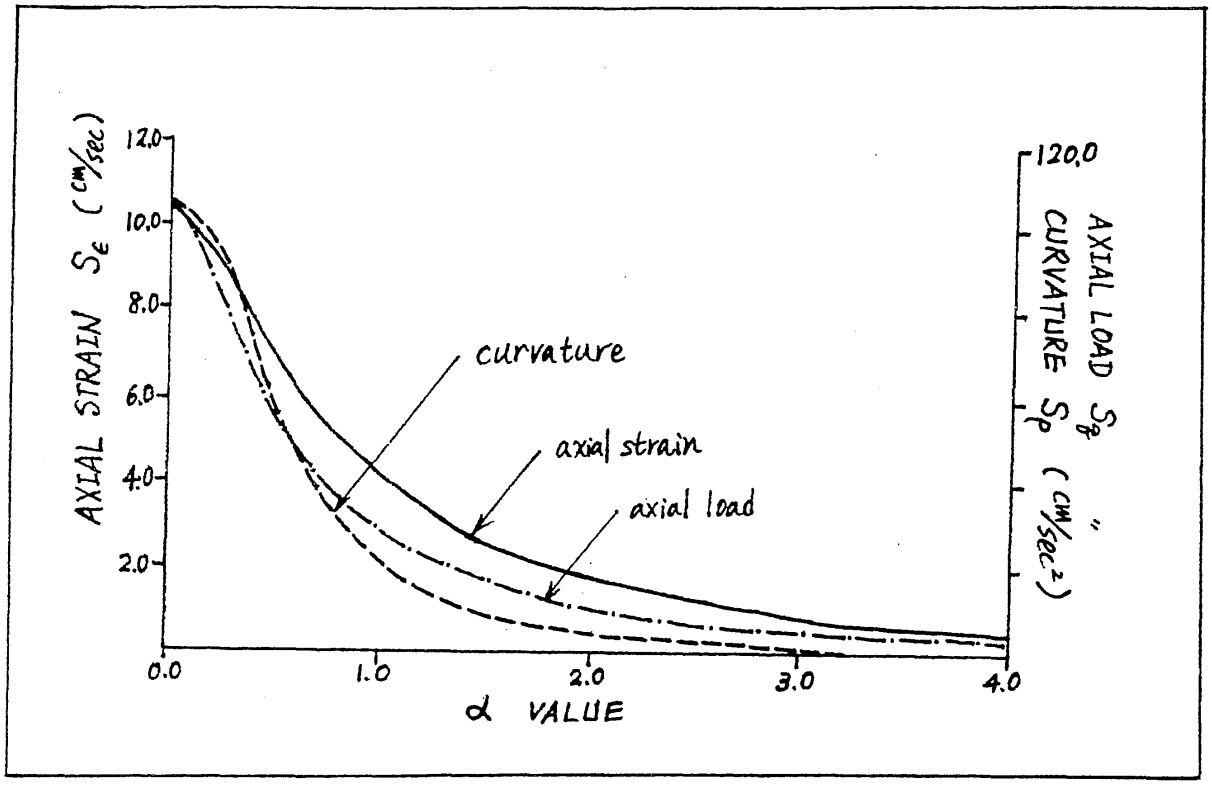

Figure 4.2 Variation of Axial Strain, Axial Load, Curvature of Buried Pipe With α

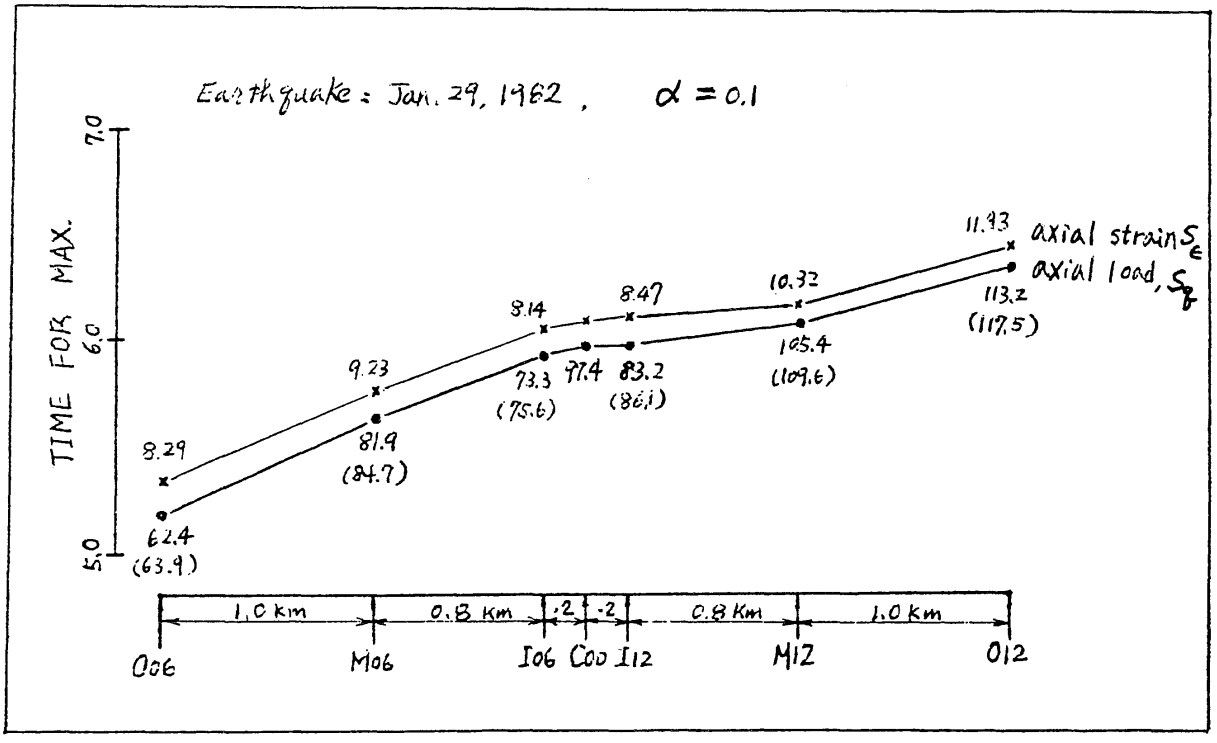

Figure 4.3 Variation of Axial Strain S_ε, Axial Load S_q and Time of Maximum as Wave Propagates Along Station 006 to 012.

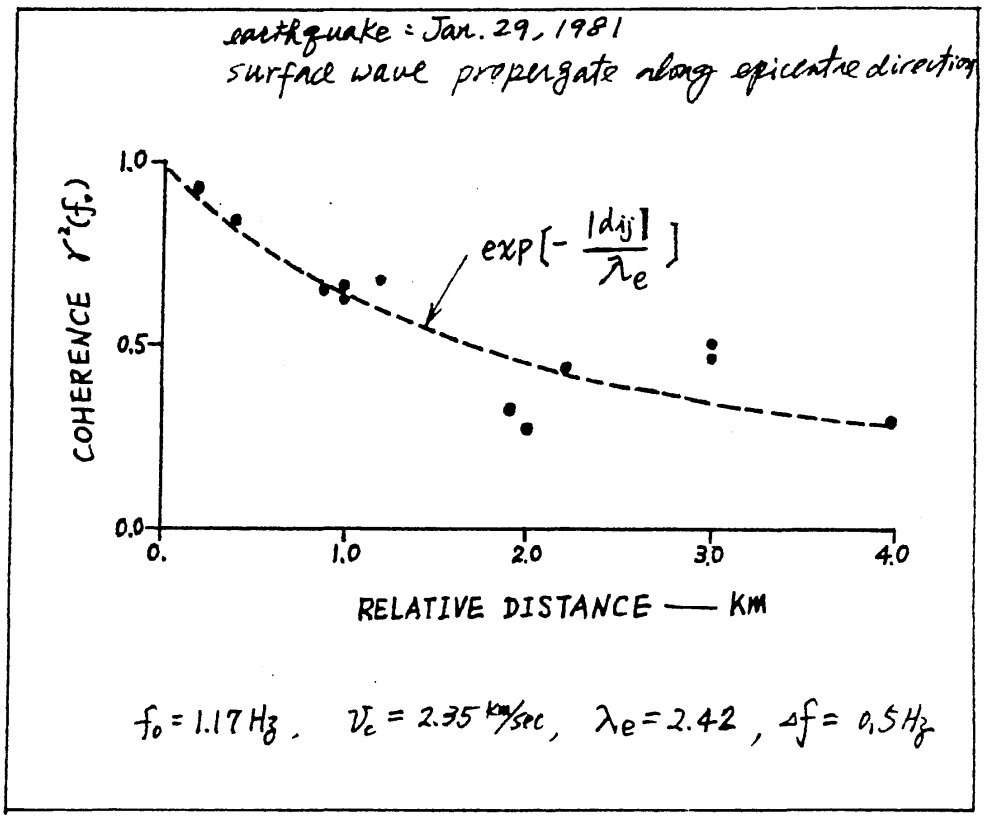

Figure 5.1 Spatial Correlation of Surface Wave Propagating Along Epicenter Direction of f = 1.17 Hz

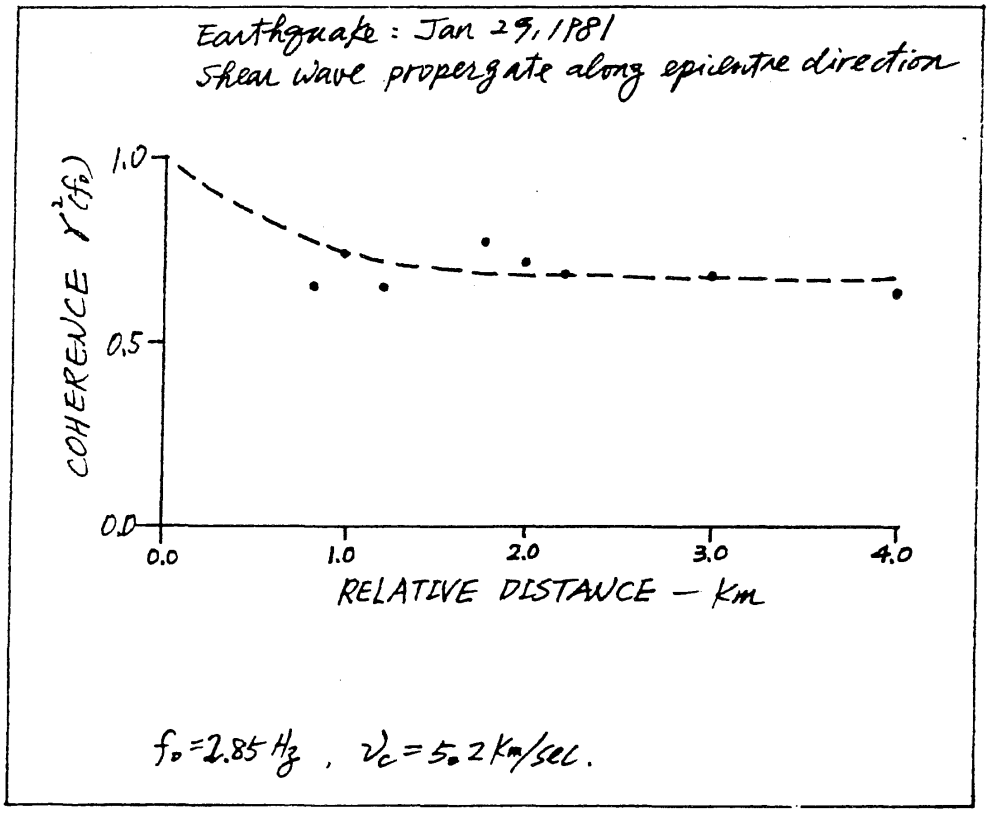

Figure 5.2 Spatial Correlation of Shear Wave Propagating Along Epicenter Direction at f = 2.85 Hz

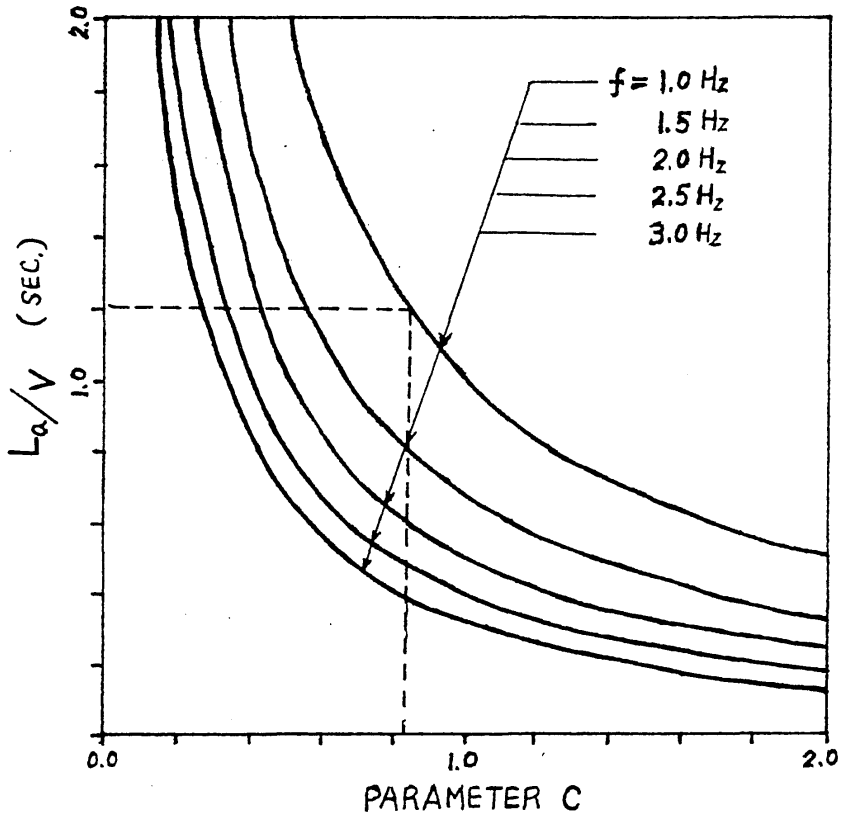

Figure 5.3 Variation of Correlation Length with Parameter C at Different Frequencies

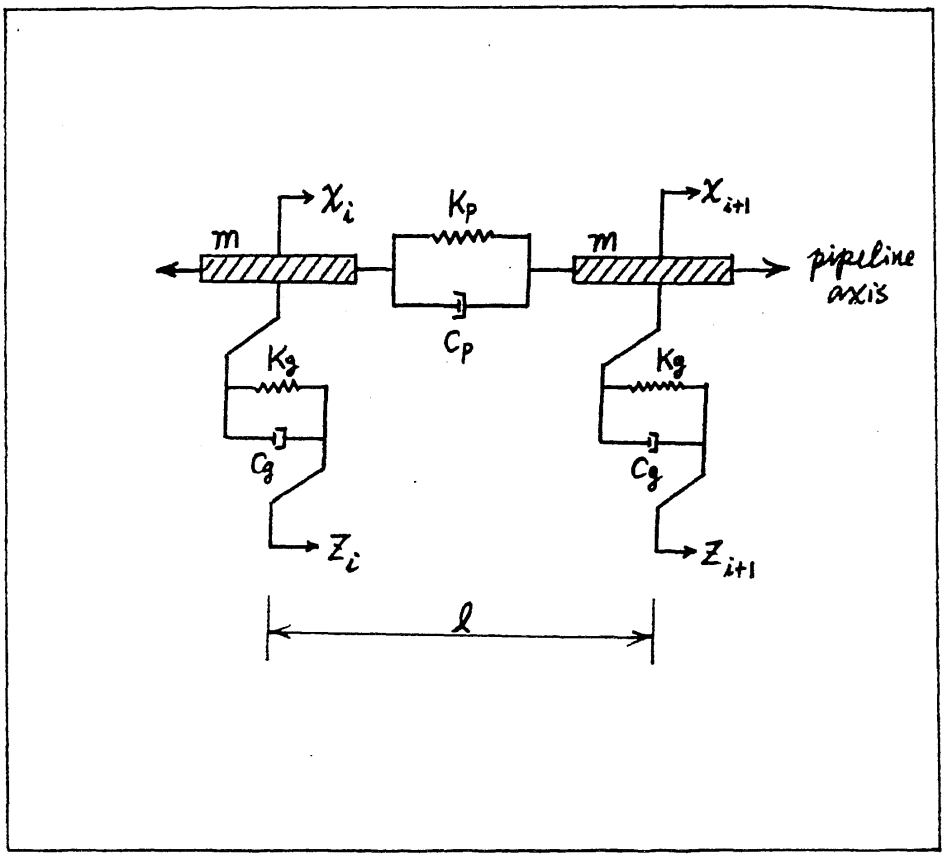

Figure 5.4 Discrete Model of Lifeline Element (Longitudinal Motion)

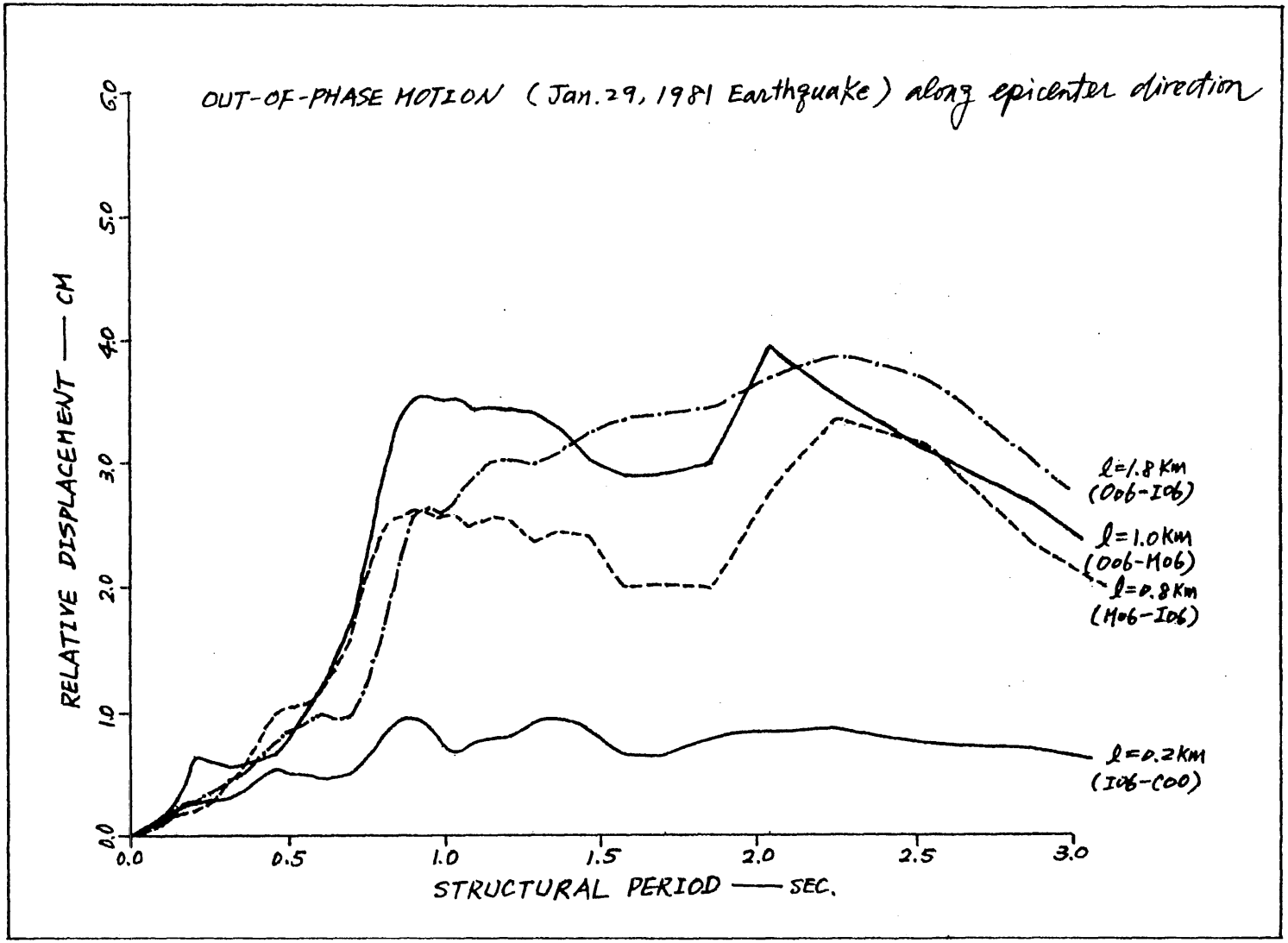

Figure 5.5 Displacement Response Spectrum for Out-of-Phase Input Motion

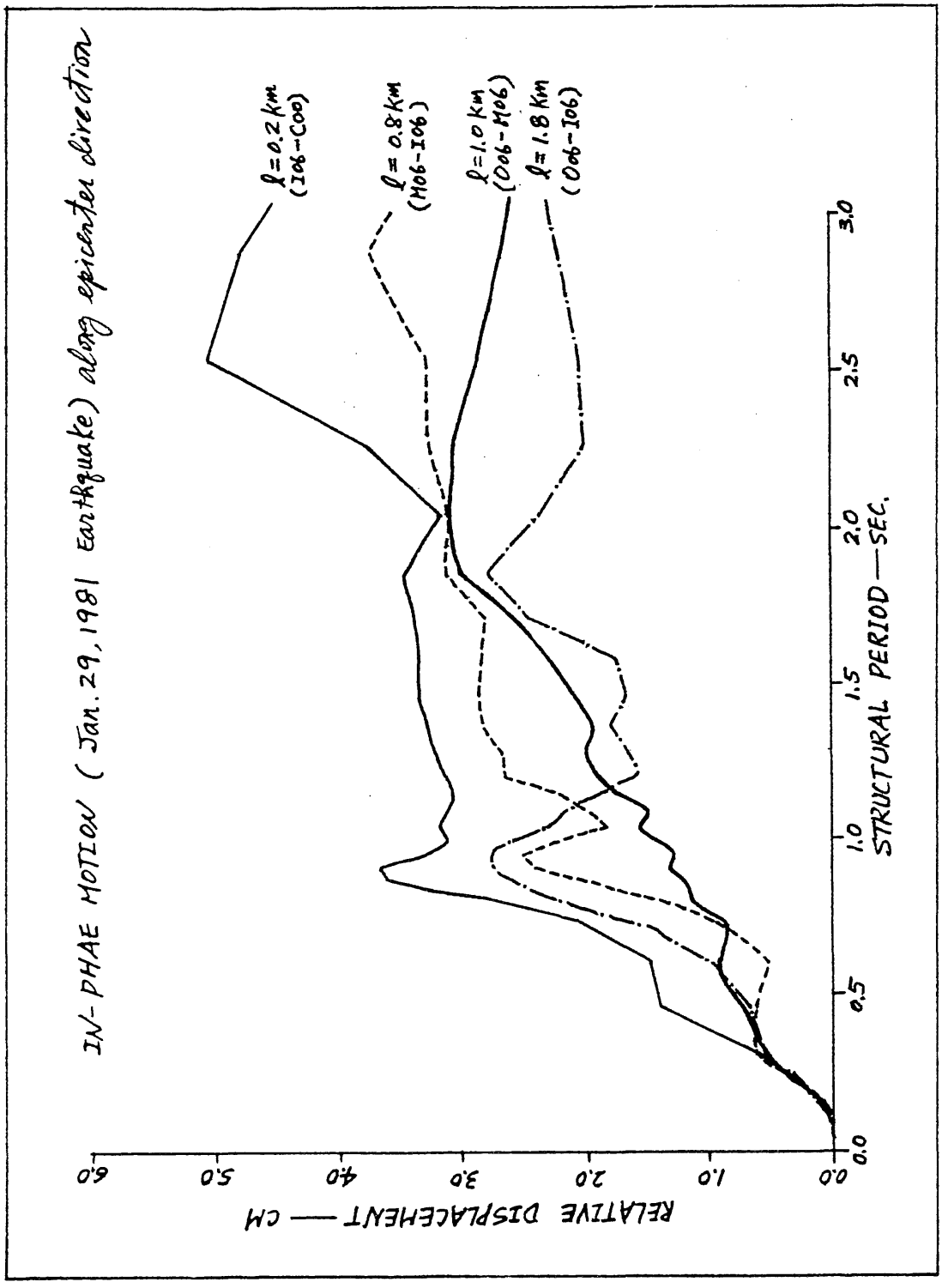

Figure 5.6 Displacement Response Spectrum for In-Phase Input Motion

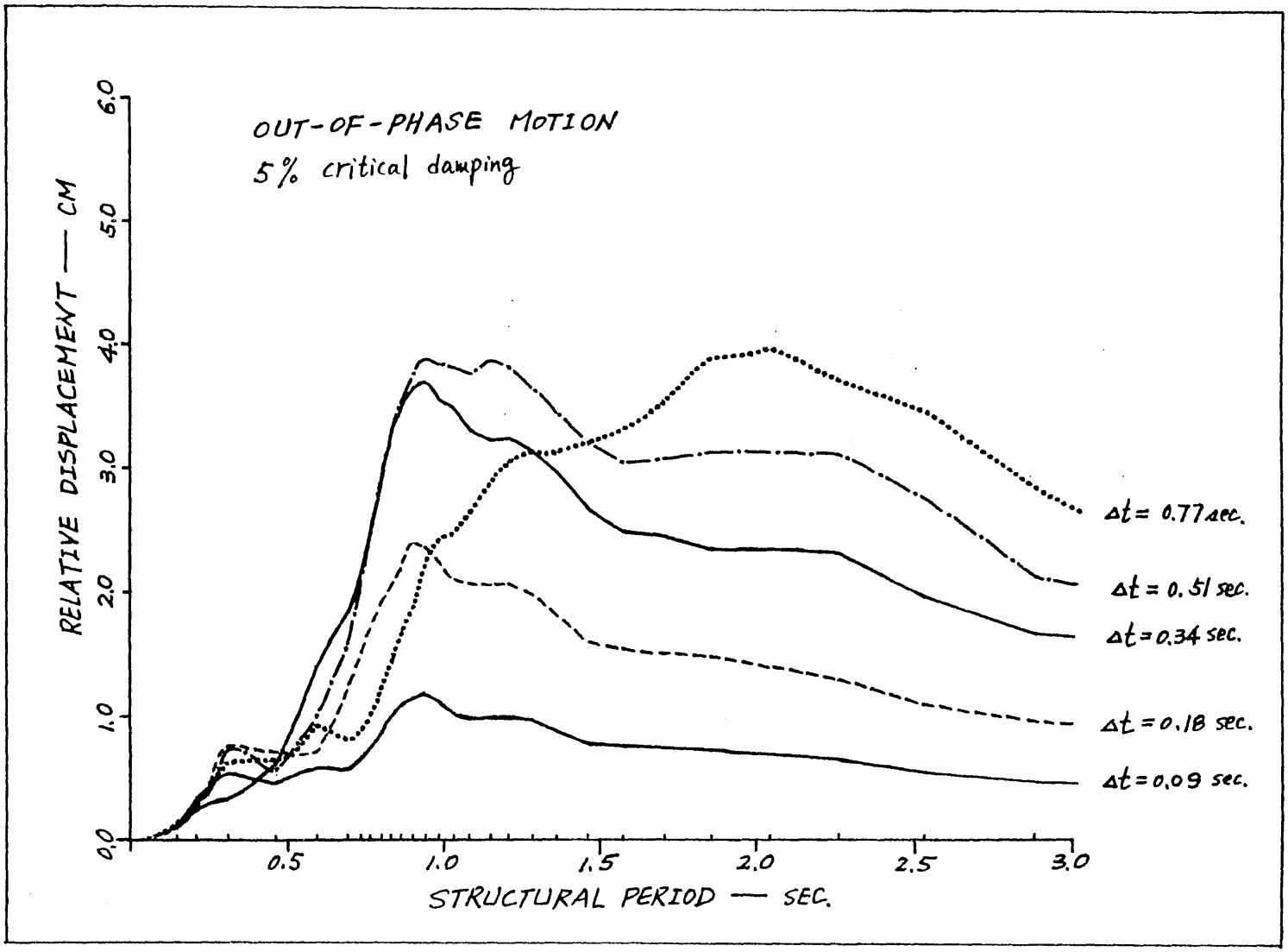

Figure 5.7 Displacement Response Spectrum for Out-of-Phase Input Motion with Different Phase Delay

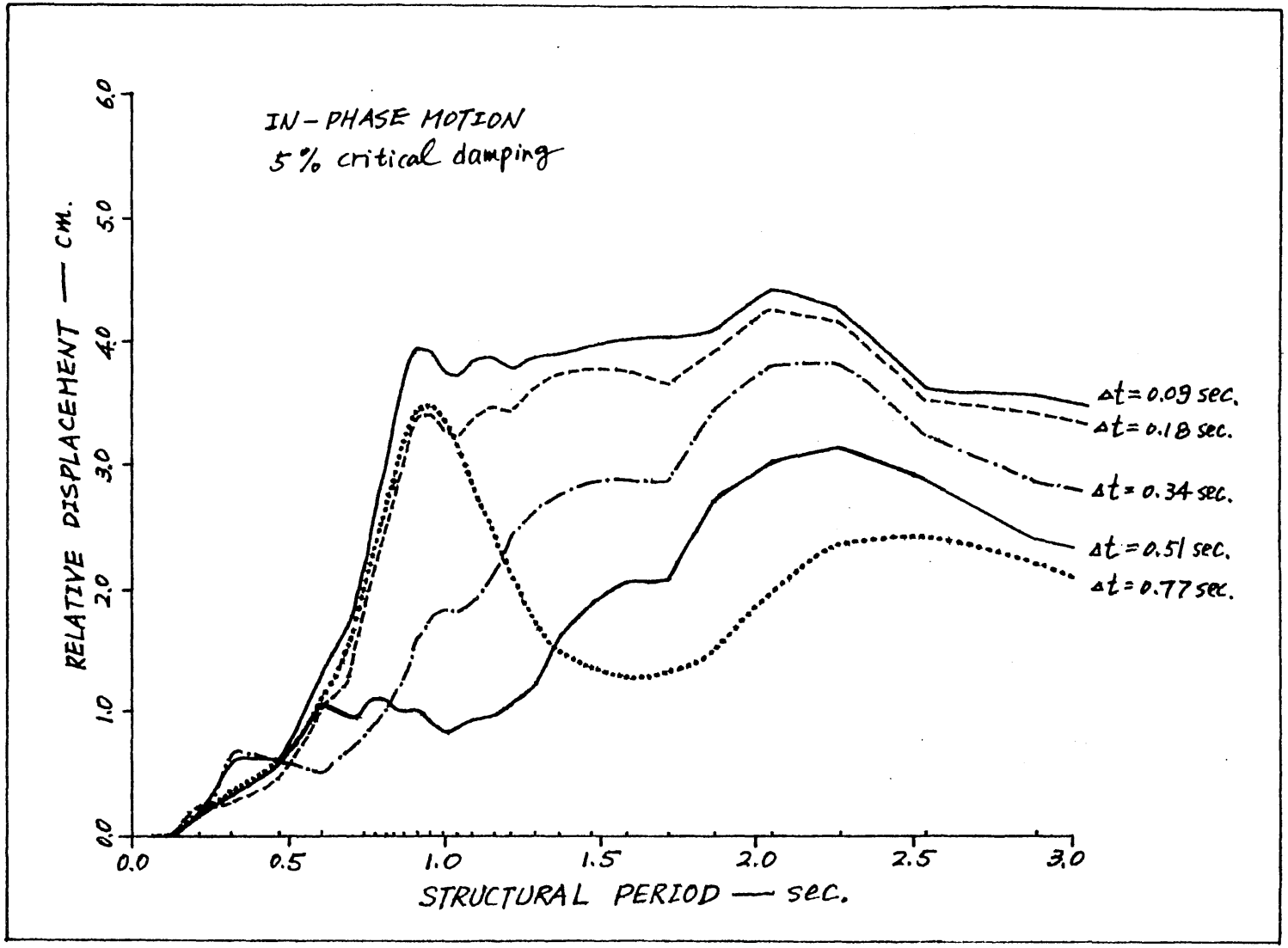

Figure 5.8 Displacement Response Spectrum for In-Phase Input Motion with Different Phase Delay

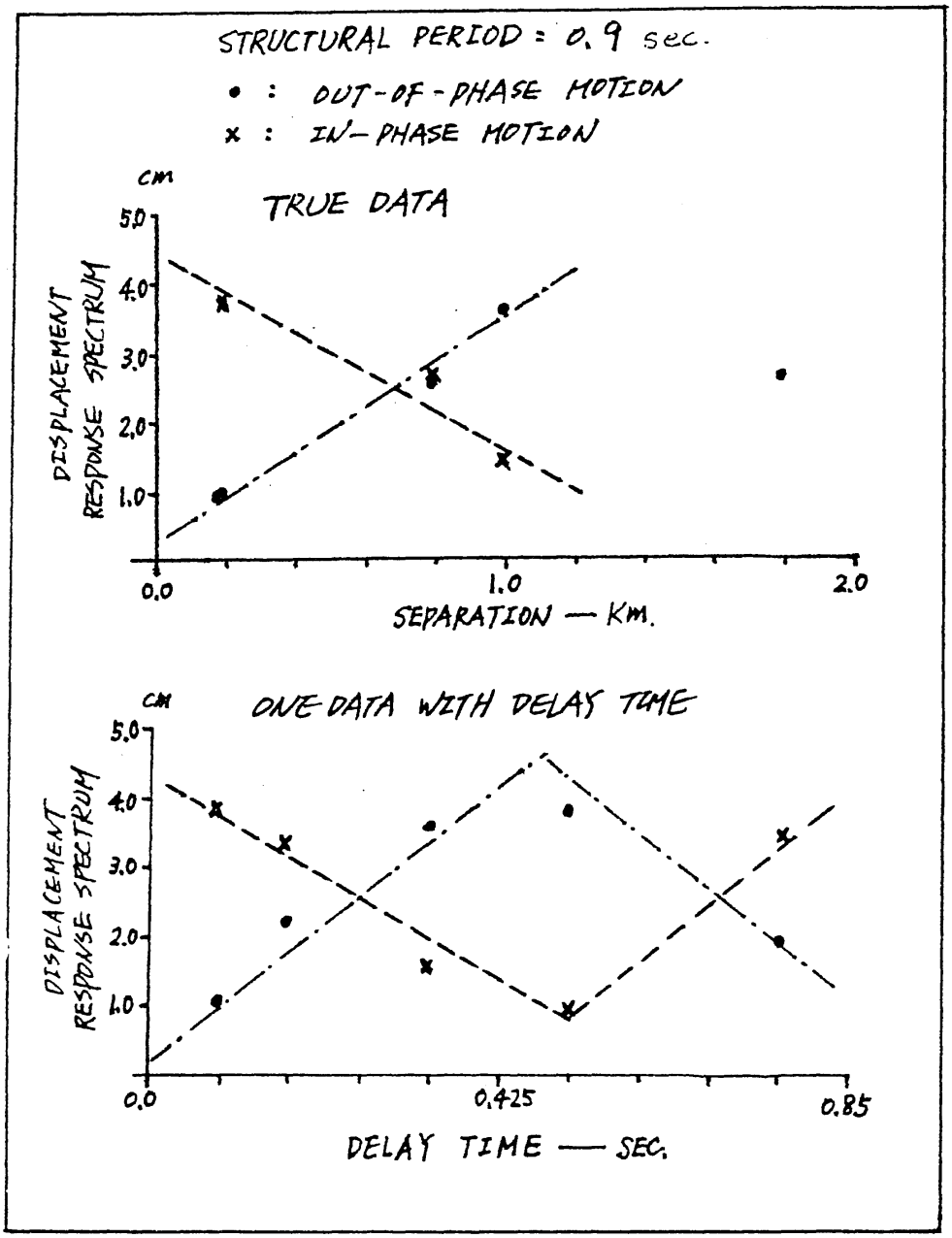

Figure 5.9 Comparison of Displacement Response Spectrum for Out-of-Phase Input Motion at Structural Period of 0.9 sec.

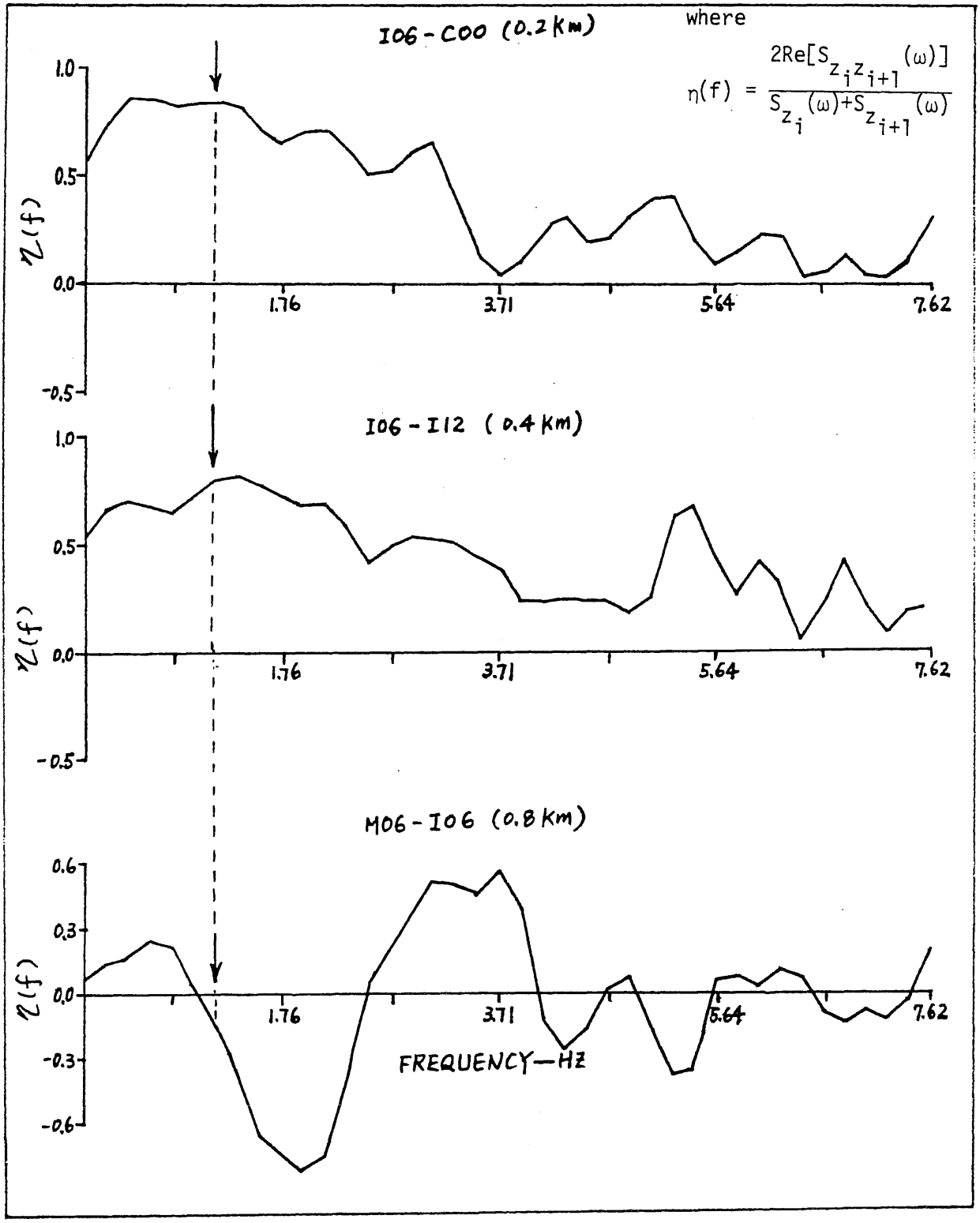

Figure 5.10a Variation of $\eta(f)$ with Frequency for Different Station Pairs

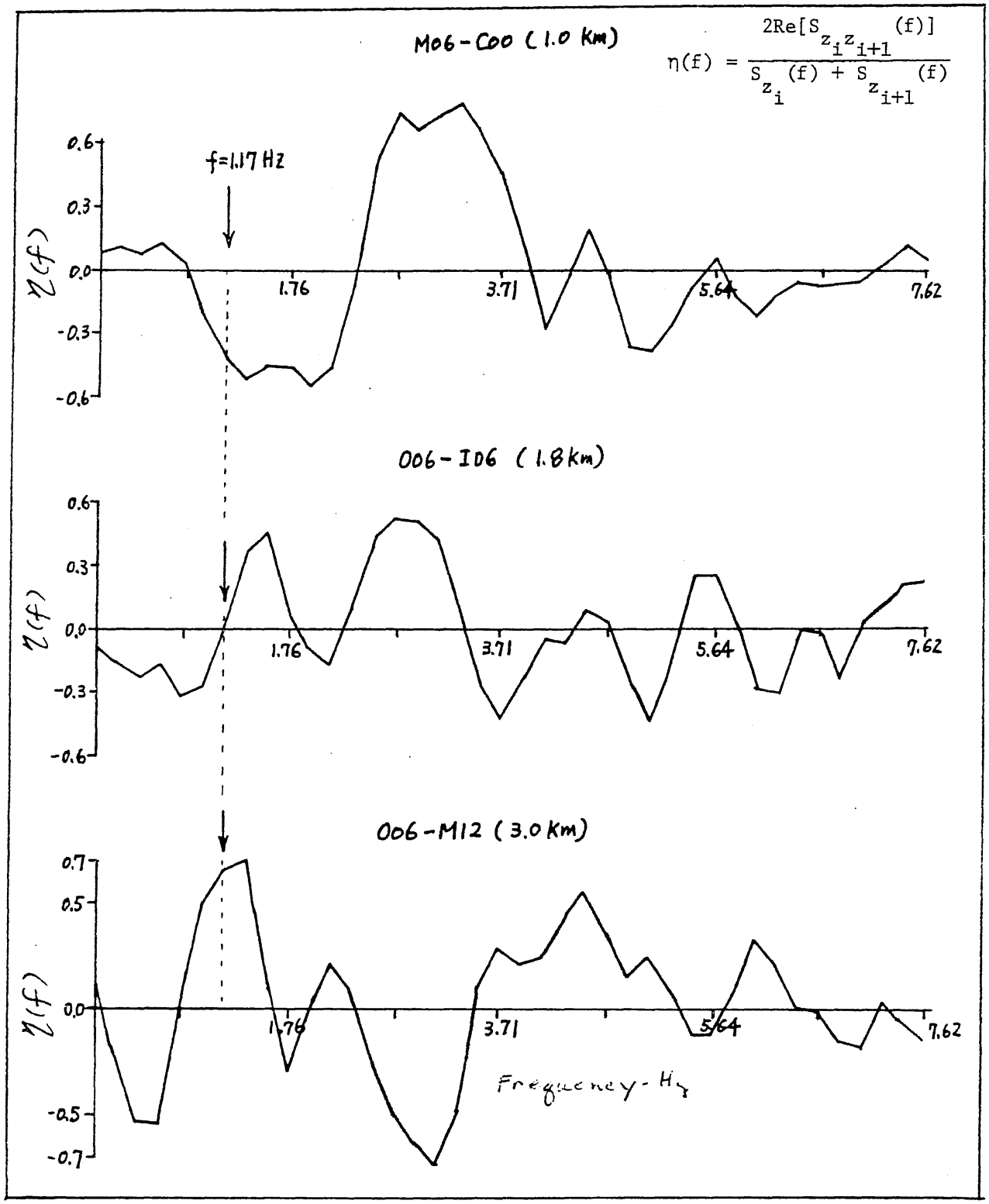

Figure 5.10b Variation of η(f) with Frequency for Different Station Pairs

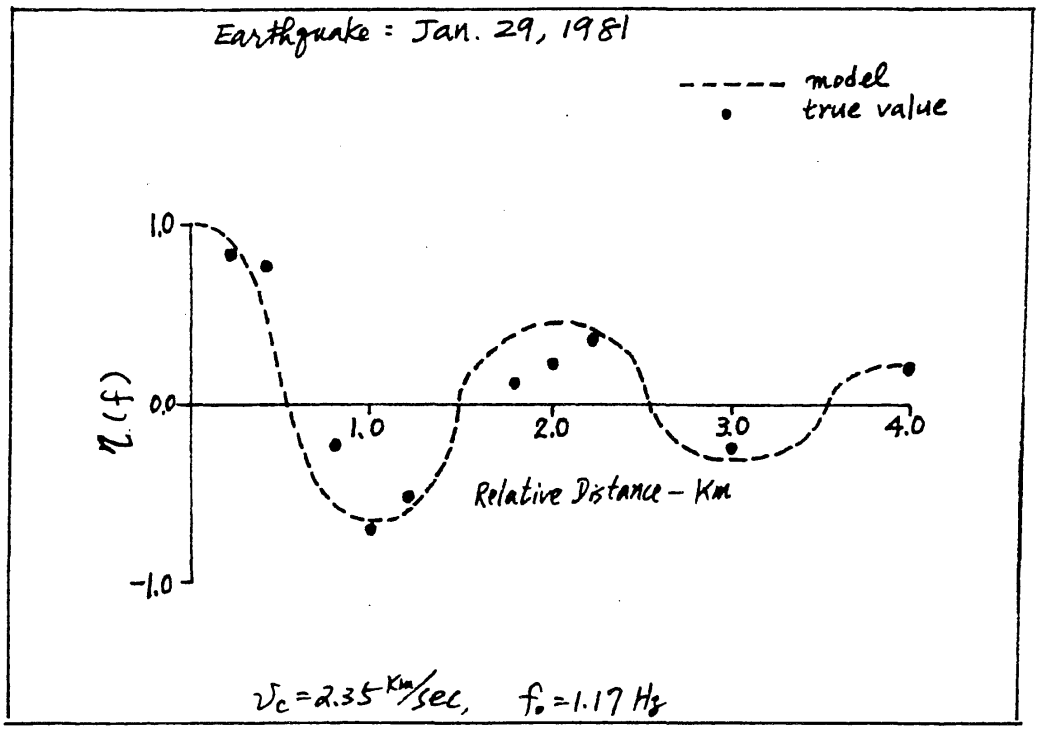

Figure 5.11 Variation of η(f) with Relative Distance at Frequency f = 1.17 Hz

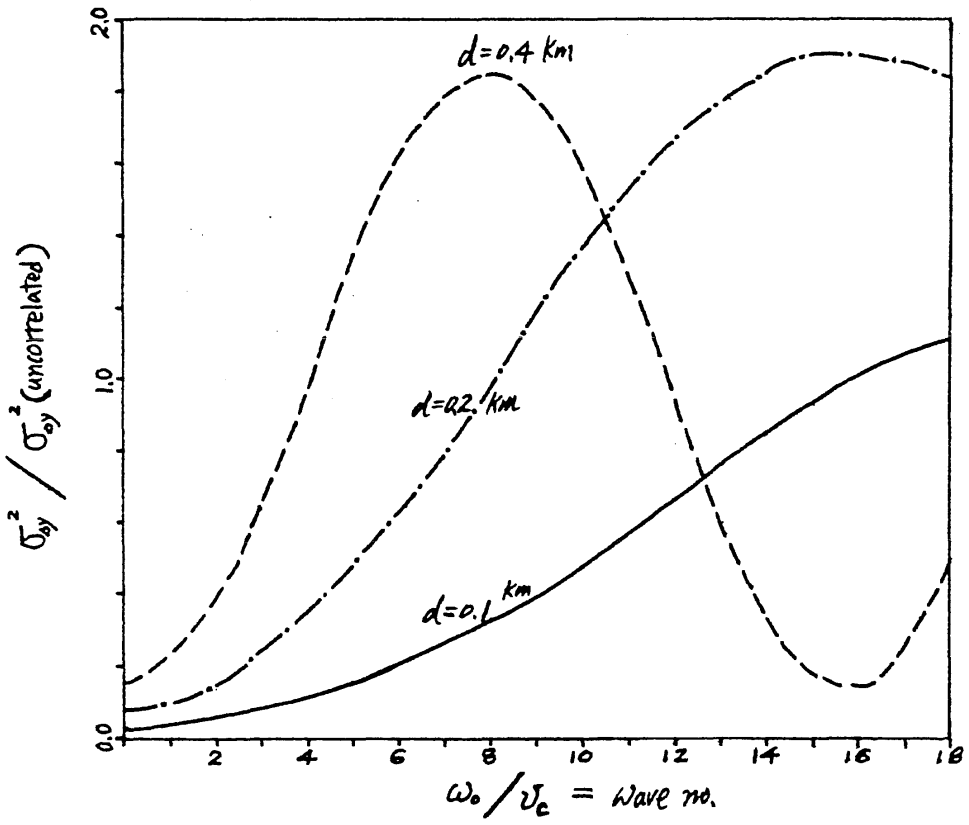

Figure 5.12 Variation of the Ratio of σ_{oy} Between Correlated and Uncorrelated Inputs with with Different Wave Members

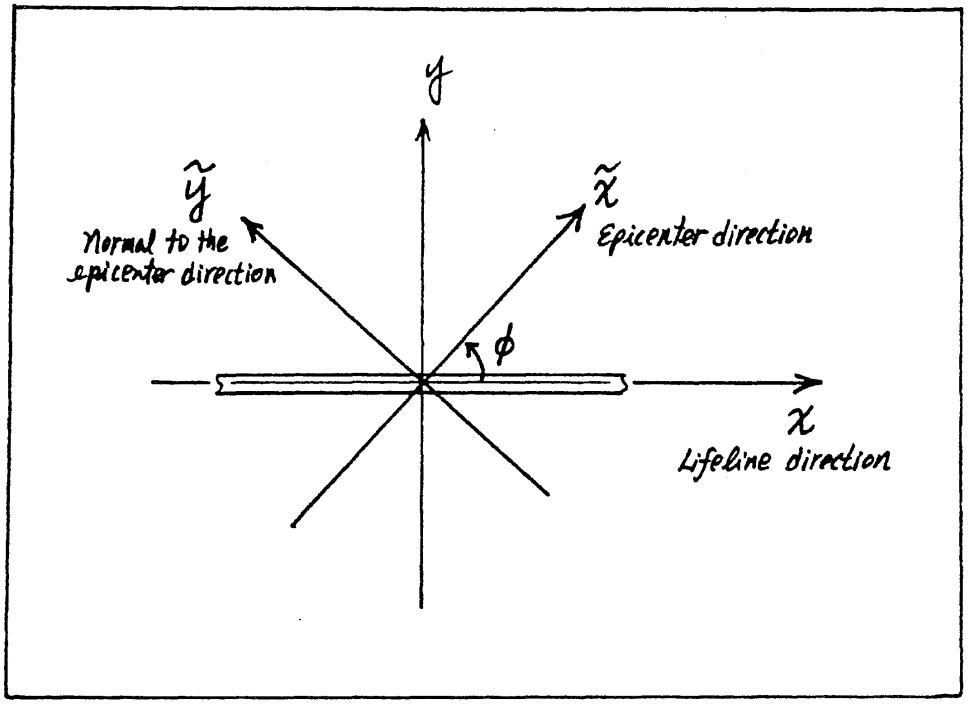

Figure 6.1 Coordinate Relationship Between Lifeline Direction and Epicenter Direction

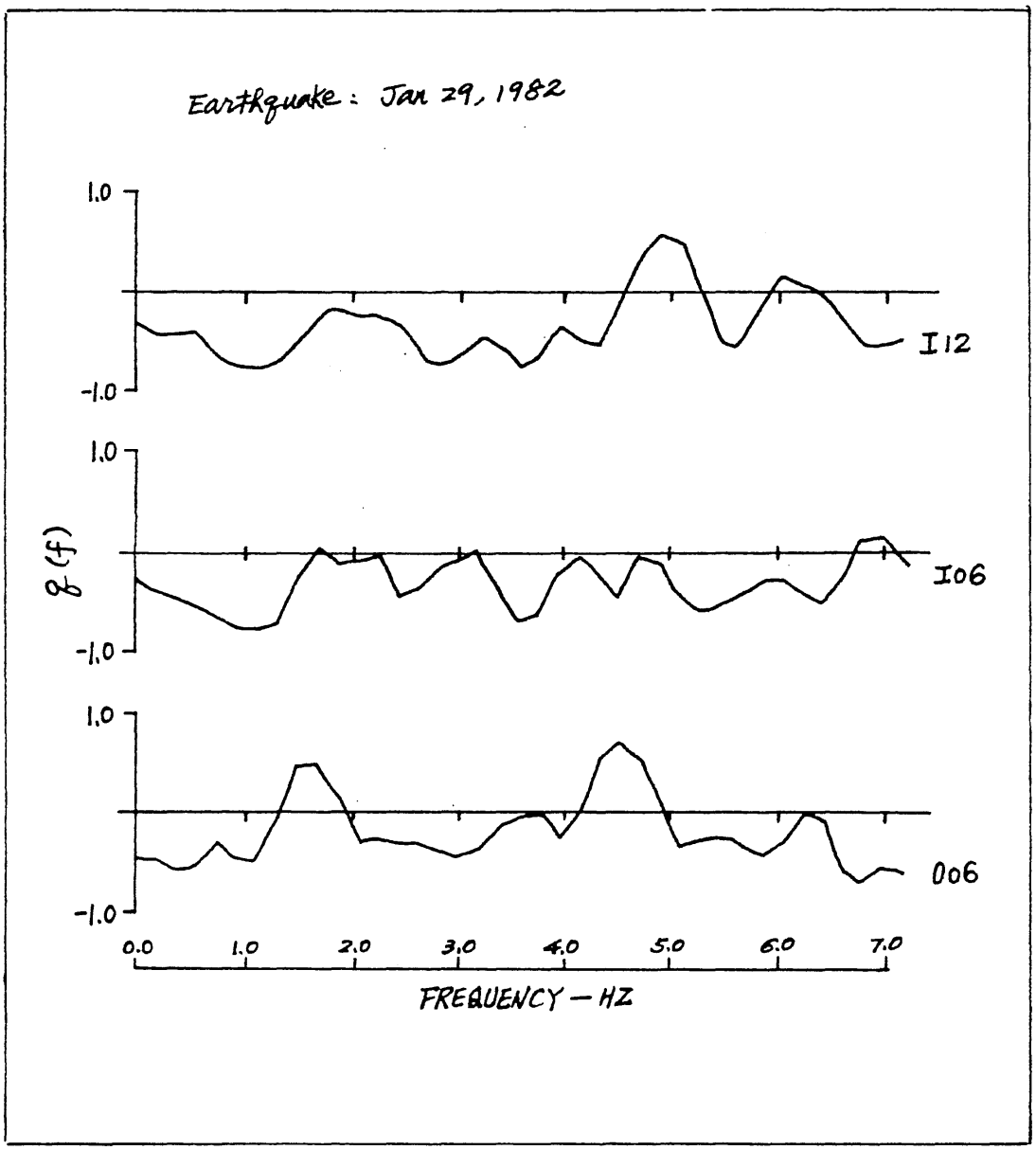

Figure 6.2 Variation of q(f) at Station I12, I06 and 006 for Earthquake of January 29, 1982

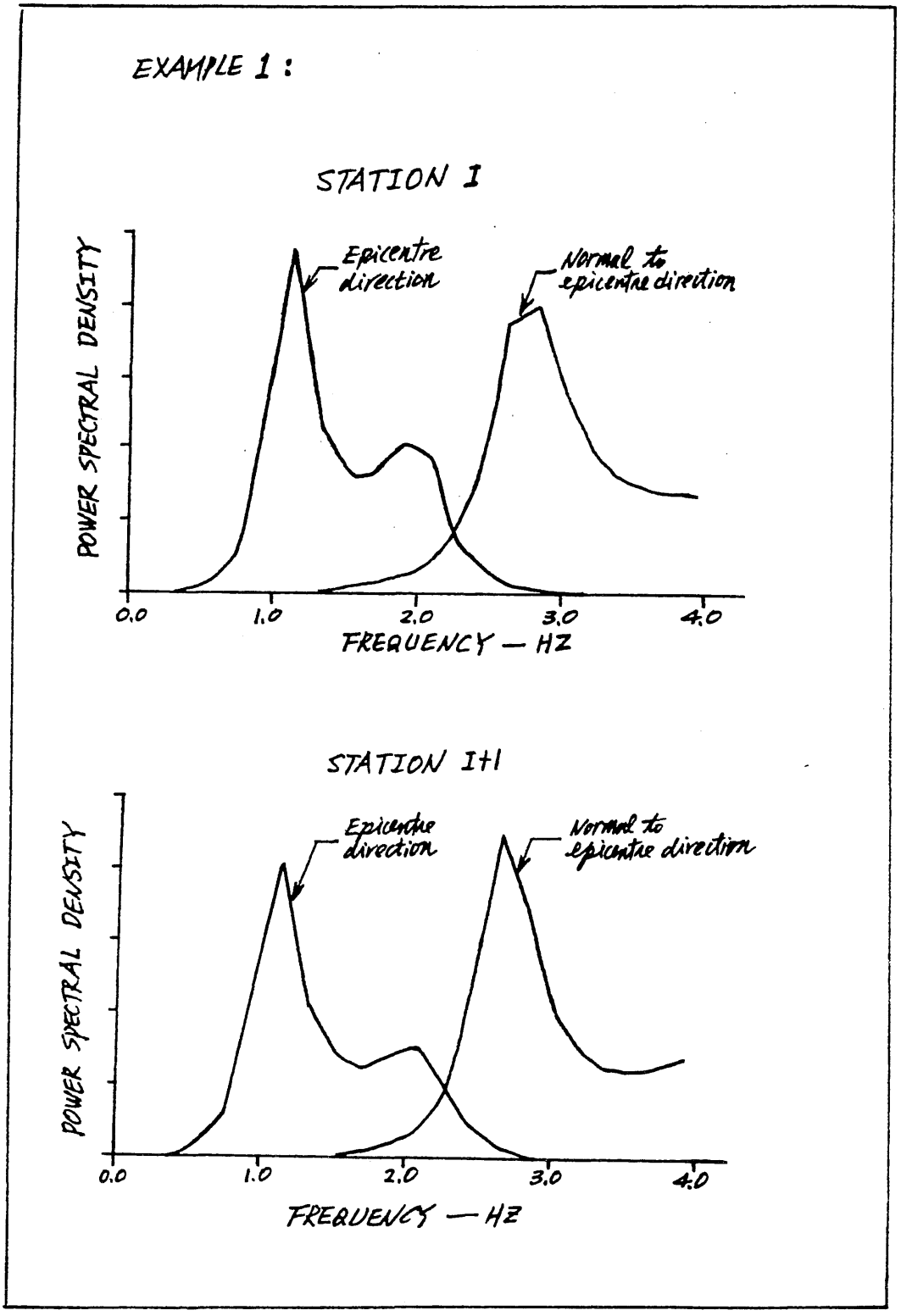

Figure 6.3 Variation of Power Spectral Density Function Along and Normal to the Epicenter Direction at Station i and i+1 (Example 1)

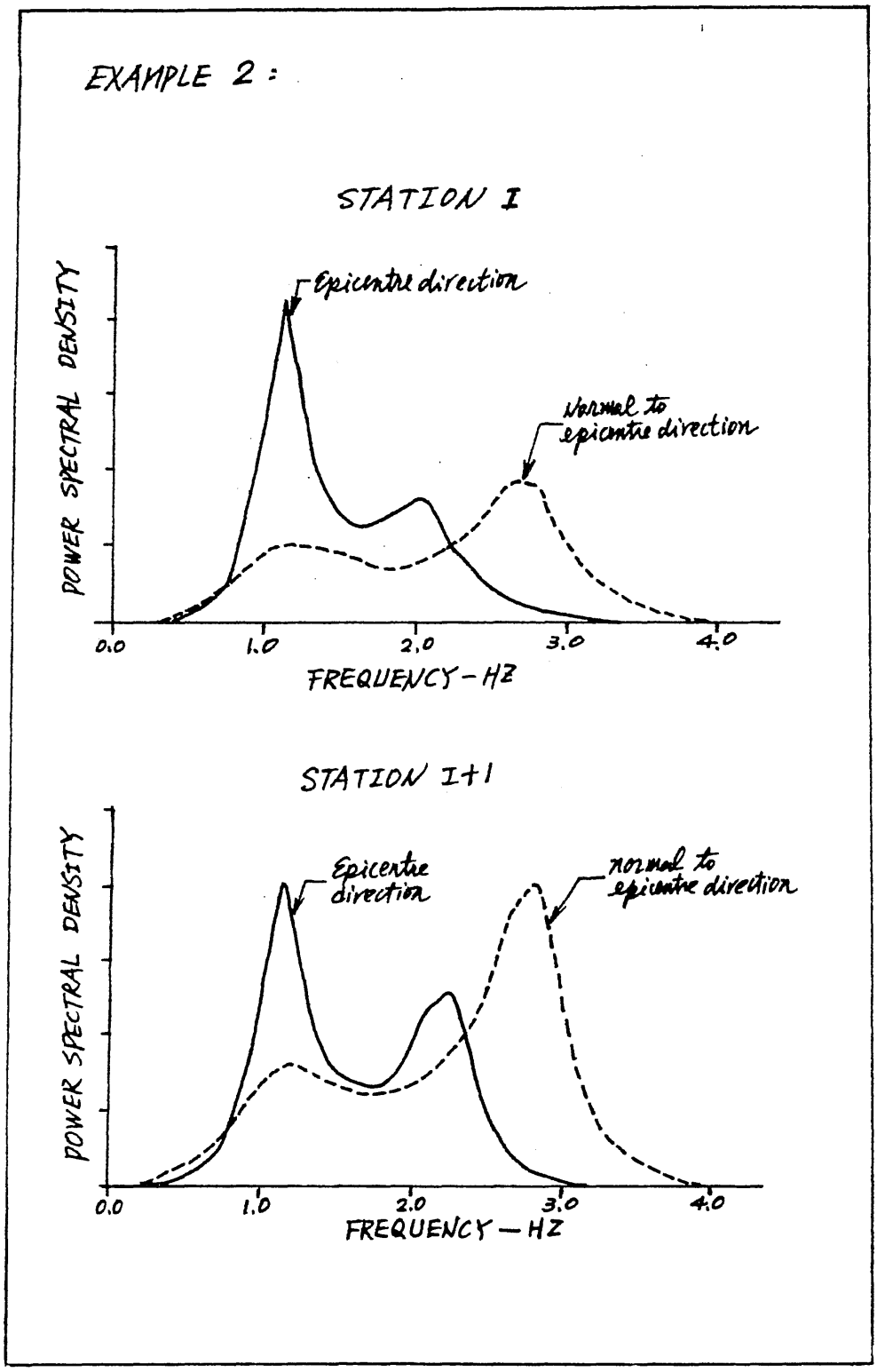

Figure 6.4 Variation of Power Spectral Density Function Along and Normal to the Epicenter Direction at Station i and i+1 (Example 2)

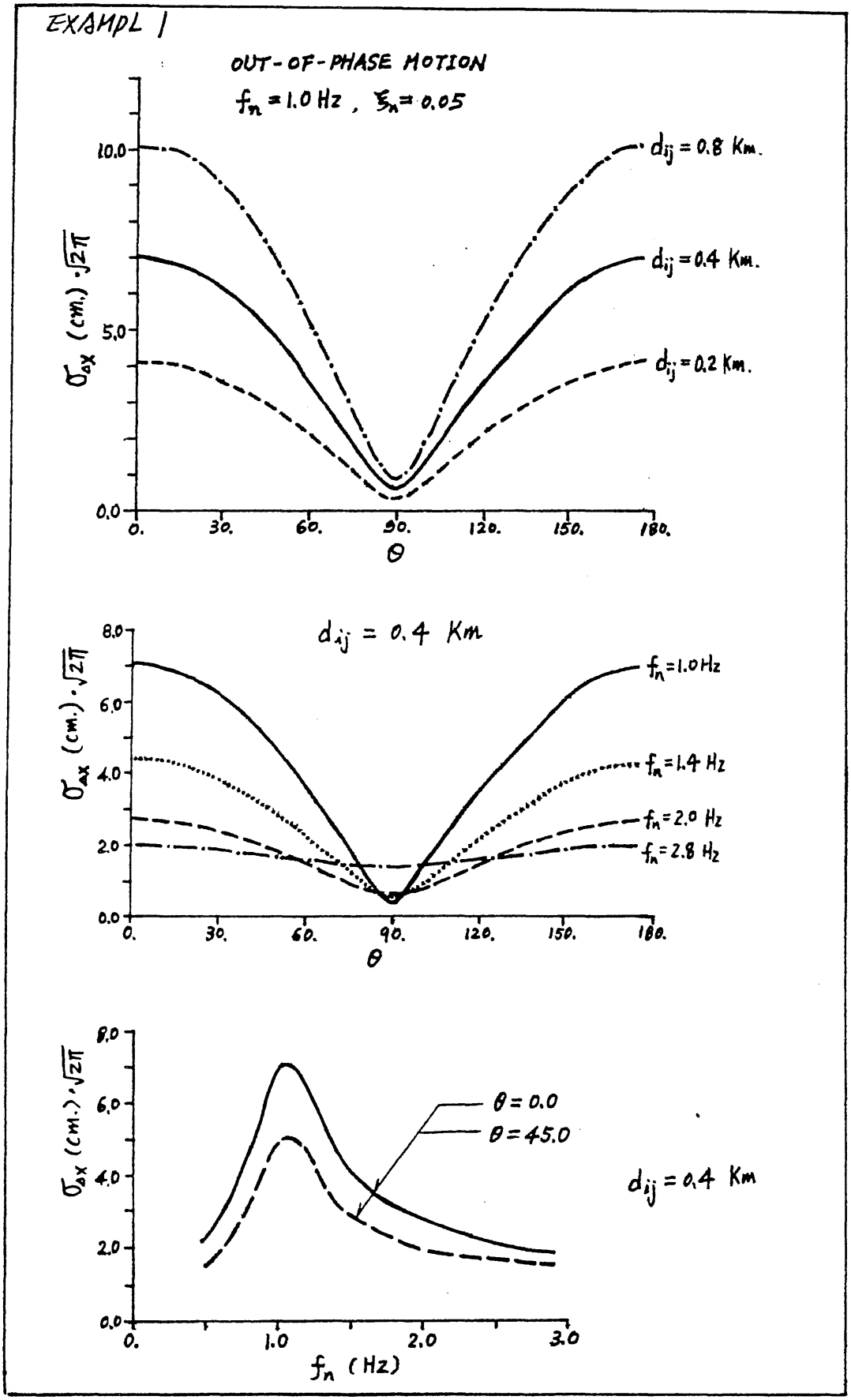

Figure 6.5 Variation of $\sigma_{\Delta x}$ with θ for longitudinal Response (Example 1)

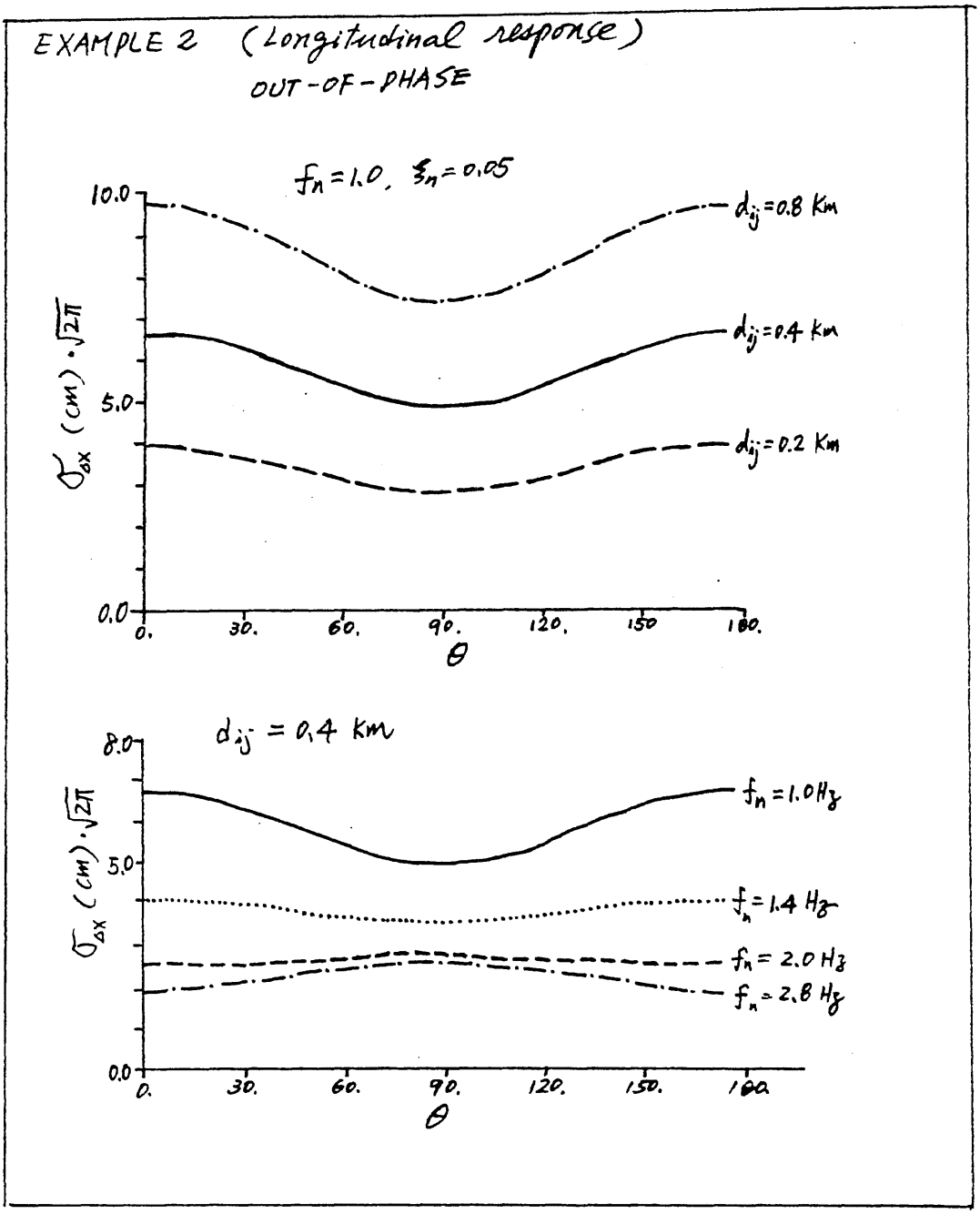

Figure 6.6 Variation of $\sigma_{\Delta x}$ with θ for Longitudinal Response (Example 2)

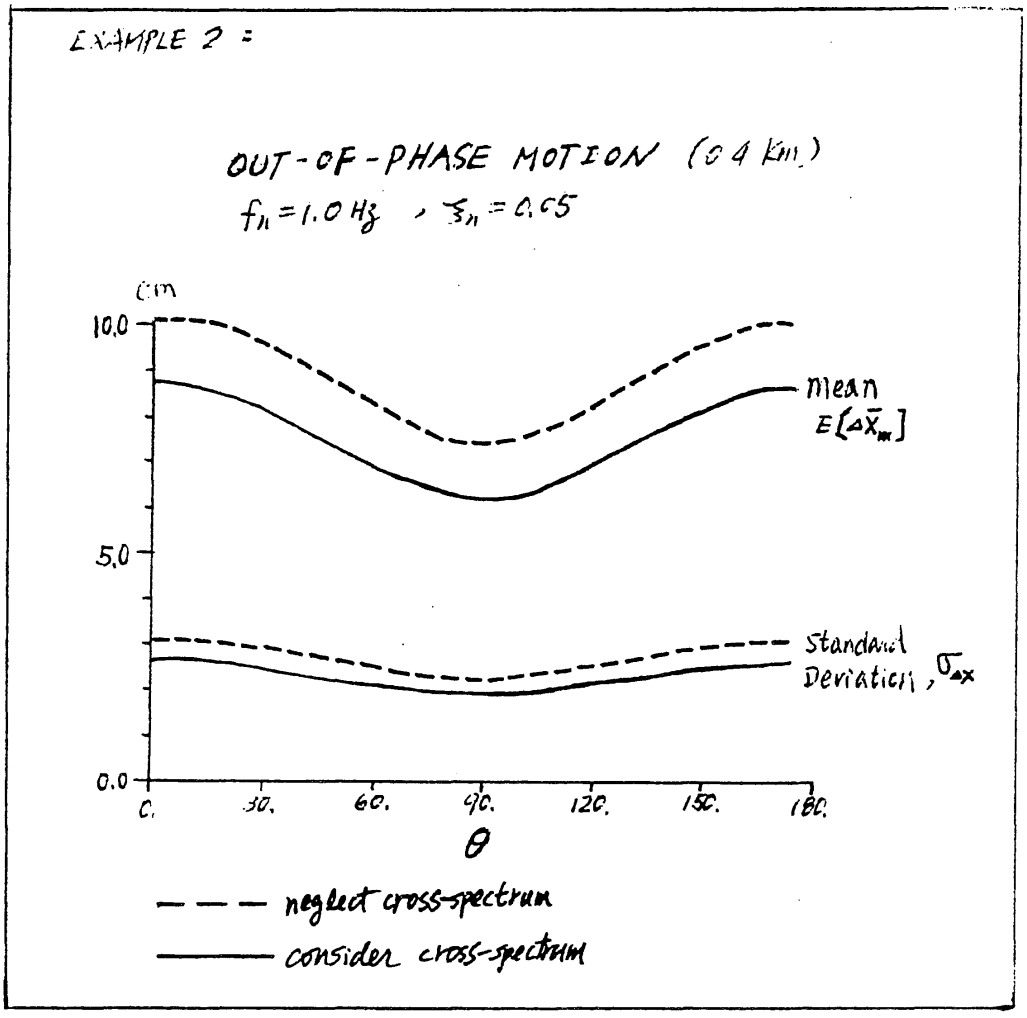

Figure 6.7 Variation of $\sigma_{\Delta x}$ and $E[\Delta\bar{x}_m]$ with θ

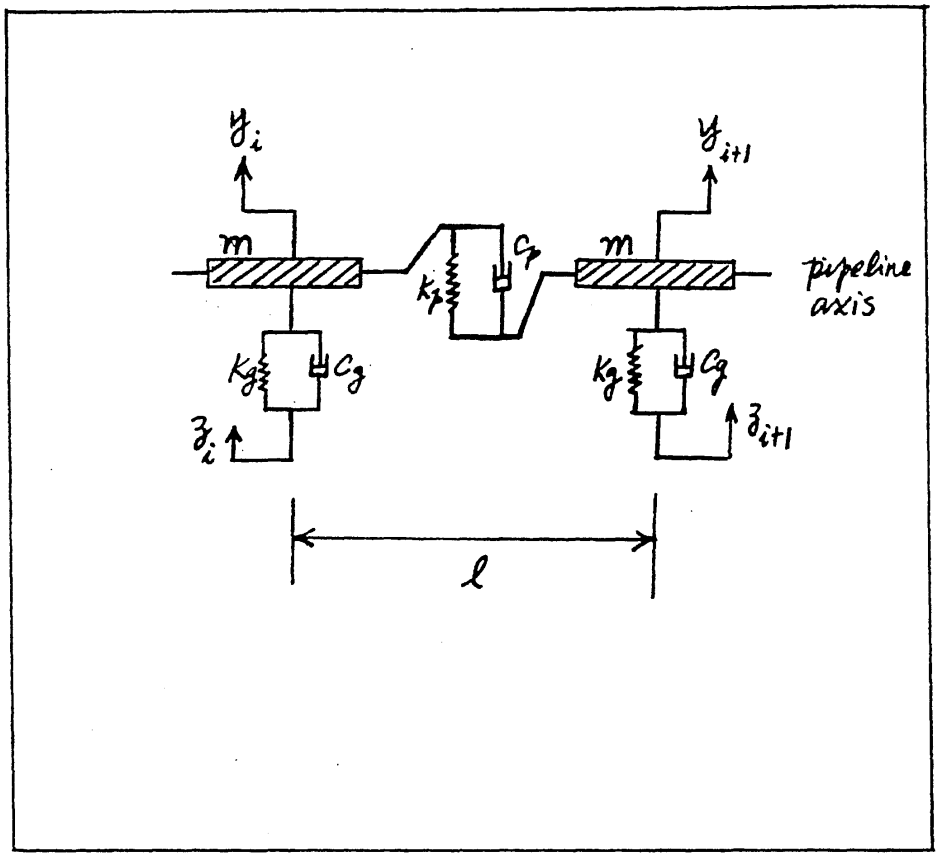

Figure 6.8 Discrete Model of Lifeline Element (Transverse Motion)

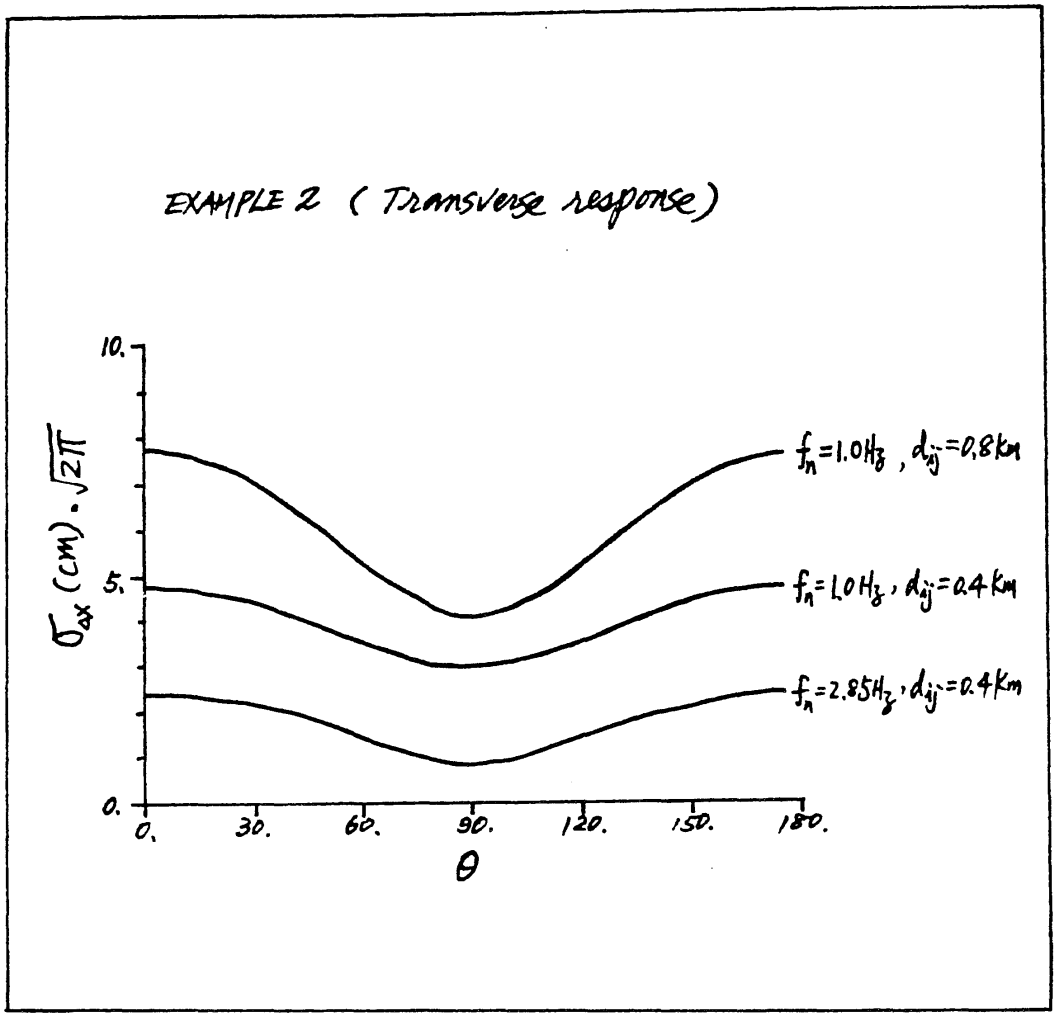

Figure 6.9 Variation of $\sigma_{\Delta x}$ with θ (Transverse Response)

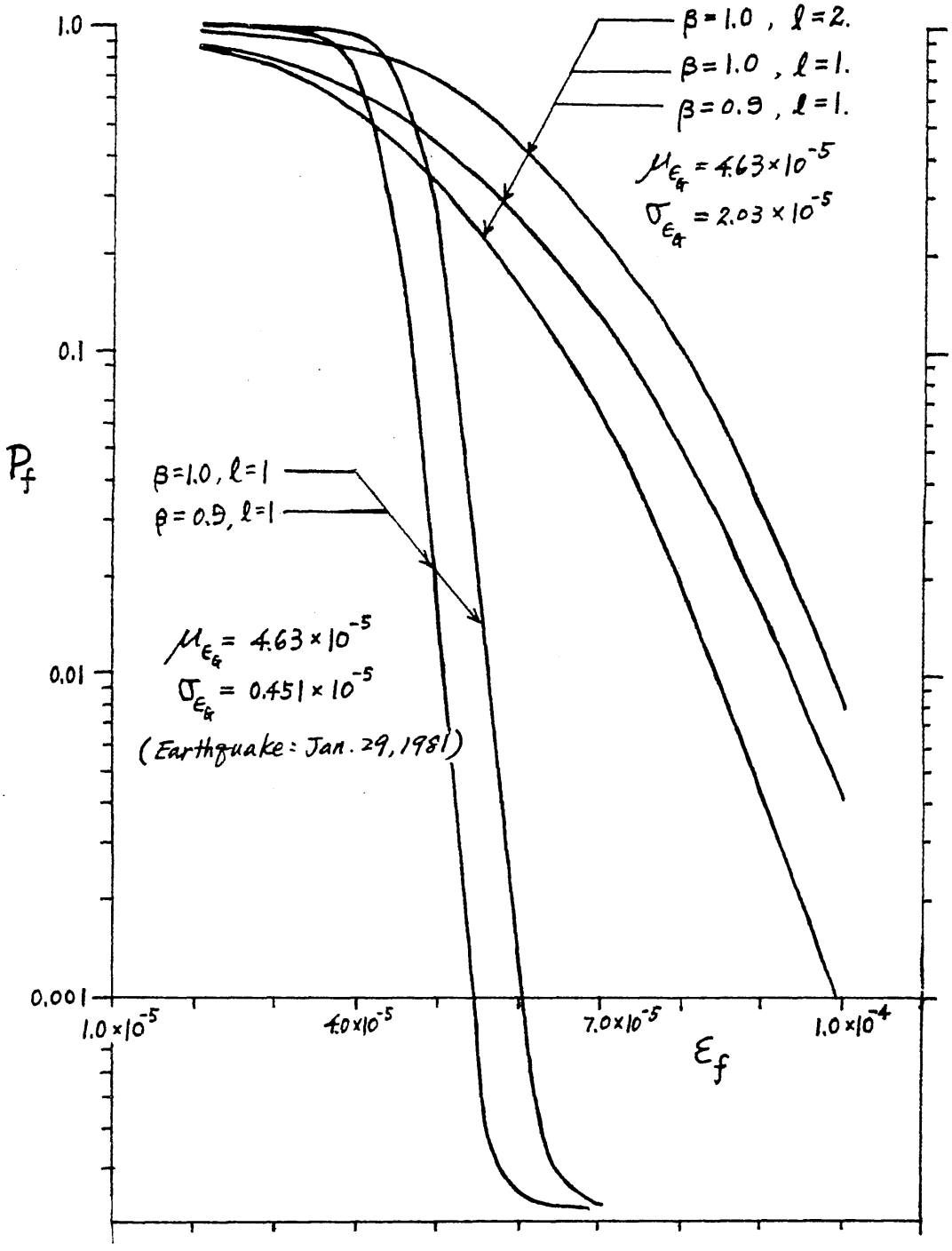

Figure 7.1 Probability of Damage for Different Values of the Failure Strain ϵ_f

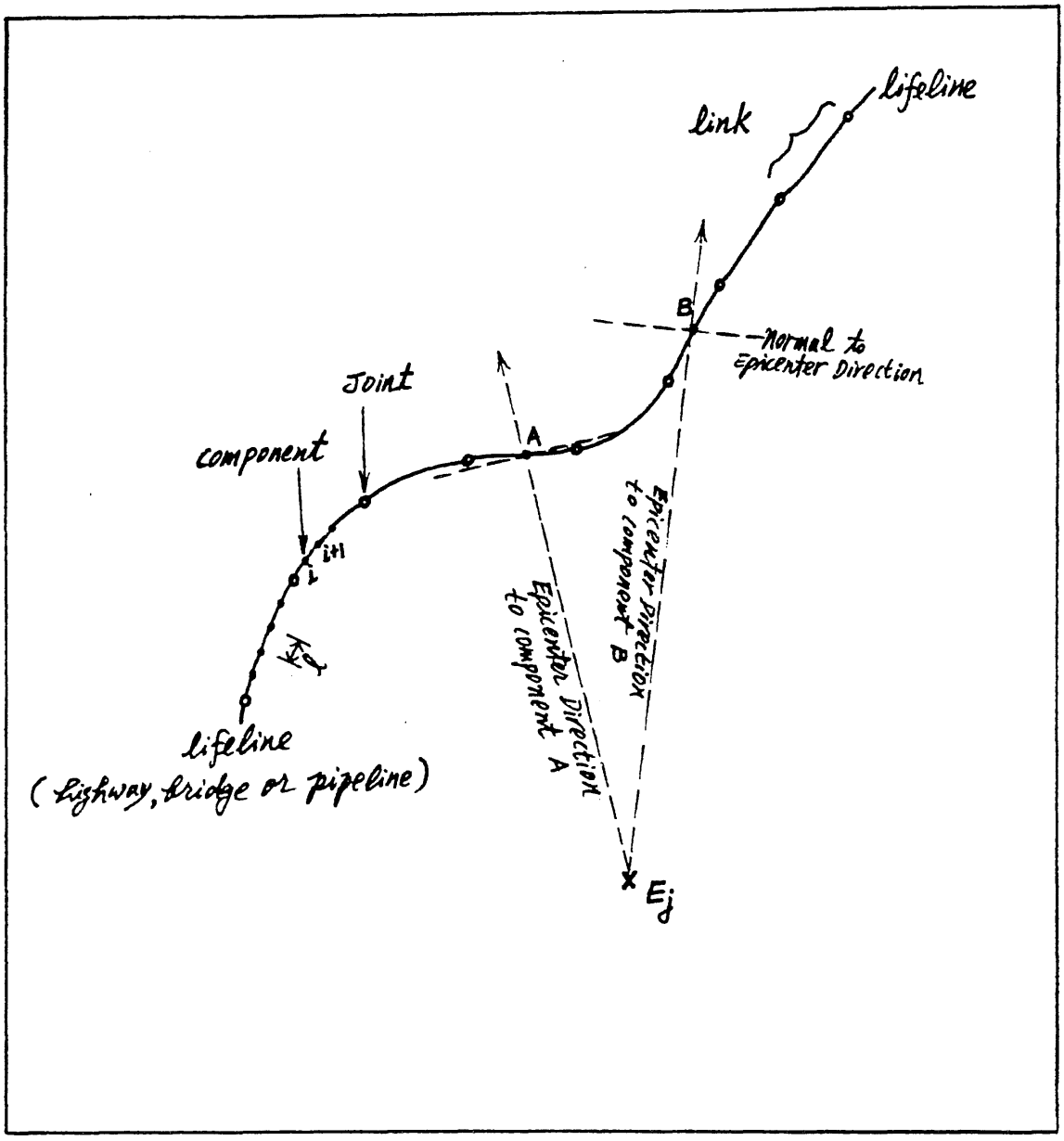

Figure 7.2 An Example Lifeline System

APPENDIX

A. Coherence of Ground Accelerations At One Station

The ratio R(f) defined by Eq. 2.3, is plotted in Figs. A-1 and A-2 with respect to frequency for the stations along 006 to 012 and 003 to 009. The dominant direction at low values of R(f) (< 0.3) is also indicated in these figures. As pointed out earlier, certain kind of wave may exist at low values of R if there is also a peak power spectral density value at that frequency. On the other hand, if there is no obvious peak spectral density function and also the value of R is large, then this particular point may be chosen as the separation point to differentiate between different kinds of waves along the frequency axis. Then within each frequency band, one can study the coherence of the two orthogonal ground motions at one station or the coherence of the ground motions at two different stations.

When $R(f_o) = 1$ there is no principal direction because the harmonic motion at frequency f_o moves along a circular path at constant angular velocity, $2\pi f_o$. When $R(f_o) < 1$, principal directions exist with the motion being along a straight line for $R(f_o) = 0$. It is significant to note that only for $R(f_o) = 0$ can a pure single harmonic wave exist.

In most studies of structures under multiple ground excitations, the two horizontal ground motion components are assumed to be uncorrelated. From the present study of the SMART-1 data, a certain level of coherence obviously exists between the motions along and normal to the epicenter direction at some specific frequency. Figure A-3 shows the coherence curve and the ratio R(f). The epicenter direction of the January 29, 1981 earthquake is at $\phi = 76$; therefore, if the dominant wave is not in this direction, it will create a high coherence at this particular frequency (e.g., at f = 2.85 Hz). To estimate the co-spectrum (real part of cross-spectral density function) for multiple inputs, the function q(f) as defined in Eq. 6.3 is calculated from the array data and shown in Fig. A-4 with R(f). Using

the previously discussed method of separation of frequency axis into bounds, q(f) can be assumed to be a constant (the average) within each frequency band. This is more reasonable than assuming a constant for all frequencies.

From the January 29, 1981 earthquake data, q(f) may be modeled as

$$q(f) = \begin{cases} -0.169 & 0 < f \leq 1.563 \text{ Hz} \\ 0.186 & 1.536 < f \leq 2.344 \text{ Hz} \\ -0.361 & 2.344 < f \leq 3.320 \text{ Hz} \\ -0.220 & 3.320 < f \leq 4.60 \text{ Hz} \end{cases}$$

Note that q(f) may vary from earthquake to earthquake.

Table A-1 Characteristics of the January 29, 1981 Earthquake

January 29, 1981 Earthquake (SMART-1)	Ground Motion in Epicenter Direction	Ground Motion Normal to Epicenter Direction
Data Used Along Stations 006-012	Figure: A-6 Dominant Frequency: 1.17 Hz (Surface Waves) Obvious phase change and loss of coherence along spatial coordinate.	Figure: A-8 Dominant Frequency: 2.98 Hz (Shear Waves) Obvious phase change but spatial correlation is strong in III.
Data Used Along Stations 003-009	Figure: A-10 Dominant Frequency: 1.17 Hz No obvious phase change up to 1 km.	Figure: A-12 Dominant Frequency: 2.93 Hz No obvious loss of coherence in III. The phase change are not obvious at 2.93 Hz up to 1 km separation.

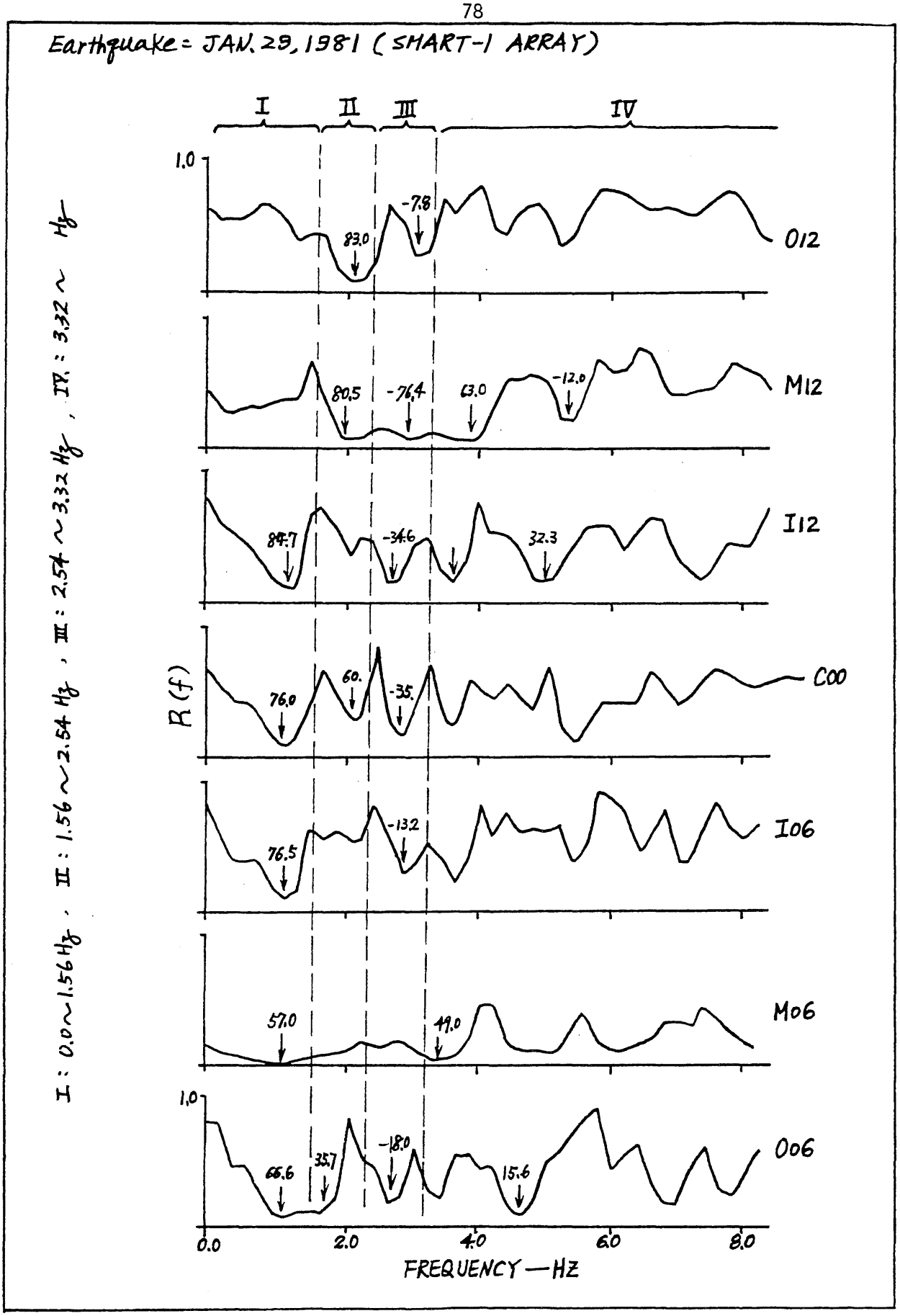

Figure A-1 Variation of R(f) with Frequency Showing Dominant Direction at Low Value of R(f)

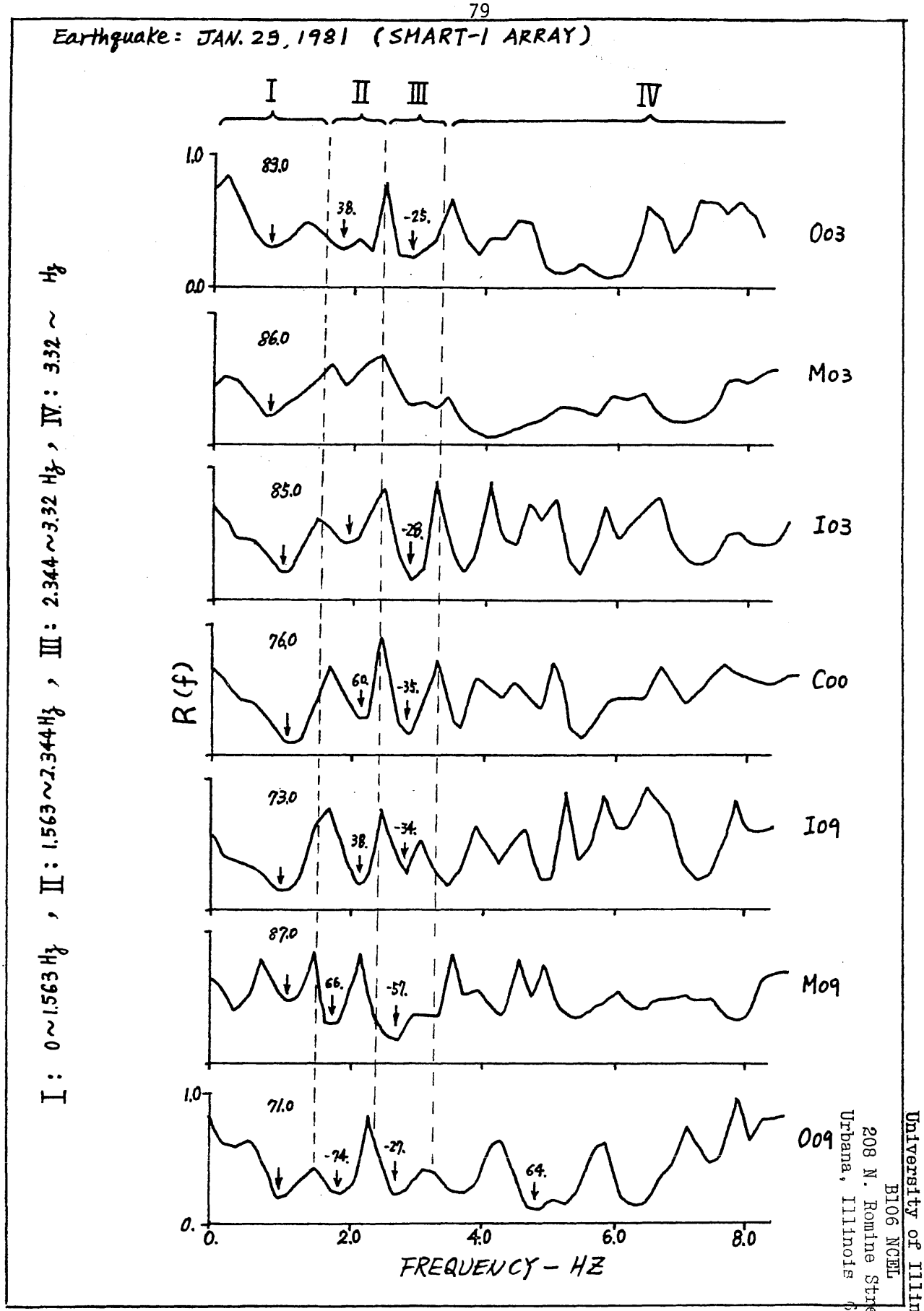

University of Illinois
B106 NCEL
208 N. Romine Street
Urbana, Illinois 61801

Figure A-2 Variation of R(f) with Frequency Showing Dominant Direction at Low Value of R(f)

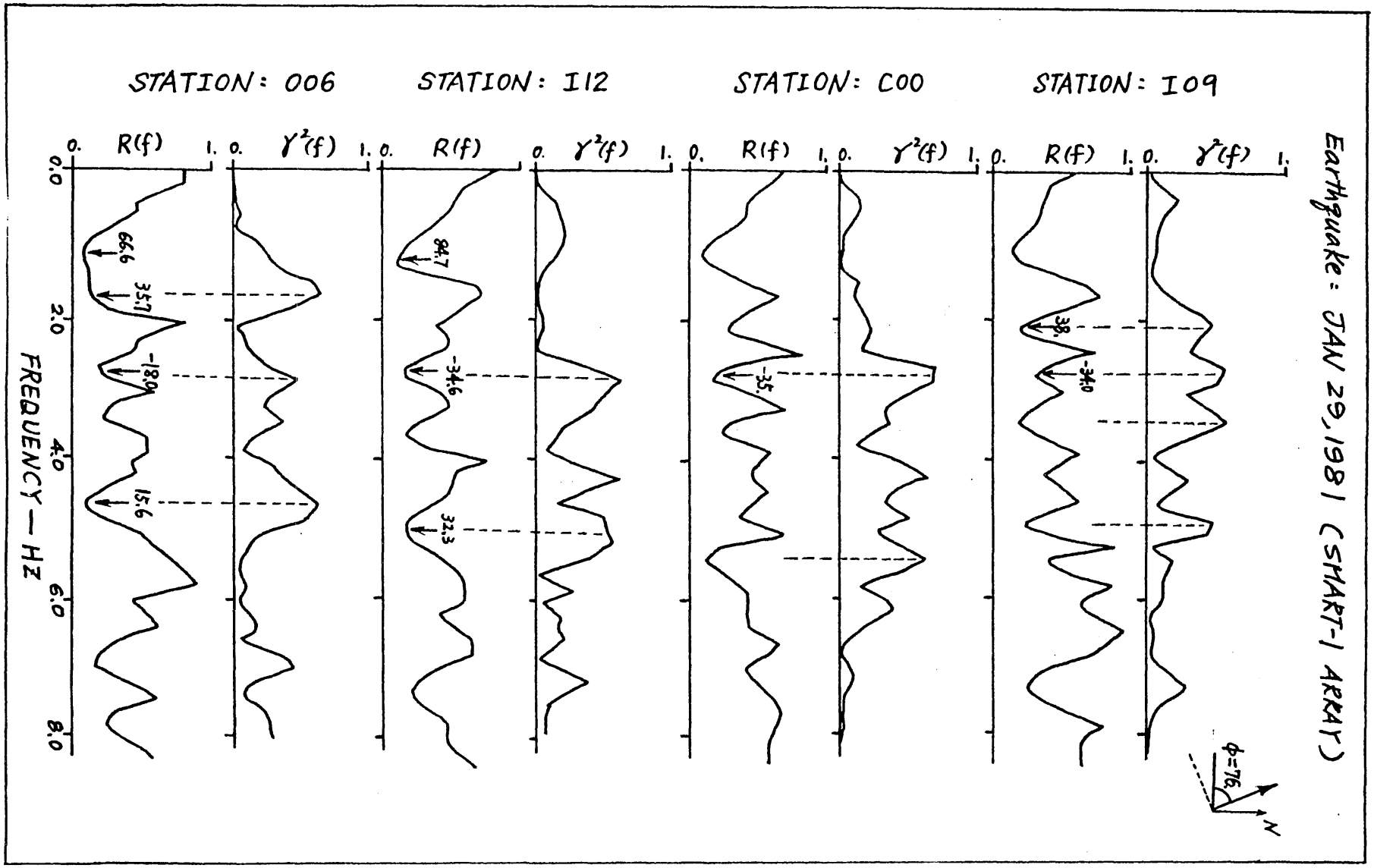

Figure A-3 Comparison of R(f) and Coherence $\gamma^2(f)$ at Station C00, I09, I12, C00

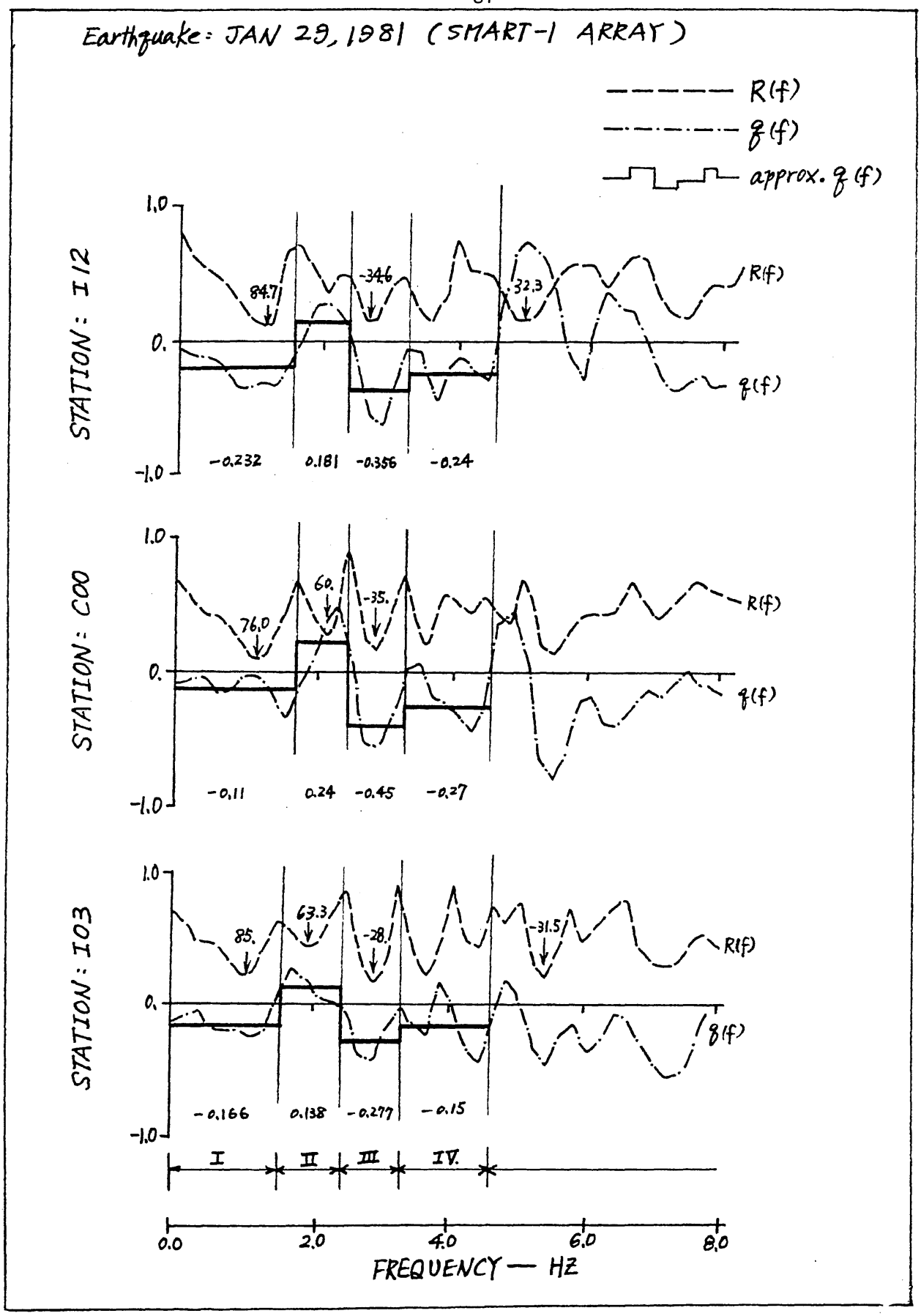

Figure A-4 Variation of R(f) and q(f) with Frequency and Approximate q(f) at Different Frequency Band

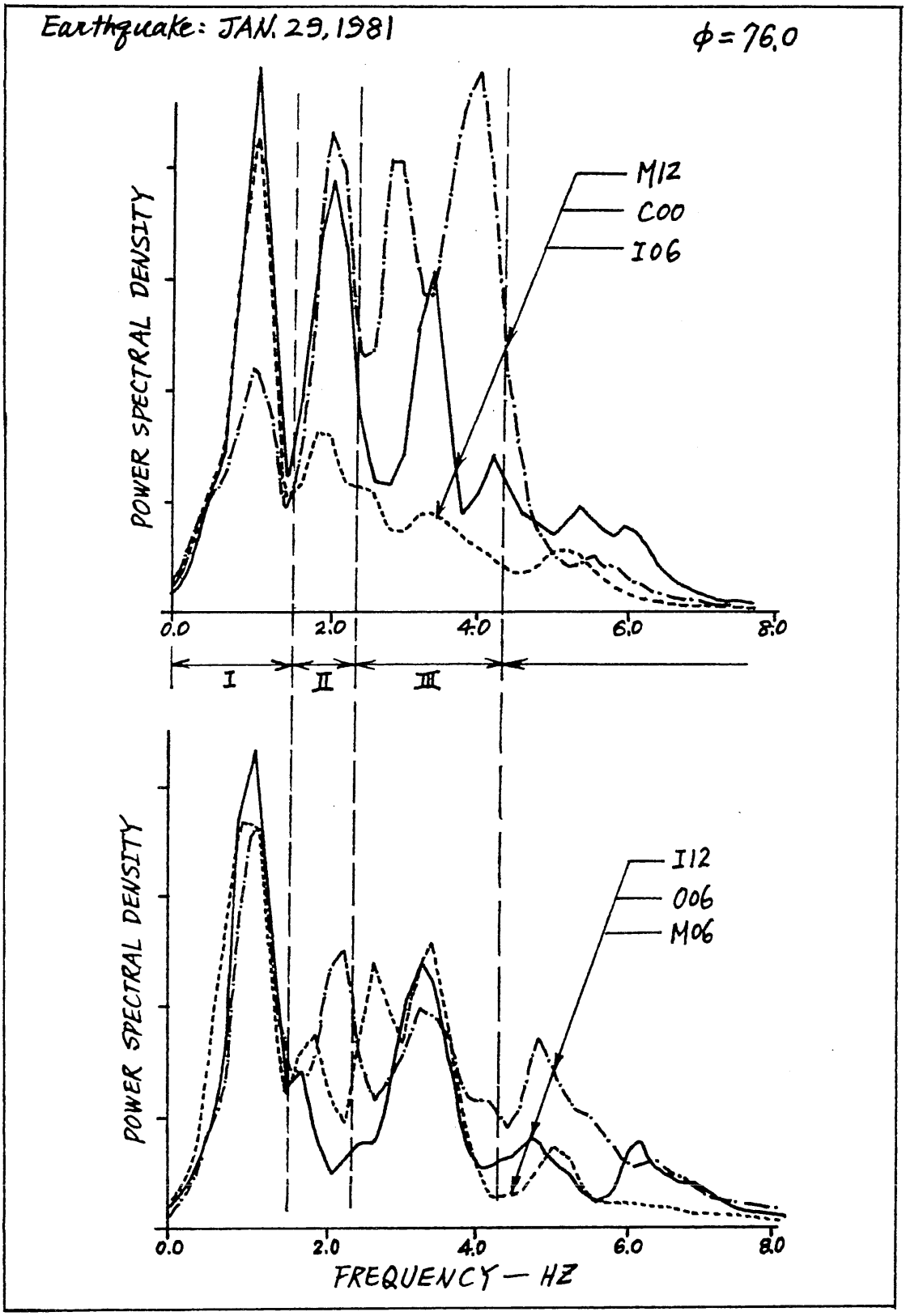

Figure A-5 Power Spectral Density of Stations C00, I06, I12, M12, M06, 006 Along ϕ = 76.0°

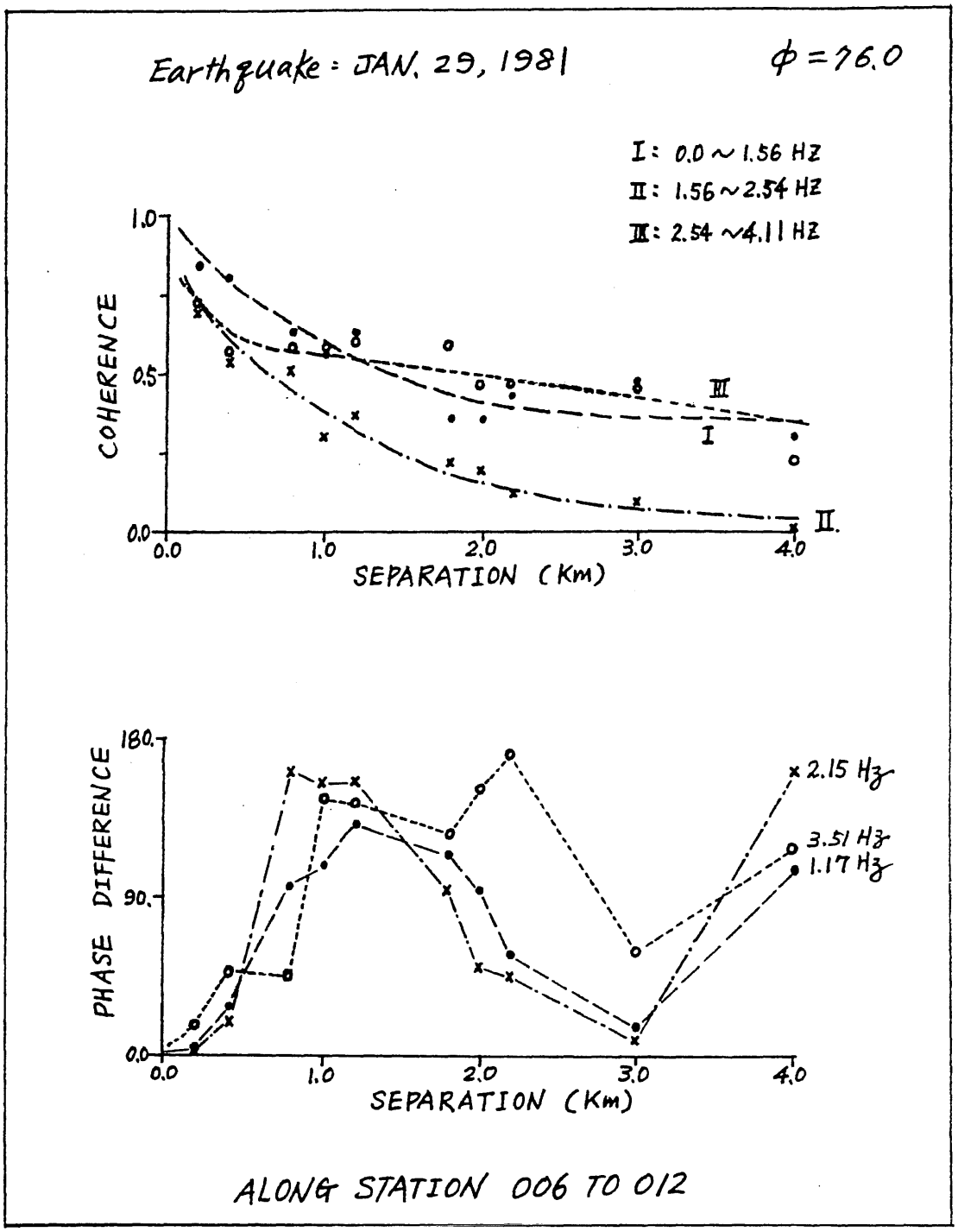

Figure A-6 Variation of Coherence and Phase Difference of Data Along Stations 006 to 012, at ϕ = 76.0°

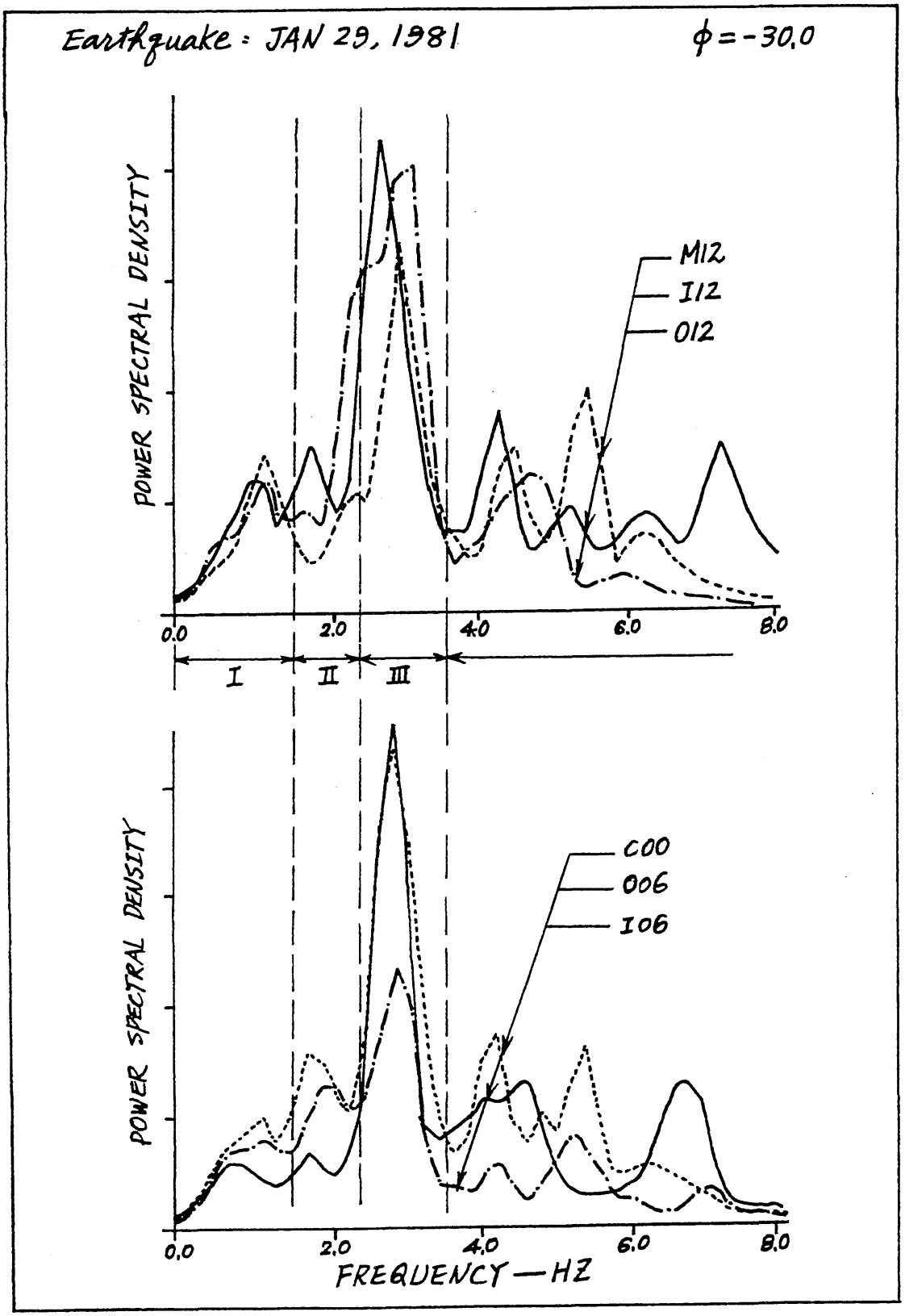

Figure A-7 Power Spectral Density of Stations C00, I06, I12, M12, 006, 012 Along ϕ = -30.0°

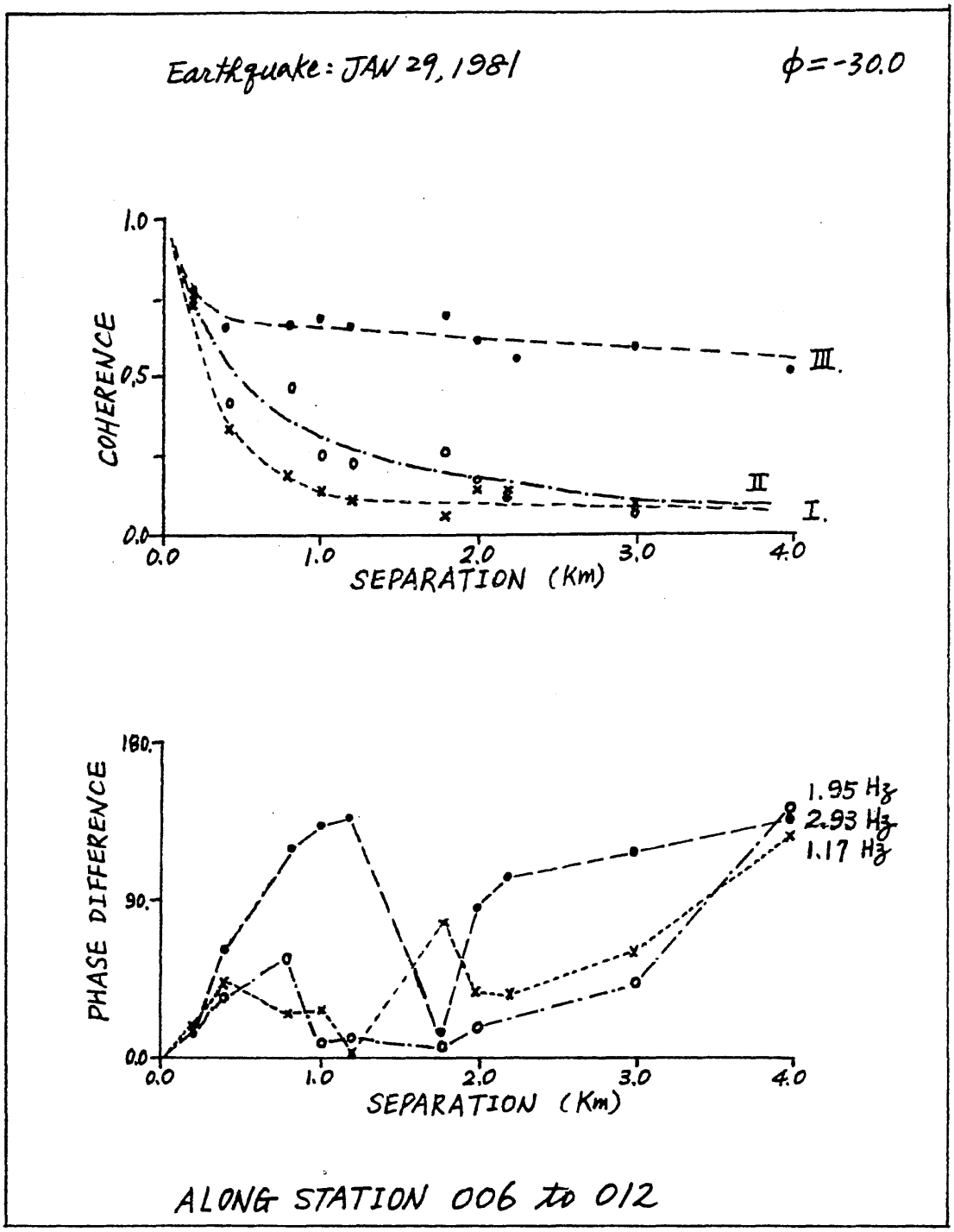

Figure A-8 Variation of Coherence and Phase Difference of Data Along Stations 006 to 012 at ϕ = -30.0°

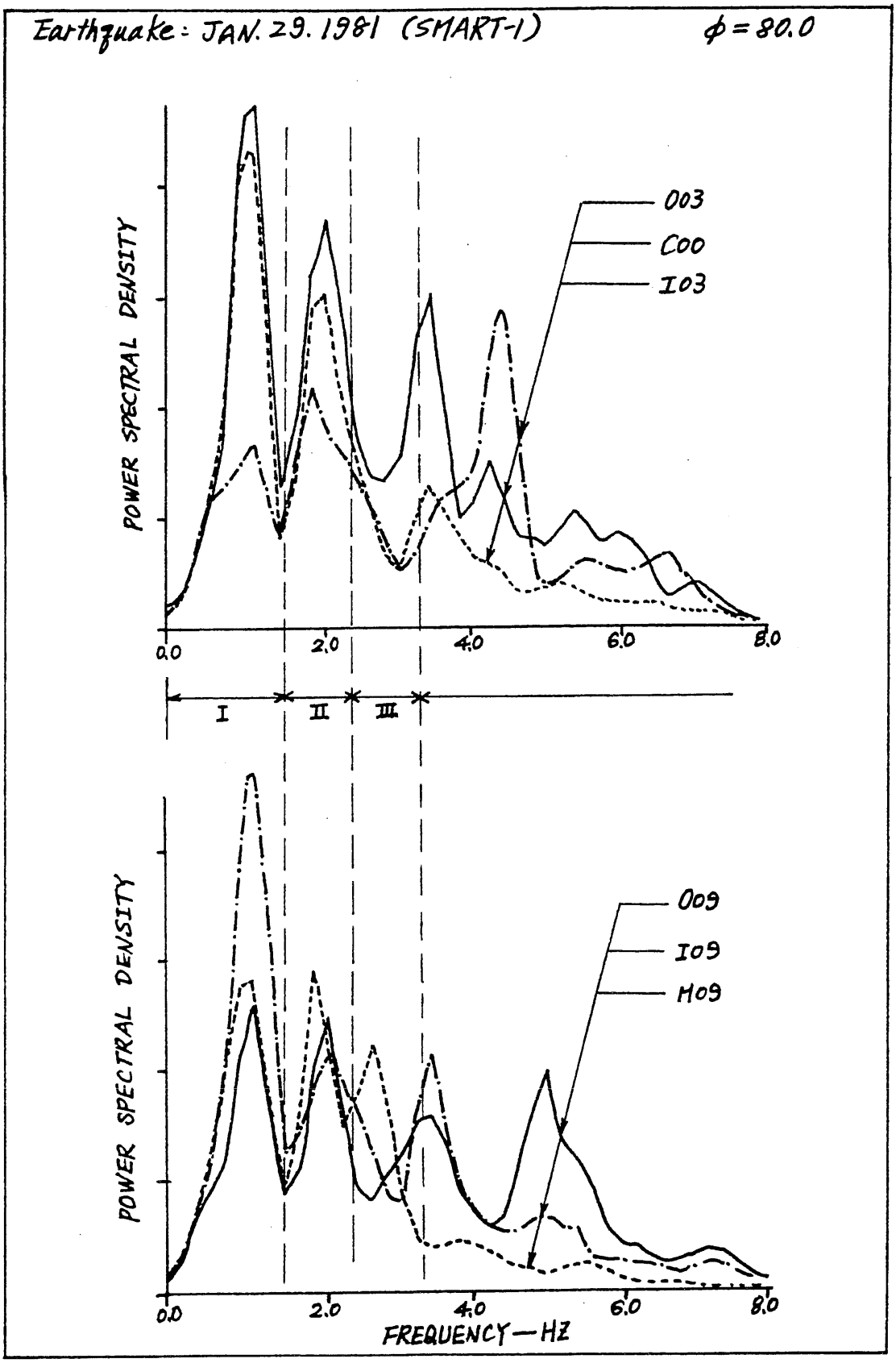

Figure A-9 Power Spectral Density of Stations C00, I03, I09, M09, 003, 009 Along ϕ = 80.0°

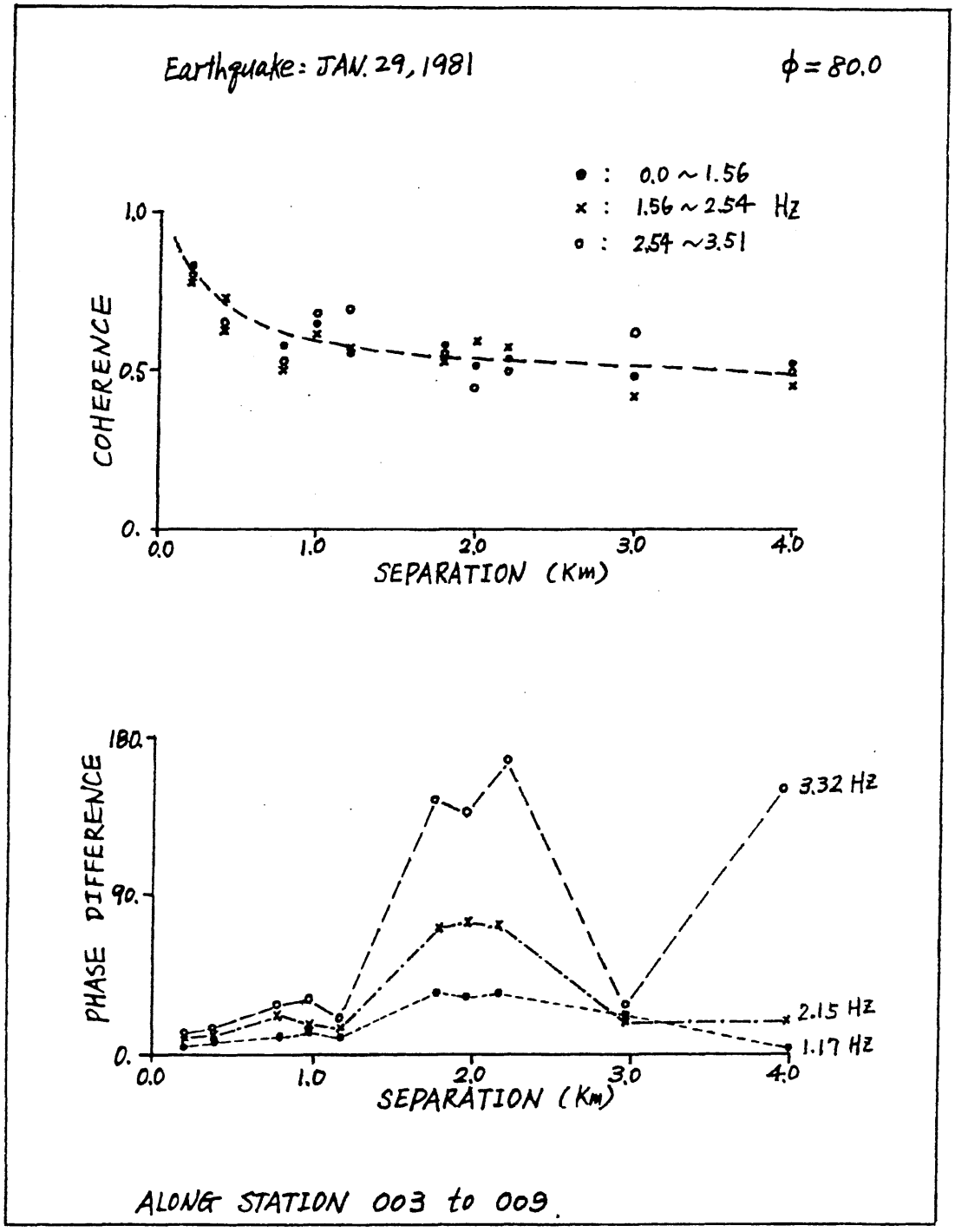

Figure A-10 Variation of Coherence and Phase Difference of Data Along Stations 003 to 009 at ϕ = 80.0°

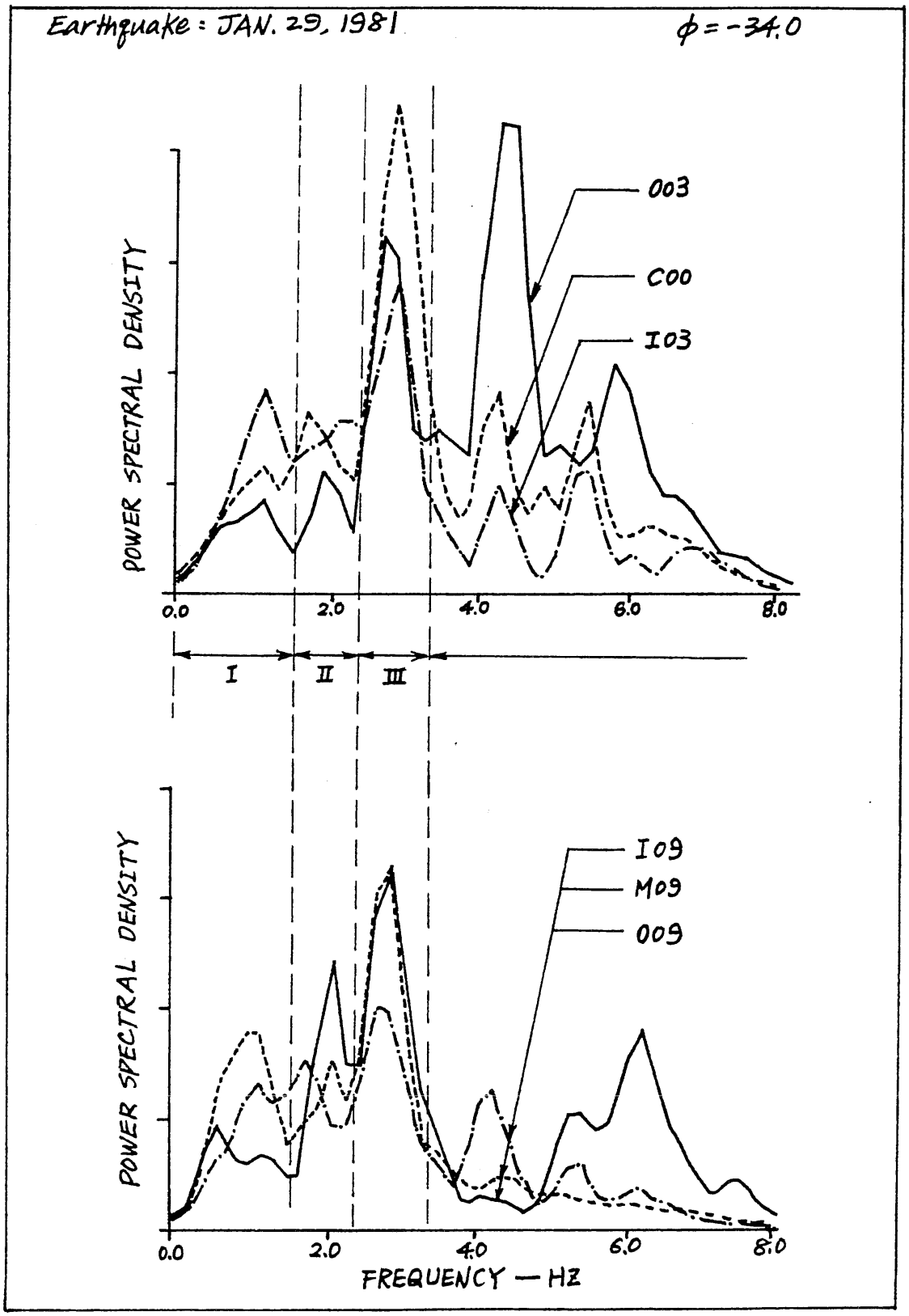

Figure A-11 Power Spectral Density of Stations COO, I03, I09, M09, 003, 009 Along ϕ = -34.0°

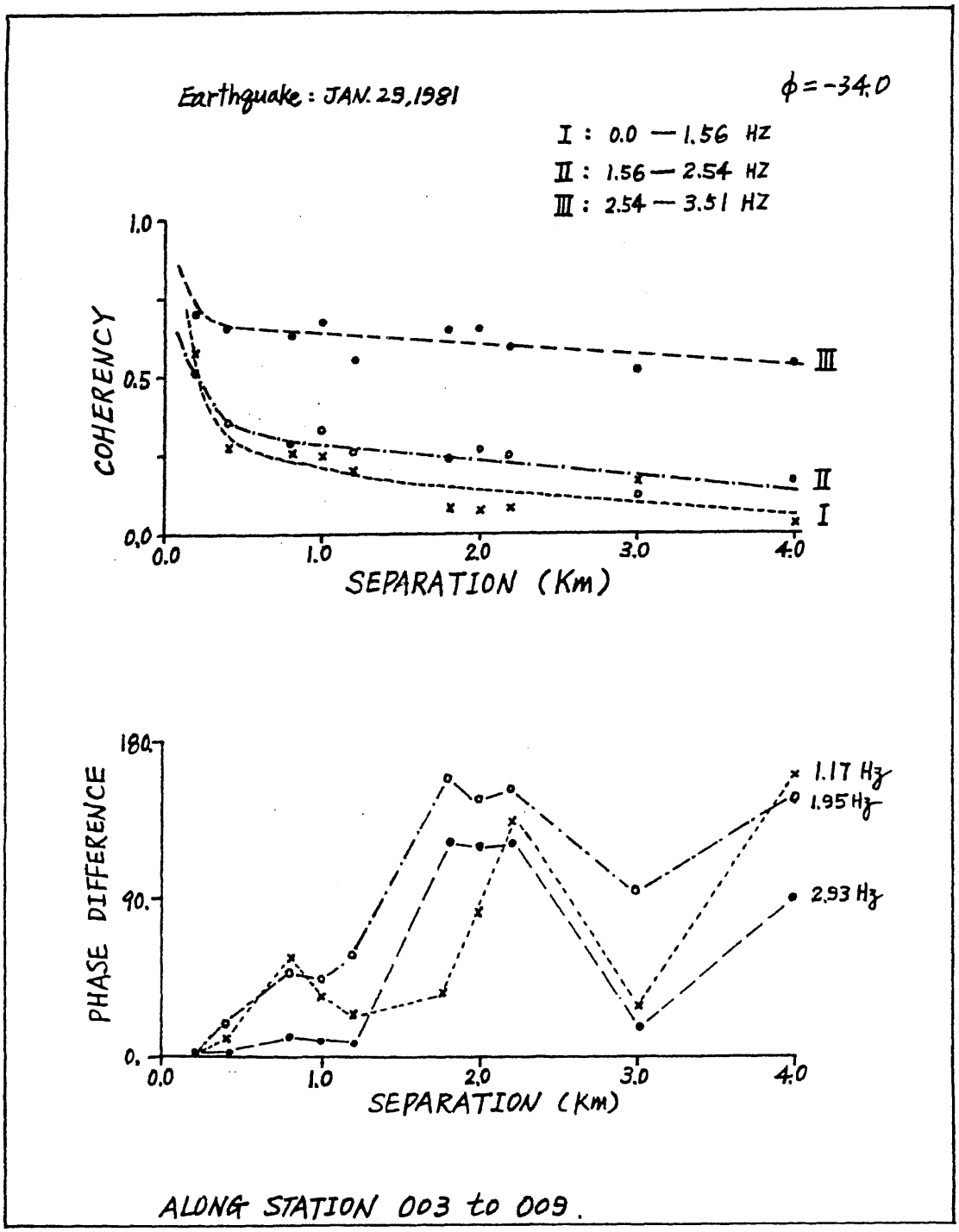

Figure A-12 Variation of Coherence and Phase Difference of Data Along Stations 003 to 009 at ϕ = -34.0°

B. Spatial Correlation of Ground Motions Along and Normal to Epicenter Direction

The fact that the array stations from 006 to 012 are along the epicenter direction makes it easy to study the spatial correlation of seismic waves. By choosing different frequency bands (I:0.0 ~ 1.56 Hz; II:1.56 ~ 2.54 Hz; III:2.54 ~ 4.11 Hz), the spatial coherence and phase difference with respect to station separation are calculated for the January 29, 1981 earthquake. The result is shown in Table A-1. The phase change for the dominant waves (surface waves and shear waves) in the direction of wave propagation is quite obvious. Figures A-5, A-7, A-9, and A-11 plot the power spectral density functions of the ground accelerations at different stations. The previously chosen frequency bands correspond well with the peaks in the power spectral density. This means that there exists a certain kind of wave in a particular frequency band, and thus makes the estimation of coherence more meaningful.

For different earthquakes the frequency bands may be different, and the estimated loss of correlation and phase difference of ground motions due to spatial separation may also have different values.

C. Computer Programs

PROGRAM TO IDENTIFY THE DOMINANT DIRECTION

```
      PROGRAM DIRECT(INPUT,OUTPUT,D1,D2,TAPE6=OUTPUT
     &,TAPE4=INPUT,TAPE10=D1,TAPE20=D2)
      DIMENSION X1(2048),X2(2048),COV1(256),COV2(256)
      DIMENSION COV3(256),COV4(256),EV(256),OD(256)
      MAX=256
      N=2048
      READ(10,10)(X1(I),I=1,N)
      READ(20,10)(X2(I),I=1,N)
      READ(4,3) IM,IN
  222 FORMAT(1X,11HTIME WINDOW,2I8)
      WRITE(6,222)IM,IN
    3 FORMAT(I5)
      K=1
      DO 2 I=IM,IN
      X1(K)=X1(I)
      X2(K)=X2(I)
    2 K=K+1
      INM=IN-IM+1
      DO 4 I=INM,N
      X1(I)=0.
    4 X2(I)=0.
   10 FORMAT(5F12.4)
      CALL COVF(X1,X1,N,COV1,MAX,0,V1)
      CALL COVF(X2,X2,N,COV2,MAX,0,V2)
      CALL COVF(X1,X2,N,COV3,MAX,0,V3)
      CALL COVF(X2,X1,N,COV4,MAX,0,V4)
      DO 12 I=1,MAX
      EV(I)=(COV3(I)+COV4(I))*0.5
      OD(I)=(COV3(I)-COV4(I))*0.5
      COV3(I)=EV(I)
   12 COV4(I)=OD(I)
      CALL AUTO(X1,COV3,MAX,0)
C     CALL AUTO(X1,COV4,MAX,1)
      CALL AUTO(X1,COV1,MAX,0)
      CALL AUTO(X1,COV2,MAX,0)
      PI=3.141592653
      DO 101 I=1,MAX
      EV(I)=2.*COV3(I)
  101 OD(I)=COV1(I)-COV2(I)
      DO 8 I=1,MAX
      IF((EV(I).GT.0.).AND.(OD(I).GE.0.)) ANG=ATAN(EV(I)/OD(I))
      IF((EV(I).LT.0.).AND.(OD(I).LT.0.)) ANG=-PI+ATAN(EV(I)/OD(I))
      IF((EV(I).LT.0.).AND.(OD(I).GE.0.)) ANG=-ATAN(-EV(I)/OD(I))
      IF((EV(I).GT.0.).AND.(OD(I).LT.0.)) ANG=PI-ATAN(-EV(I)/OD(I))
      X1(I)=(ANG/2.)
      X2(I)=(ANG/2.)*180./PI
    8 CONTINUE
      WRITE(6,333)
  333 FORMAT(1X,18HDOMINANT DIRECTION)
      WRITE(6,110)(X2(I),I=1,48)
      DO 104 I=1,MAX
      AA=COS(X1(I))
      BB=SIN(X1(I))
      EV(I)=COV1(I)*AA*AA+COV2(I)*BB*BB+2.*COV3(I)*AA*BB
      OD(I)=COV1(I)*BB*BB+COV2(I)*AA*AA-2.*COV3(I)*AA*BB
  104 CONTINUE
```

> TWO ORTHOGONAL HORIZONTAL GROUND ACCELERATION.

```
      WRITE(6,444)
  444 FORMAT(1X,13HMAX. SPECTRUM)
      WRITE(6,110)(EV(I),I=1,48)
      DO 105 I=1,MAX
  105 X2(I)=OD(I)/EV(I)
      WRITE(6,666)
  666 FORMAT(1X,9HFREQUENCY)
      OD(1)=0.
      DF=50./256.
      DO 107 I=2,58
  107 OD(I)=OD(I-1)+DF
      WRITE(6,110)(OD(I),I=1,48)
      WRITE(6,555)
  555 FORMAT(1X,5HRATIO)
      WRITE(6,110)(X2(I),I=1,48)
  110 FORMAT(10F10.3)
      STOP
      END
      SUBROUTINE COVF(X,Y,N,C,M,NN,V)
      DIMENSION X(1),Y(1),C(1)
      DO 25 KK=1,M
      K=KK-1
      S=0.
      NN1=NN+1
      L=N-NN-K
      DO 15 I=NN1,L
   15 S=S+X(I)*Y(I+K)
      C(KK)=S/FLOAT(L-NN)
   25 CONTINUE
      V=C(1)
      CONTINUE
      RETURN
      END
      SUBROUTINE AUTO(X,Y,M,IM)
      DIMENSION X(1),Y(1)
      S=0.
      DO 10 L=1,M
      K=M-L+1
      X(2*K)=0.
      PI=3.141592653
   10 X(2*K-1)=(Y(K)-S)*0.5*(1.+COS(PI*FLOAT(K-1)/FLOAT(M-1)))
      M21=2*M+1
      M4=4*M
      DO 20 L=M21,M4
   20 X(L)=0.
      CALL FOUR1(X,2*M,-1)
      DO 40 L=1,M
   40 Y(L)=X(2*L-1+IM)
      RETURN
      END
```

PROGRAM TO CALCULATE THE ROOT MEAN SQUARE RESPONE OF LIFELINE ELEMENT.

```
      PROGRAM EPICEN(INPUT,OUTPUT,DATA,VCX,TAPE5=DATA,TAPE6=
     &OUTPUT,TAPE4=INPUT,TAPE10=VCX)
      DIMENSION SX1(100),SX2(100),SY1(100),SY2(100),SS(100),X(100)
      DIMENSION RSX(100),RSY(100),A(100),QSXY(100),PSXY(100)
      DIMENSION VCX(100),VCY(100),STAN(50),CSXY(100),DSXY(100)
      DIMENSION VA(100),XMEAN(100),VV(100),ST(100)
      READ(4,2) Q,DIS,ABX,ABY
      WRITE(6,13) Q,DIS,ABX,ABY
   13 FORMAT(4F12.3)
      READ(10,11)(VCX(I),I=1,60)
   11 FORMAT(5F6.3)
      WRITE(6,11)(VCX(I),I=1,44)
      READ(5,3) WG1,DA1,WF1,DP1,S1
      READ(5,3) WG2,DA2,WF2,DP2,S2
    2 FORMAT(F10.4)
      WRITE(6,3) WG1,DA1,WF1,DP1,S1
      WRITE(6,3) WG2,DA2,WF2,DP2,S2
C     CALCULAT SPECTRAUM AT STATION I ALONG X &Y DIRECTION
      CALL SPECTR(S1,WG1,DA1,WF1,DP1,SX1)
      CALL SPECTR(S2,WG2,DA2,WF2,DP2,SY1)
      WRITE(6,20)(SX1(I),I=1,42)
      WRITE(6,20)(SY1(I),I=1,42)
      READ(5,3) WG3,DA3,WF3,DP3,S3
      READ(5,3) WG4,DA4,WF4,DP4,S4
      WRITE(6,3) WG3,DA3,WF3,DP3,S3
      WRITE(6,3) WG4,DA4,WF4,DP4,S4
    3 FORMAT(4F6.3,F6.1)
C     CALCULATE SPECTRUM AT STATION I+1 ALONG X & Y DIREC.
      CALL SPECTR(S3,WG3,DA3,WF3,DP3,SX2)
      CALL SPECTR(S4,WG4,DA4,WF4,DP4,SY2)
      WRITE(6,20)(SX2(I),I=1,42)
      WRITE(6,20)(SY2(I),I=1,42)
C     CALCULATE  CO-SPECTRUM AT STATION I
      CALL REALSP(SX1,SY1,Q,PSXY)
      CALL REALSP(SX2,SY2,Q,QSXY)
      WRITE(6,20)(PSXY(I),I=1,42)
      WRITE(6,20)(QSXY(I),I=1,42)
C     CALCULATE CROSS SPECTRUM BETWEEN STATION I & I+1, X-AXIS
      CALL CROSS(SX1,SX2,DIS,VCX,ABX,RSX)
C     CALCULATE CROSS SPECTRUM BETWEEN  STATION I&I+1 ,Y-AXIS
      CALL CROSS(SY1,SY2,DIS,VCX,ABY,RSY)
C     CALCULATE CO-SPECTRUM OF XI & YI+1
      CALL REALSP(SX1,SY2,Q,CSXY)
      CALL REALSP(SX2,SY1,Q,DSXY)
      WRITE(6,20)(CSXY(I),I=1,42)
      WRITE(6,20)(DSXY(I),I=1,42)
      PI=3.141592653
      AG=0.0
      READ(4,2) WG,DAMP
```

DIS = Distance between two different stations
Q = $\phi(f)$

Wave velocity at each frequency, of = $\frac{25}{256}$ Hz

$> Eq.(6.3)$

(structural system)

```
      DO 100 K=1,36
      ANG=AG*PI/180.
      DO 10 I=1,60
      SS(I)=(SX1(I)+SX2(I)-2.*RSX(I))*COS(ANG)*COS(ANG)
     &+(SY1(I)+SY2(I)-2.*RSY(I))*SIN(ANG)*SIN(ANG)
     &+2.*(CSXY(I)+DSXY(I)-QSXY(I)-PSXY(I))*COS(ANG)*SIN(ANG)
      SS(I)=(SX1(I)+SX2(I))*COS(ANG)*COS(ANG)+(SY1(I)+SY2(I))
     &*SIN(ANG)*SIN(ANG)
  10 CONTINUE
      CALL SYSTEM(WG,DAMP,X)
      CALL MULTIP(X,SS,A)
      CALL INTEGR(A,VA,ST,K)
      VV(K)=(ST(K)/VA(K))/(2.*PI)
 100 AG=AG+5.0
      DO 110 I=1,36
 110 STAN(I)=SQRT(VA(I))
      WRITE(6,20)(STAN(I),I=1,36)
      DO 120 I=1,36
      TEMP=SQRT(2.*ALOG(20.48*VV(I)))
 120 XMEAN(I)=STAN(I)*(TEMP+0.5772/TEMP)
      WRITE(6,20)(XMEAN(I),I=1,36)
  20 FORMAT(5F12.4)
      STOP
      END
      SUBROUTINE SYSTEM(WG,DAMP,X)
      DIMENSION X(1)
      FREQ=50./256.
      PI=3.141592653
      X(1)=0.
      DO 10 I=2,60
      W=FLOAT(I-1)*FREQ
      A=2.*DAMP*W/WG
      B=1.-(W/WG)**2
      C=(1.+A*A)/(B*B+A*A)
  10 X(I)=C/(2.*PI*W)**4
      RETURN
      END
      SUBROUTINE MULTIP(X,Y,A)
      DIMENSION X(1),Y(1),A(1)
      DO 10 I=1,60
  10 A(I)=X(I)*Y(I)
      RETURN
      END
      SUBROUTINE INTEGR(SS,STAN,ST,K)
      DIMENSION SS(1),STAN(1),ST(1)
      PI=3.141592653
      DF=50./256.
      XUM=0.
      SUM=0.
      DO 100 I=1,60
      W=FLOAT(I-1)*DF
      XUM=XUM+DF*SS(I)*(W*2.*PI)**2
 100 SUM=SUM+SS(I)*DF
      STAN(K)=SUM
      ST(K)=XUM
      RETURN
      END
```

```
      SUBROUTINE SPECTR(S,WG,DF,WF,DF,SP)
      DIMENSION SP(1)
      PI=3.141592653
      FF=50./256.
      DO 100 I=1,60
      W=FLOAT(I-1)*FF
      A=(1.0-(W/WG)**2)**2
      B=4.0*(DF*(W/WG))**2
      C=1.0+B
      D=(W/WF)**2
      E=(1.0-(W/WF)**2)**2+(2.0*DF*W/WF)**2
  100 SP(I)=S*(C/(A+B))*(D/E)
      RETURN
      END
      SUBROUTINE REALSP(SX,SY,Q,SXY)
      DIMENSION SX(1),SY(1),SXY(1)
      DO 100 I=1,60
  100 SXY(I)=Q*SQRT(SX(I)*SY(I))
      RETURN
      END
      SUBROUTINE CROSS(SX,SY,DIS,VC,AR,RSXY)
      DIMENSION SX(1),SY(1),RSXY(1),VC(1)
      DF=50./256.
      PI=3.141592653
      RSXY(1)=0.5*(SX(1)+SY(1))
      DO 10 I=2,60
      W=FLOAT(I-1)*DF*2.*PI
      IF(AR.NE.0.) A=EXP(-DIS/AR)
      IF(AR.EQ.0.) A=1.0
      IF(AR.NE.0.) B=COS(W*DIS/VC(I))
      IF(AR.EQ.0.) B=1.0
      D=0.5*(SX(I)+SY(I))
      RSXY(I)=D*A*B
   10 CONTINUE
      RETURN
      END
```

PROGRAM TO CALCULATE GROUND DISPLACEMENT & GROUND STRAIN, GIVEN CONSTANT WAVE NUMBER.

```
      PROGRAM DISPL(INPUT,OUTPUT,BI12EW,BI12NS,TAPE4=INPUT
     *,TAPE6=OUTPUT,TAPE10=BI12EW,TAPE20=BI12NS)
C     CALCULATE GROUND DISPLACEMENT
      DIMENSION XA(2048),XXA(4096),TXV(2048),XV(2048)
      EQUIVALENCE (TXV(1),XXA(1)),(XV(1),XXA(2049))
      WRITE(6,33)
   33 FORMAT(1X,39HWAVE NO. 1 & 2, ANG, FREQUENCY BAND 1-4)
      READ(4,2) WNO1,WNO2,ANG
    2 FORMAT(F6.2)
      READ(4,3) N1,N2,N3,N4,KKK
    3 FORMAT(I5)
      READ(10,10)(XA(I),I=1,2048)
      READ(20,10)(XV(I),I=1,2048)
      ANG=ANG*3.141592653/180.
      DO 11 I=1,2048
   11 XA(I)=XA(I)*COS(ANG)+XV(I)*SIN(ANG)
   10 FORMAT(5F12.4)
      M=2048
      IF(KKK.EQ.1) GO TO 777
      IF(KKK.EQ.2) GO TO 888
      IF(KKK.EQ.3) GO TO 666
  888 NXX=N1
      NYY=N2
      WRITE(6,444)
  444 FORMAT(1X,9HPASS BAND)
      ABC=2.
      GO TO 333
  666 NXX=N3
      NYY=N4
      N1=0
      N2=0
      ABC=2.0
      GO TO 333
  777 NXX=1
      NYY=2048
      ABC=1.
      WRITE(6,555)
  555 FORMAT(1X,17HFULL ACCEL.RECORD)
      GO TO 333
  333 XV(1)=XA(1)*0.01/2.
      SM=XV(1)
      M1=M-1
      DO 112 I=1,M1
      SM=SM+(XA(I)+XA(I+1))*0.01/2.
  112 XV(I+1)=SM
      CALL LEAST(XV,M,COF1,COF2,0.01)
      WRITE(6,10) COF1,COF2
      DO 4 I=1,M
    4 XV(I)=XV(I)-COF1-COF2*FLOAT(I)*0.01
      DO 5 I=1,M
    5 XA(I)=XV(I)
      CALL ORMSBY(XXA,XA,NXX,NYY,M)
      DO 8 I=1,M
    8 TXV(I)=XXA(2*I-1)*ABC
```

```
      DO 9 I=1,M
    9 XA(I)=TXV(I)
      CALL SORT(XA,2048,AMAX,NX)
      WRITE(6,77)
   77 FORMAT(1X,32HGROUND VELOCITY/MAX(CM/SEC),TIME)
      TIME=FLOAT(NX)*0.01
      WRITE(6,99) AMAX,TIME
      DO 302 I=1,M
  302 XA(I)=TXV(I)
      XV(1)=0.01*XA(1)/2.0
      SUM=XV(1)
      DO 13 I=1,M1
      SUM=SUM+(XA(I)+XA(I+1))*0.01/2.
   13 XV(I+1)=SUM
      DO 311 I=1,M
  311 XA(I)=XV(I)
      CALL ORMSBY(XXA,XA,NXX,NYY,M)
      DO 15 I=1,M
   15 TXV(I)=XXA(2*I-1)*ABC
      DO 305 I=1,M
  305 XA(I)=TXV(I)
      CALL SORT(TXV,2048,AMAX,NX)
      TIME=FLOAT(NX)*0.01
      WRITE(6,98)
   98 FORMAT(1X,25HGROUNDDISP./MAX(CM),TIME/)
      WRITE(6,99) AMAX,TIME
   99 FORMAT(2F15.7)
C     INVERSE FOURIER TRANSFORM AND CALCULATE GROUND STRAIN
      PI=3.141592653
      DO 21 J=1,2048
      JJ=2048-J+1
      XXA(2*JJ)=0.
   21 XXA(2*JJ-1)=XA(JJ)
      CALL FOUR1(XXA,2048,-1)
      DO 31 I=1,300
   31 XA(I)=(XXA(2*I-1)**2+XXA(2*I)**2)/(2.*PI*20.48)
      DO 350 I=3,100
  350 XV(I)=(XA(I-2)+XA(I-1)+XA(I)+XA(I+1)+XA(I+2))/5.
      XV(1)=0.333*(XA(1)+XA(2)+XA(3))
      XV(2)=0.2*XA(1)+XA(2)*0.4+XA(3)*0.2+XA(4)*0.2
      WRITE(6,32)(XV(I),I=1,98)
   32 FORMAT(10F10.3)
      DO 22 I=N1,N2
      T1=XXA(2*I-1)
      T2=XXA(2*I)
      XXA(2*I-1)=-T2*WNO1
   22 XXA(2*I)=T1*WNO1
      DO 23 I=N3,N4
      T1=XXA(2*I-1)
      T2=XXA(2*I)
      XXA(2*I-1)=-T2*WNO2
   23 XXA(2*I)=T1*WNO2
      N1M1=N1-1
      DO 24 I=1,N1M1
      XXA(2*I-1)=0.
   24 XXA(2*I)=0.
      DO 25 I=N2,N3
      XXA(2*I-1)=0.
   25 XXA(2*I)=0.
```

```
      DO 26 I=N4,2048
      XXA(2*I-1)=0.
   26 XXA(2*I)=0.
      CALL FOUR1(XXA,2048,1)
      DO 27 I=1,2048
   27 XA(I)=XXA(2*I-1)*2./FLOAT(2048)
      CALL SORT(XA,2048,AMAX,NX)
      TIME=FLOAT(NX)*0.01
      WRITE(6,101)
  101 FORMAT(1X,21HMAXIMUM GROUND STRAIN)
      WRITE(6,100) AMAX,TIME
  100 FORMAT(2F15.3)
      STOP
      END
      SUBROUTINE LEAST(T1,M,COF1,COF2,DT)
      DIMENSION T1(1)
      SUM=0.
      DO 10 I=1,M
   10 SUM=SUM+T1(I)
      XUM=0.
      DO 15 I=1,M
   15 XUM=XUM+FLOAT(I)*T1(I)
      COF1=(2.*(2.*FLOAT(M)+1.)*SUM-6.*XUM)/(FLOAT(M)*FLOAT(M-1))
      COF2=(12.*XUM-6.*FLOAT(M+1)*SUM)/(DT*FLOAT(M)*FLOAT(M-1)
     **FLOAT(M+1))
      RETURN
      END
      SUBROUTINE ORMSBY(XXA,A,K,IJ,M)
      DIMENSION XXA(1), A(1)
      N=2048
      M1=M+1
      DO 3 I=M1,N
    3 A(I)=0.
      DO 4 J=1,N
      JJ=N-J+1
      XXA(2*JJ)=0.
      XXA(2*JJ-1)=A(JJ)
    4 CONTINUE
      PI=3.141592653
      TOF=FLOAT(N)*0.01
      DO 100 I=1,N
      T=0.01*FLOAT(I)
      IF(T-TOF/10.) 80,60,60
   60 IF(T-9.0*TOF/10.) 100,100,80
   80 THETA=5.*PI*T/TOF
      XXA(2*I-1)=XXA(2*I-1)*(1.-(COS(THETA))**2)
  100 CONTINUE
      CALL FOUR1(XXA,N,-1)
   50 K2=K*2
      DO 6 I=1,K2
      XXA(I)=0.
    6 CONTINUE
      XXA(2*K+1)=0.5*XXA(2*K+1)
      XXA(2*K+2)=0.5*XXA(2*K+2)
      IJ1=2*IJ+1
      N2=N*2
      DO 7 I=IJ1,N2
    7 XXA(I)=0.
```

```
70 CALL FOUR1(XXA,N,1)
   N2=N*2
   DO 8 I=1,N2
 8 XXA(I)=XXA(I)/FLOAT(N)
   RETURN
   END
   SUBROUTINE SORT(Y,N,AMAX,NO)
   DIMENSION Y(1)
   DO 10 I=1,N
10 Y(I)=ABS(Y(I))
   NM1=N-1
   DO 20 I=1,NM1
   IF(Y(I+1).GT.Y(I)) GO TO 6
   YK=Y(I+1)
   Y(I+1)=Y(I)
   Y(I)=YK
   GO TO 7
 6 NO=I+1
 7 AMAX=Y(I+1)
20 CONTINUE
   RETURN
   END
   SUBROUTINE FOUR1(DATA,NN,ISIGN)
   DIMENSION DATA(1)
   N=2*NN
   J=1
   DO 5 I=1,N,2
   IF(I-J) 1,2,2
 1 TEMPR=DATA(J)
   TEMPI=DATA(J+1)
   DATA(J)=DATA(I)
   DATA(J+1)=DATA(I+1)
   DATA(I)=TEMPR
   DATA(I+1)=TEMPI
 2 M=N/2
 3 IF(J-M) 5,5,4
 4 J=J-M
   M=M/2
   IF(M-2) 5,3,3
 5 J=J+M
   MMAX=2
 6 IF(MMAX-N) 7,9,9
 7 ISTEP=2*MMAX
   DO 8 M=1,MMAX,2
   THETA=3.141592653*FLOAT(ISIGN*(M-1))/FLOAT(MMAX)
   WR=COS(THETA)
   WI=SIN(THETA)
   DO 8 I=M,N,ISTEP
   J=I+MMAX
   TEMPR=WR*DATA(J)-WI*DATA(J+1)
   TEMPI=WR*DATA(J+1)+WI*DATA(J)
   DATA(J)=DATA(I)-TEMPR
   DATA(J+1)=DATA(I+1)-TEMPI
   DATA(I)=DATA(I)+TEMPR
   DATA(I+1)=DATA(I+1)+TEMPI
 8 CONTINUE
   MMAX=ISTEP
   GO TO 6
 9 RETURN
   END
```

PROGRAM TO CALCULATE THE COHERENCE OF TWO SIGNALS

```
      PROGRAM COHER(INPUT,OUTPUT,D1,D2,D3,D4,TAPE6=OUTPUT
     &,TAPE4=INPUT,TAPE10=D1,TAPE20=D2,TAPE30=D3,TAPE40=D4)
      DIMENSION X1(2048),X2(2048),COV1(256),COV2(256)
      DIMENSION X3(2048),X4(2048),X5(2048),X6(4096)
      DIMENSION COV3(256),COV4(256),EV(256),OD(256)
      EQUIVALENCE (X5(1),X6(2049))
      MAX=256
      N=2048
      READ(10,10)(X3(I),I=1,N)
      READ(20,10)(X4(I),I=1,N)
      READ(30,10)(X5(I),I=1,N)
      READ(40,10)(X6(I),I=1,N)
      READ(4,1) ANG
    1 FORMAT(F6.2)
C     READ(4,2) II,JJ
    2 FORMAT(I5)
      PI=3.141592653
      AG=ANG*PI/180.
      DO 5 I=1,N
    5 X1(I)=X3(I)*COS(AG)+X4(I)*SIN(AG)
      DO 6 I=1,N
    6 X2(I)=X5(I)*COS(AG)+X6(I)*SIN(AG)
C     CALL TRANSF(X1,X6,N,II,JJ)
C     CALL TRANSF(X2,X6,N,II,JJ)
   10 FORMAT(5F12.4)
      N=2048
      CALL COVF(X1,X1,N,COV1,MAX,0,V1)
   15 FORMAT(10F8.2)
      CALL COVF(X2,X2,N,COV2,MAX,0,V2)
      CALL COVF(X1,X2,N,COV3,MAX,0,V3)
      CALL COVF(X2,X1,N,COV4,MAX,0,V4)
      TEMP=V3/SQRT(V1*V2)
      WRITE(6,10) TEMP
      DO 12 I=1,MAX
      EV(I)=(COV3(I)+COV4(I))*0.5
      OD(I)=(COV3(I)-COV4(I))*0.5
      COV3(I)=EV(I)
   12 COV4(I)=OD(I)
      CALL AUTO(X1,COV3,MAX,0)
      CALL AUTO(X1,COV4,MAX,1)
      CALL AUTO(X1,COV1,MAX,0)
      CALL AUTO(X1,COV2,MAX,0)
      WRITE(6,15)(COV1(I),I=1,42)
      WRITE(6,15)(COV2(I),I=1,42)
      DO 13 I=1,MAX
   13 EV(I)=(COV3(I)**2+COV4(I)**2)/(COV1(I)*COV2(I))
      WRITE(6,20)(EV(I),I=1,42)
      DO 14 I=1,MAX
      IF((COV3(I).GE.0.).AND.(COV4(I).GE.0.)) PH=ATAN(COV4(I)/
     &COV3(I))
      IF((COV3(I).LE.0.).AND.(COV4(I).GE.0.)) PH=PI-ATAN(-COV4
     &(I)/COV3(I))
      IF((COV3(I).GE.0.).AND.(COV4(I).LE.0.)) PH=-ATAN(-COV4(I)
     &/COV3(I))
      IF((COV3(I).LE.0.).AND.(COV4(I).LE.0.)) PH=-PI+ATAN(COV4(I)
     &/COV3(I))
```

```
      WRITE(6,20)(OD(I),I=1,42)
   20 FORMAT(5F12.3)
      STOP
      END
      SUBROUTINE TRANSF(X1,X6,N,II,JJ)
      DIMENSION X1(1),X6(1)
      DO 3 I=1,N
      X6(2*I-1)=X1(I)
    3 X6(2*I)=0.
      CALL FOUR1(X6,N,-1)
      II1=II-1
      DO 4 I=1,II1
      X6(2*I-1)=0.
    4 X6(2*I)=0.
      JJ1=JJ+1
      DO 5 I=JJ1,2048
      X6(I*2-1)=0.
    5 X6(2*I)=0.
      CALL FOUR1(X6,N,1)
      DO 7 I=1,N
    7 X1(I)=2.*X6(2*I-1)
      RETURN
      END
      SUBROUTINE COVF(X,Y,N,C,M,NN,V)
      DIMENSION X(1),Y(1),C(1)
      DO 25 KK=1,M
      K=KK-1
      S=0.
      NN1=NN+1
      L=N-NN-K
      DO 15 I=NN1,L
   15 S=S+X(I)*Y(I+K)
      C(KK)=S/FLOAT(L-NN)
   25 CONTINUE
      V=C(1)
      CONTINUE
      RETURN
      END
      SUBROUTINE AUTO(X,Y,M,IM)
      DIMENSION X(1),Y(1)
      S=0.
      DO 10 L=1,M
      K=M-L+1
      X(2*K)=0.
      PI=3.141592653
   10 X(2*K-1)=(Y(K)-S)*0.5*(1.+COS(PI*FLOAT(K-1)/FLOAT(M-1)))
      M21=2*M+1
      M4=4*M
      DO 20 L=M21,M4
   20 X(L)=0.
      CALL FOUR1(X,2*M,-1)
      DO 40 L=1,M
   40 Y(L)=X(2*L-1+IM)
      RETURN
      END
```

PROGRAM TO CALCULATE ROOT MEAN SQUARE RESPONSE BY USING THE ACTURAL EARTHQUAKE DATA

```
      PROGRAM EPIXXX(INPUT,OUTPUT,D1,D2,D3,D4,TAPE6=OUTPUT
     &,TAPE4=INPUT,TAPE10=D1,TAPE20=D2,TAPE30=D3,TAPE40=D4)
      DIMENSION X1(2048),X2(2048),COV3(256),COV4(256)
      DIMENSION X3(2048),X4(2048),X5(2048),X6(2048)
      DIMENSION SX1(256),SX2(256),SY1(256),SY2(256),PSXY(256)
      DIMENSION QSXY(256),CSXY(256),DSXY(256),RSX(256),RSY(256)
      EQUIVALENCE (X2(1),SX1(1)),(X2(257),SX2(1)),(X2(769),SY1(1))
      EQUIVALENCE (X2(1281),PSXY(1)),(X2(1025),SY2(1))
      EQUIVALENCE (X2(1537),DSXY(1)),(X2(513),CSXY(1))
      MAX=256
      N=2048
      READ(10,10)(X1(I),I=1,N)
      READ(20,10)(X2(I),I=1,N)
      PI=3.141592653
      ANG=77.36*PI/180.
      AG=-34.0*PI/180.
      DO 5 I=1,N
      X5(I)=X1(I)*COS(AG)+X2(I)*SIN(AG)
    5 X3(I)=X1(I)*COS(ANG)+X2(I)*SIN(ANG)
      READ(30,10)(X1(I),I=1,N)
      READ(40,10)(X2(I),I=1,N)
      DO 6 I=1,N
      X6(I)=X1(I)*COS(AG)+X2(I)*SIN(AG)
    6 X4(I)=X1(I)*COS(ANG)+X2(I)*SIN(ANG)
   10 FORMAT(5F12.4)
      CALL CCVF(X3,X3,N,SX1,MAX,0,V1)
      CALL AUTO(X1,SX1,MAX,0)
      WRITE(6,10)(SX1(I),I=1,42)
      CALL COVF(X4,X4,N,SX2,MAX,0,V2)
      CALL AUTO(X1,SX2,MAX,0)
      WRITE(6,10)(SX2(I),I=1,42)
      CALL COVF(X5,X5,N,SY1,MAX,0,V3)
      CALL AUTO(X1,SY1,MAX,0)
      WRITE(6,10)(SY1(I),I=1,42)
      CALL COVF(X6,X6,N,SY2,MAX,0,V4)
      CALL AUTO(X1,SY2,MAX,0)
      WRITE(6,10)(SY2(I),I=1,42)
      CALL COVF(X3,X4,N,COV3,MAX,0,V3)
      CALL COVF(X4,X3,N,COV4,MAX,0,V4)
      DO 12 I=1,MAX
   12 RSX(I)=(COV3(I)+COV4(I))*0.5
      CALL AUTO(X1,RSX,MAX,0)
      WRITE(6,10)(RSX(I),I=1,42)
      CALL COVF(X5,X6,N,COV3,MAX,0,V3)
      CALL COVF(X6,X5,N,COV4,MAX,0,V4)
      DO 13 I=1,MAX
   13 RSY(I)=(COV3(I)+COV4(I))*0.5
      CALL AUTO (X1,RSY,MAX,0)
      WRITE(6,10)(RSY(I),I=1,42)
      CALL COVF(X3,X6,N,COV3,MAX,0,V3)
      CALL COVF(X6,X3,N,COV4,MAX,0,V4)
      DO 14 I=1,MAX
   14 CSXY(I)=(COV3(I)+COV4(I))*0.5
      CALL AUTO(X1,CSXY,MAX,0)
      WRITE(6,10)(CSXY(I),I=1,42)
```

```
      CALL COVF(X5,X4,N,COV3,MAX,0,V3)
      CALL COVF(X4,X5,N,COV4,MAX,0,V4)
      DO 15 I=1,MAX
   15 DSXY(I)=(COV3(I)+COV4(I))*0.5
      CALL AUTO(X1,DSXY,MAX,0)
      WRITE(6,10)(DSXY(I),I=1,42)
      CALL COVF(X3,X5,N,COV3,MAX,0,V3)
      CALL COVF(X5,X3,N,COV4,MAX,0,V4)
      DO 16 I=1,MAX
   16 PSXY(I)=(COV3(I)+COV4(I))*0.5
      CALL AUTO(X1,PSXY,MAX,0)
      WRITE(6,10)(PSXY(I),I=1,42)
      CALL COVF(X4,X6,N,COV3,MAX,0,V3)
      CALL COVF(X6,X4,N,COV4,MAX,0,V4)
      DO 17 I=1,MAX
   17 QSXY(I)=(COV3(I)+COV4(I))*0.5
      CALL AUTO(X1,QSXY,MAX,0)
      WRITE(6,10)(QSXY(I),I=1,42)
      AG=0.
      READ(4,2) WG,DAMP
    2 FORMAT(F12.4)
      DO 100 K=1,36
      ANG=AG*PI/180.
      DO 90 I=1,60
      X1(I)=(SX1(I)+SX2(I)-2.*RSX(I))*COS(ANG)*COS(ANG)
     &+(SY1(I)+SY2(I)-2.*RSY(I))*SIN(ANG)*SIN(ANG)
     &+2.*(CSXY(I)+DSXY(I)-QSXY(I)-PSXY(I))*COS(ANG)*SIN(ANG)
   90 CONTINUE
      CALL SYSTEM(WG,DAMP,COV3)
      CALL MULTIP(COV3,X1,COV4)
      CALL INTEGR(COV4,X3,K)
  100 AG=AG+5.0
      DO 110 I=1,36
  110 X3(I)=SQRT(X3(I))
      WRITE(6,10)(X3(I),I=1,36)
      STOP
      END
      SUBROUTINE SYSTEM(WG,DAMP,X)
      DIMENSION X(1)
      FREQ=50./256.
      PI=3.141592653
      X(1)=0.
      DO 10 I=2,60
      W=FLOAT(I-1)*FREQ
      A=2.*DAMP*W/WG
      B=1.-(W/WG)**2
      C=(1.+A*A)/(B*B+A*A)
   10 X(I)=C/(2.*PI*W)**4
      RETURN
      END
      SUBROUTINE MULTIP(X,Y,A)
      DIMENSION X(1),Y(1),A(1)
      DO 10 I=1,60
   10 A(I)=X(I)*Y(I)
      RETURN
      END
```

```
      SUBROUTINE INTEGR(SS,STAN,K)
      DIMENSION SS(1),STAN(1)
      DF=50./256.
      SUM=0.
      DO 100 I=1,60
  100 SUM=SUM+SS(I)*DF
      STAN(K)=SUM
      RETURN
      END
      SUBROUTINE COVF(X,Y,N,C,M,NN,V)
      DIMENSION X(1),Y(1),C(1)
      DO 25 KK=1,M
      K=KK-1
      S=0.
      NN1=NN+1
      L=N-NN-K
      DO 15 I=NN1,L
   15 S=S+X(I)*Y(I+K)
      C(KK)=S/FLOAT(L-NN)
   25 CONTINUE
      V=C(1)
      CONTINUE
      RETURN
      END
      SUBROUTINE AUTO(X,Y,M,IM)
      DIMENSION X(1),Y(1)
      S=0.
      DO 10 L=1,M
      K=M-L+1
      X(2*K)=0.
      PI=3.141592653
   10 X(2*K-1)=(Y(K)-S)*0.5*(1.+COS(PI*FLOAT(K-1)/FLOAT(M-1)))
      M21=2*M+1
      M4=4*M
      DO 20 L=M21,M4
   20 X(L)=0.
      CALL FOUR1(X,2*M,-1)
      DO 40 L=1,M
   40 Y(L)=X(2*L-1+IM)
      RETURN
      END
      SUBROUTINE FOUR1(DATA,NN,ISIGN)
      DIMENSION DATA(1)
      N=2*NN
      J=1
      DO 5 I=1,N,2
      IF(I-J) 1,2,2
    1 TEMPR=DATA(J)
      TEMPI=DATA(J+1)
      DATA(J)=DATA(I)
      DATA(J+1)=DATA(I+1)
      DATA(I)=TEMPR
      DATA(I+1)=TEMPI
    2 M=N/2
    3 IF(J-M) 5,5,4
    4 J=J-M
      M=M/2
      IF(M-2) 5,3,3
```

```
      MMAX=2
    6 IF(MMAX-N) 7,9,9
    7 ISTEP=2*MMAX
      DO 8 M=1,MMAX,2
      THETA=3.141592653*FLOAT(ISIGN*(M-1))/FLOAT(MMAX)
      WR=COS(THETA)
      WI=SIN(THETA)
      DO 8 I=M,N,ISTEP
      J=I+MMAX
      TEMPR=WR*DATA(J)-WI*DATA(J+1)
      TEMPI=WR*DATA(J+1)+WI*DATA(J)
      DATA(J)=DATA(I)-TEMPR
      DATA(J+1)=DATA(I+1)-TEMPI
      DATA(I)=DATA(I)+TEMPR
      DATA(I+1)=DATA(I+1)+TEMPI
    8 CONTINUE
      MMAX=ISTEP
      GO TO 6
    9 RETURN
      END
```

REFERENCES

1. Ang, A. H-S., "Structural Risk Analysis and Reliability-Based Design," J. Structural Division, ASCE, ST9, September 1973.

2. Ang, A. H-S. and Y. K. Wen, "Risk and Safety Analysis in Design for Natural Hazards Protection," Proc. U.S.-Southeast Asia Symposium on Earthquake Engineering for Natural Hazard Protection, (edited by A. H-S. Ang), 1977.

3. Aoki, Y. and S. Hayashi, "Spectra for Earthquake Resistive Design of Underground Long Structures," Proc. Fifth World Conference on Earthquake Engineering, Rome, 1973.

4. Bolt, B. A., C. H. Loh, J. Penzien, Y. B. Tsai, and Y. T. Yeh, "Preliminary Report on the SMART-1 Strong Motion Array in Taiwan," UCB-EERC 82/13, University of California, Berkeley, 1982.

5. Campbell, K. W, R. T. Eguchi, and C. M. Duke, "Reliability in Lifeline Earthquake Engineering," J. Technical Council of ASCE, December 1979.

6. Christian, J. T., "Relative Motion of Two Points During an Earthquake," J. Geotechnical Engineering Division, ASCE, GT11, November 1976.

7. Der Kiureghian, A. and A. H-S. Ang, "A Fault-Rupture Model for Seismic Risk Analysis," B.S.S.A., 67, 4, August 1977.

8. Der Kiureghian, A., "Seismic Risk Analysis of Structural System," J. Engineering Mechanics Division, ASCE, 107, EM6, December 1981.

9. Esteva, L., S. E. Ruiz, and A. Ryeus, "Seismic Response of Multi-Support Structures," Proc. Seventh World Conference on Earthquake Engineering, Turkey, 1980.

10. Feng, Qimin and Yuxian Hu, "Spatial Correlation of Earthquake Motion and Its Effect on Structural Response," Proc. U.S.-PRC Bilateral Workshop on Earthquake Engineering, August 1982.

11. Goto, H., H. Kameda, S. Takada, and H. Sugito, "Earthquake Motion Estimation for Buried Lifelines," Specialty Conference on Lifeline Earthquake Engineering, Oakland, August 1981.

12. Goto, H., M. Sugito, H. Kameda, and A. Isoda, "Microzonation of Ground Strain for Estimation of Earthquake Damage to Buried Pipelines," Third International Earthquake Microzonation Earthquake Engineering, Oakland, August 1981.

13. Hindy, A. and M. Novak, "Earthquake Response of Underground Pipeline," Int. J. Earthquake Engineering and Structural Dynamics, 7, 1979.

14. Hindy, A. and M. Novak, "Pipeline Response to Random Ground Motions," J. Engineering Mechanics Division, ASCE, April 1980.

15. Iyer, H. M. and J. H. Hlaby, "Evidence for the Existence of Locally Generated Body Waves in the Short-Period Noise at the Large Apperture Seismic Array," B.S.S.A., 62, 1, 1972.

16. Kameda, H., H. Goto, M. Sugito, and K. Asaoka, "Seismic Risk and Performance of Water Lifeline," Probabilistic Methods in Structure Engineering, ASCE, October 1981.

17. Kameda, H. and M. Shinozuka, "Simplified Formula for Axial Strains of Buried Pipes Induced by Propagating Seismic Waves," Memoirs of the Faculty of Engineering, Kyoto University, 44, Part 2, April 1982.

18. Kameda, H., M. Sugito, and H. Goto, "Microzonation and Simulation of Spatially Correlated Earthquake Motions," Third International Earthquake Microzonation Conference, Seattle, July 1982.

19. Kubo, K., T. Katayama, and M. Ohashi, "Lifeline Earthquake Engineering in Japan," J. Technical Council of ASCE, April 1979.

20. Loh, C. H., J. Penzien, and Y. B. Tsai, "Engineering Analysis of SMART-1 Array Data," Int. J. Earthquake Engineering and Structural Dynamics, 1982.

21. Loh, C. H. and J. Penzien, "Identification of Waves Types, Directions and Velocities Using SMART-1 Strong Motion Array Data," paper submitted to 8WCEE, 1984.

22. Moghtaderizadeh, M., R. K. Wood, A. D. Kiureghian, and R. E. Barlow, "Seismic Reliability of Lifeline Networks," J. Technology Council, ASCE, TC1, May 1982.

23. Mohammadi, J. and A. H-S. Ang, "Seismic Hazard Analysis of Lifelines," J. Structural Division, ASCE, 108, ST6, June 1982.

24. Nelson, I. and P. Weidlinger, "Dynamic Seismic Analysis of Long Segments Lifelines," J. Pressure Vessel Technology, February 1979.

25. Pazargadi, S., "Lifeline Response Analysis Under Nonstationary Traveling Seismic Wave Loading," Proc. Seventh World Conference on Earthquake Engineering, Turkey, 1980.

26. Penzien, J., "Aoki Spectrum for the Design of Underground Long Structures," Private communication.

27. "Research Needs in Lifeline Earthquake Engineering," J. Technical Councils of ASCE, December 1979.

28. Shinozuka, M., S. Takada, and H. Kawakami, "Risk Analysis of Underground Lifeline Network System," Proc. U.S.-Southeast Asia Symposium on Earthquake Engineering for Natural Hazard Protection, (edited by A. H-S. Ang), Manila, 1977.

29. Shinozuka, M., S. Takada, and H. Ishikawa, "Some Aspects of Seismic Risk Analysis of Underground Lifeline Systems," J. Pressure Vessel Technology, ASME, February 1979.

30. Shinozuka, M., R. Y. Tan, and T. Koike, "Serviceability of Water Transmission Systems Under Seismic Risk," Proc. Specialty Conference on Lifeline Earthquake Engineering, ASCE, Oakland, 1981.

31. Shinozuka, M., H. Kameda, and T. Koike, "Ground Strain Estimation for Seismic Risk Analysis of Underground Lifelines," ASME, 80-C2/PVP-69, 1981.

32. Taleb-Agha, G., "Seismic Risk Analysis of Lifeline Networks," B.S.S.A., 67, 6, December 1977.

33. Wang, L.R.L., "Vibration Frequency of Buried Pipelines," J. Technology Councils of ASCE, November 1978.

34. Wirsching, P. H. and J. T-P. Yao, "Monte Carlo Study of Seismic Structural Safety," J. of the Structural Division, ASCE, 97, ST5, May 1971.

35. Yang, J. N., S. Sae-Ung, and Y. K. Lin, "Variability of Tall Building Response to Earthquakes with Changing Epicentral Direction," J. Earthquake Engineering and Structural Dynamics, 10, 1982.